

NASA CONTRACTOR REPORT



NASA CR-170909

LIGHTNING MAPPER SENSOR DESIGN STUDY

By L. R. Eaton, C. W. Poon,
J. C. Shelton, N. P. Laverty
and R. D. Cook

TRW Space & Technology Group

(NASA-CR-170909) LIGHTNING MAPPER SENSOR
DESIGN STUDY Final Report (TRW Space
Technology Labs.) 153 p HC A08/MF A01

N84-13732

CSSL 04B

Unclas

G3/47

42601

Final Report

September 1983

Prepared for

NASA - Marshall Space Flight Center
Marshall Space Flight Center, Alabama 35812

TECHNICAL REPORT STANDARD TITLE PAGE

1. REPORT NO. NASA CR-170909		2. GOVERNMENT ACCESSION NO.		3. RECIPIENT'S CATALOG NO.	
4. TITLE AND SUBTITLE Lightning Mapper Sensor Design Study				5. REPORT DATE September 1983	
				6. PERFORMING ORGANIZATION CODE	
7. AUTHOR(S) L. K. Eaton, C. W. Poon, J. C. Shelton, N. P. Laverty and R. D. Cook				8. PERFORMING ORGANIZATION REPORT #	
9. PERFORMING ORGANIZATION NAME AND ADDRESS TRW Space & Technology Group One Space Park Redondo Beach, CA 90278				10. WORK UNIT NO.	
				11. CONTRACT OR GRANT NO. NAS8-34941	
				13. TYPE OF REPORT & PERIOD COVERED Contractor Report	
12. SPONSORING AGENCY NAME AND ADDRESS National Aeronautics & Space Administration Washington, D. C. 20546				14. SPONSORING AGENCY CODE	
15. SUPPLEMENTARY NOTES Final Report Technical Monitor: Hugh Christian, Atmospheric Science Division, Systems Dynamics Laboratory, Marshall Space Flight Center, Alabama					
16. ABSTRACT World-wide continuous measurement of lightning location, intensity, and time during both day and night is to be provided by the Lightning Mapper (LITMAP) instrument. This study is primarily a technology assessment to determine if the LITMAP requirements can be met using existing sensor and electronic technologies. The baseline concept discussed in this report is a compromise among a number of opposing requirements (e.g., ground resolution versus array size; large field of view versus narrow bandpass filter). The concept provides coverage for more than 80 percent of the lightning events as based on recent above-cloud NASA/U2 lightning measurements.					
17. KEY WORDS Lightning mapper Optical sensors			18. DISTRIBUTION STATEMENT Unclassified-Unlimited <i>G. F. McDonough</i> G. F. McDonough Director, Systems Dynamics Laboratory		
19. SECURITY CLASSIF. (of this report) Unclassified		20. SECURITY CLASSIF. (of this page) Unclassified		21. NO. OF PAGES 155	22. PRICE NTIS

ACKNOWLEDGMENT

The work reported herein was supported by the National Aeronautics and Space Administration, Marshall Space Flight Center, Systems Dynamics Laboratory, Atmospheric Sciences Division, under NASA Contract NAS8-349.1 and under the sponsorship of Dr. James C. Dodge, Mesoscale Atmospheric Processes Program Manager, NASA Headquarters, Washington, D.C.

Special thanks are given also to Dr. H. J. Christian (scientific monitor of this study) and other NASA and university lightning research team members who provided technical advice and input to the final documentation.

TABLE OF CONTENTS

1. OVERVIEW	1
1.1 STUDY	1
1.2 DRIVERS	1
1.3 CONCEPT SELECTION	2
1.4 BASELINE DEFINITION	3
1.5 FINAL REPORT CONTENTS	3
2. SYSTEMS PARAMETERS	5
2.1 REQUIREMENTS	5
2.2 DESIGN PARAMETERS	6
2.3 SUMMARY	9
3. SYSTEMS ANALYSIS	11
3.1 DAYTIME OPERATION	11
3.2 NIGHT OPERATION	11
3.3 ADJUSTABLE THRESHOLD	13
3.4 PARAMETRIC TRADES	14
3.5 KEY SENSOR PARAMETERS	15
3.6 SOLUTIONS TO SYSTEM DRIVERS	16
3.7 SUMMARY	20
4. CONCEPT DESCRIPTION	21
4.1 GENERAL	21
4.2 OPTICAL CONCEPT	22
4.2.1 Requirements	22
4.2.2 Telescope Concepts	23
4.2.3 Optical Partitioning	25
4.2.4 Filter Design	29
4.2.5 Transmission	31
4.2.6 Baseline Performance Summary	31
4.3 DETECTOR	32
4.3.1 Selection of Detector Type	32
4.3.2 Frame Transfer Methods	37
4.3.3 Focal Plane Configuration	39
4.3.4 Required Modifications	42

TABLE OF CONTENTS (Continued)

4.4 SIGNAL PROCESSING	46
4.4.1 Design Requirements	46
4.4.2 Background Substraction	48
4.4.2.1 Analog Versus Digital	49
4.4.2.2 Digital Approach	50
4.4.2.3 Analog Approach	52
4.4.3 Proposed System	52
4.4.3.1 Data Processor	54
4.4.3.2 Control Logic	63
4.4.3.3 Data Formatter	64
4.4.3.4 Power Control	66
4.4.4 Alternate Design Approaches	66
4.4.5 Other Design Considerations	67
4.4.5.1 Product Design	67
4.4.5.2 Spacecraft Interface	68
4.5 RADIATION EFFECTS IN SILICON DEVICES	69
4.5.1 General	69
4.5.2 Soft Damage	69
4.5.3 Transient Effects	69
4.5.4 Hard Damage	70
4.5.5 LITMAP Electronics Hardening Approaches	70
5.0 TECHNOLOGY ASSESSMENT	73
5.1 CCD REQUIREMENTS	73
5.2 SENSOR CONCEPTS	74
5.3 CURRENTLY AVAILABLE CCD's	76
5.4 DISCUSSION WITH MANUFACTURERS REGARDING DEVICE OPTIMIZATION	79
5.4.1 Texas Instruments	79
5.4.2 RCA Electro Optics and Devices Solid State Division	80
5.4.3 RCA David Sarnoff Research Laboratories	81
5.4.4 Hughes Aircraft Co., Industrial Electronics Technology Center	81
5.4.5 Westinghouse Advanced Technology Laboratory	83
5.4.6 Fairchild CCD Imaging	83
5.5 CONCLUSIONS	83
6. REFERENCES	85

TABLE OF CONTENTS

APPENDICES

A.	PARAMETER SPECIFICATIONS	87
A.1	INTRODUCTION	87
A.2	FIELD OF VIEW: FOV	87
A.3	AREA PER PIXEL: A_b	93
A.4	SOURCE CHARACTERISTICS	94
A.4.1	Source Area: A_s	94
A.4.2	Geometric Splitting Factor: ν	95
A.4.3	Lightning Pulse Duration: T_L	98
A.4.4	Pulse Time Splitting: ξ	100
A.4.5	Source Energy Strength: $E_{s,\lambda}$	101
A.5	SIGNAL/NOISE RATIO: SNR	103
A.6	BACKGROUND: I_b , ALBEDO	105
A.7	OPTICS:F/NO., K	107
A.8	FILTER: $\Delta\lambda$, η	108
A.9	SENSOR CHARACTERISTICS	110
A.9.1	Quantum Efficiency: Q	110
A.9.2	Pixel Dimensions: δ_p	112
A.9.3	Sensor Noise: ϵ	114
A.9.4	Integration Time: T_i	115
A.9.5	Full Well Capacity: FW	117
A.10	DYNAMIC RANGE	121
A.11	SUMMARY	122

APPENDICES (Con't)

B. PARAMETRIC TRADES	125
B.1 INTRODUCTION	125
B.2 BASELINE PARAMETER SET	125
B.3 OPTIMISTIC SET	129
B.4 LIGHTNING PULSE DURATION	130
B.5 FILL FACTOR	131
B.6 PIXEL SIZE	133
B.7 READOUT NOISE	135
B.8 WAVELENGTH	138
B.9 FILTER BANDPASS	139
B.10 EVENT SOURCE SIZE	140
B.11 EXISTING DEVICES	141
B.12 SUMMARY	145

FIGURES

1.1	LIGHTNING MAPPER TECHNICAL ELEMENTS	1
2.1	PRIMARY SYSTEM ELEMENTS AND ASSOCIATED PARAMETERS	8
3.1	BASELINE DEVICE PIXEL AND FULL WELL REQUIREMENTS	16
4.1	CASSEGRAIN	24
4.2	REFRACTIVE	24
4.3	FOUR CCD'S WITH INDIVIDUAL OPTICS AND SPECTRAL FILTERS.	25
4.4	QUADRI-FURCATED FIBER OPTICS	26
4.5	MINIFICATION OF FIBER OPTICS IMAGE	27
4.6	IMAGE SLICER, TWO WAY	27
4.7	FOUR-WAY IMAGE SLICER CONCEPT	28
4.8	FILTER HALF POWER BANDWIDTH VERSUS MAXIMUM ANGLE OF INCIDENCE	29
4.9	SOLC FILTER	30
4.10	GENERIC DETECTOR ALTERNATIVES	33
4.11	MULTI-ANODE MICROCHANNEL ARRAY	35
4.12	ANAMORPHIC OPTICAL SUBSYSTEM	36
4.13	ORGANIZATION OF 5040 AREA ARRAY	37
4.14	WESTINGHOUSE 5040	38
4.15	LITMAP SYSTEM CONCEPTUAL BLOCK DIAGRAM	47
4.16	PROPOSED LITMAP ELECTRONICS SYSTEM BLOCK DIAGRAM	53
4.17	BACKGROUND SUBTRACTION WITH RUNNING AVERAGE	55
4.18	DATA BUFFER FUNCTIONAL BLOCK DIAGRAM	61
4.19	DATA BUFFER MEMORY STAGE FORMAT	62
4.20	MASTER CONTROL LOGIC	63
4.21	DATA FORMATTER FUNCTIONAL BLOCK DIAGRAM	64
4.22	DATA FORMATTER MEMORY STORAGE FORMAT	65
4.23	RADIATION DOSE VERSUS SHIELDING THICKNESS	72
5.1	SENSOR CONCEPTS	76

FIGURES

APPENDIX

A.1	Key Geometric Dimensions for a Geosynchronous Observation Vantage Point (B) and Geometric Overlay of Sensor Array onto Earth's Cross-section (A).	88
A.2	Distance Along Earth's Surface as Function of Sensor Observation Angle (A) and Earth's Latitude (B).	90
A.3	Linear and Area Variations (for equal steps) Normalized to the Respective Dimension at the Subsatellite Point Relative to Sensor Observation Angle (A) and Earth's Latitude (B).	91
A.4	Variation of Earth's Latitude (fixed longitude) with Observation Angle.	92
A.5	Distribution of Horizontal Cloud Dimensions.	95
A.6	Average Illuminance Within a Pixel as a Function of Pixel Size δ_B Normalized Relative to Event Size δ_S Pixel Focal Plane.	96
A.7	Effective Pulse Duration (peak energy/integrated power) (see text).	98
A.8	Maximum Radiant Energy vs. Maximum Peak Power (A) and all Strokes (B).	
A.9	Time Factor Effect on SNR	101
A.10	Energy Distribution for Lightning.	102
A.11	FAR vs. SNR.	104
A.12	Probability of Detection vs. SNR.	106
A.13	Cloud Top Altitudes.	106
A.14	Angular Shift for Interference Filters.	109
A.15	Image Spreading in Array Detectors.	111
A.16	Resolution vs. Aperture.	112
A.17	Aperture vs. Pixel Dimensions.	113
A.18	Focal Plane Partitioning vs. Sample Time.	115
A.19	Full Well Capacity.	118
A.20	Dynamic Range vs. Allowable Noise.	118
A.21	Dynamic Range as Percent of Full Well.	119
A.22	Absolute Noise Limits Relative to Full Well Capacity.	120
A.23	Relative Dynamic Range vs. Probability.	122

FIGURES

APPENDIX (Continued)

B.1	Threshold Energy for 8683A as a Function of Integration Time for the 126 Baseline Set of Parameters Given in Table 2.2.	
B.2	Computer Printout Format for Baseline/Day	127
B.3	Computer Printout for Baseline/Night	128
B.4	Baseline with (—) and without (---) Spatial and Time Splitting Factors	
B.5	Optimistic Performance	130
B.6	Pulse Duration Effects	131
B.7	FOV Effects - Day	132
B.8	FOV Effects - Night	133
B.9	Threshold Dependency on FOV. Baseline conditions and $L_s = 11$ km.	134
B.10	Pixel Size Effects - Day	136
B.11	Pixel Size Effects - Night	136
B.12	Amplifier Noise Effects - Day	137
B.13	Amplifier Noise Effects - Night	137
B.14	Wavelength Selection	138
B.15	Optical Bandpass Effects	139
B.16	Source Size Effects - Day	140
B.17	Source Size Effects - Night	141
B.18	Actual Devices - RCA, TI	142
B.19	Actual Devices - 8683A	142
B.20	Actual Devices - 7774A	143
B.21	RCA: 8683A and 7774A (SID 501D)	143
B.22	Westinghouse: 8683A and 7774A (5040)	144
B.23	Hughes: 8683A and 7774A (H4068)	144

TABLES

2.1	Statement of Work Specification	5
2.2	Definition of Terms	7
3.1	Parametric Analysis Summary	14
3.2	Summary of Sensor Configurations	18
4.1	RCA SID 501D Performance	43
4.2	TI 800 x 800 Performance	45
4.3	Array Size and Data Rate Trades	48
5.1	Summary - Characteristics of Available Imaging CCD's	77

APPENDIX

A.1	Observation Parameters from Geosynchronous Orbit	89
A.2	SNR vs. FAR	105
A.3	Filter/Optics Figure of Merit	108
A.4	Parametric Analysis Selection Summary	123
B.1	Parametric Trade Results	145

1. OVERVIEW

1.1 STUDY

World wide, continuous measurement of lightning location, intensity (or energy) and time during both day and night is to be provided by the Lightning Mapper (LITMAP) instrument. This study was primarily a technology assessment to determine if the LITMAP requirements can be met using existing sensor and electronic technologies. The baseline concept discussed in this final report is a compromise among a number of opposing requirements (e.g., ground resolution versus array size; large field of view versus narrow bandpass filter). The concept does provide coverage for more than 80% of the lightning events as based on recent above cloud NASA/U2 and satellite lightning measurements.

1.2 DRIVERS

The elements making up the Lightning Mapper (LITMAP) sensor system are illustrated in Figure 1.1. Those elements enclosed

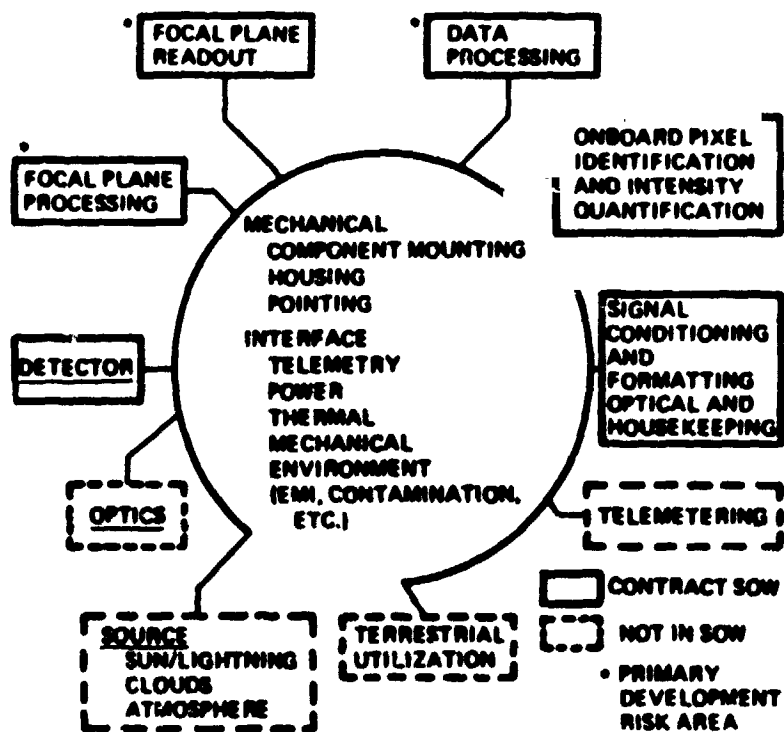


FIGURE 1.1 LIGHTNING MAPPER TECHNICAL ELEMENTS

within solid lines fall within the bounds of the study statement of work (SOW). The primary development risk areas are indicated with an asterisk and include focal plane preprocessing, focal plane readout and residual data processing. The remaining elements enclosed in the dashed lines, (source characteristics, optics, telemetry and utilization) did not have to be defined in detail as an official part of this study.

The prime scientific drivers are rapid frame time coupled with high spatial resolution and operation in a night and high background day environment while maintaining a low energy detection threshold. These scientific requirements translate into the engineering requirements of very high data rate and pixel by pixel background subtraction. Additional technology drivers identified during the system trades were: focal plane array type and size, narrowband filter and a wide field of view.

1.3 CONCEPT SELECTION

As with any application, there are multiple approaches that can be taken which must then be evaluated against schedule, cost and risk factors. A minimum cost, low risk approach for LITMAP was selected as the baseline design from which parametric systems trades were made. An approach using a single mosaic array could be implemented but it would have up to several tens of kilometers undetected strips where the mosaic elements are butted together. Operationally, slight field of view directional adjustments could provide the desired full coverage. An alternate approach for a single optical train is to use fiberoptic field splitting. Both of these approaches face a large field of view (FOV) versus narrow band filter technology problem. This technology problem can be solved by either reducing systems performance requirements (25A bandwidth rather than 5A) or higher development risk (birefringent instead of interference filter). Thus, there is latitude to implement alternate variations of the baseline concept as driven by final user considerations, trades and desires.

1.4 BASELINE DEFINITION

The low risk baseline sensor concept discussed in the following sections is built around existing imaging CCD arrays which require minimal design and development. Since the optics aperture is only around ten centimeters, separate telescopes are used to minimize the FOV of each array thus permitting the use of state-of-the-art narrow band interference filters. The focal plane must be partitioned to handle the data rate, but RCA has suggested to TRW an approach which leaves the focal plane sensors intact and only modifies the output mux, hence minimizing development cost and risk.

1.5 FINAL REPORT CONTENT

Section 2 summarizes three sets of data: a. LITMAP design goals as extracted from the statement of work (SOW); b. baseline design parameters and; c. an optimistic parameter set which should be attainable with only a slight increase in risk. The optimistic parameters set could be pushed even further if a development effort is implemented to combine the best attributes of the various technologies and manufacturer's techniques. Details defining these parameters are provided in Appendix A.

Section 3 highlights the system parametric trade conclusions. The supportive details for this section are provided in Appendix A.

Section 4 provides the concept selection and baseline concept description. The objective was to provide sufficient concept definition to permit design trades, technology assessments and flight development costing.

The technology assessment is given in Section 5.0 where device availability, cost, schedule and complexity are evaluated. Primary emphasis was placed on the focal plane array with parallel evaluations for the optics, narrow band filter and advanced processing techniques being performed under separate IR&D activities

The flight hardware development and manufacturing cost are covered in a separate volume.



2. SYSTEMS PARAMETERS

2.1. REQUIREMENTS

Exhibit A entitled "scope of work" (SOW) for the lightning mapper (LITMAP) sensor design study provided specification goals and lightning characteristics as a general guide for the technology assesement of large array sensors and background handling techniques. The primary LITMAP program objective is to provide measurements of the energy or power of individual lightning strokes along with their time and location of occurence. These measurements are to cover the full disc with a 90% probability of detection and a false alarm rate of less than 10%. A summary of these goals and characteristics is provided in Table 2.1.

From preliminary analysis, the primary system drivers are in three areas: very high data rate resulting from full time, high resolution coverage coupled with a few milliseconds of framing time; background clutter during daytime operation due to solar

TABLE 2.1 Statement of Work Specification

AREA	ITEM	VALUE	UNIT	CATEGORY	COMMENTS
Source Size	Source Size-Diameter	5	km	Characteristic	Typical Cell Size
	Resolution	5	km	Goal	Fully Illuminated Cell
	Field of View			Goal	Full Disc & Conus
Source Power	Dynamic Range	10^7-10^{12}	Watts	Goal	Total Optical Power
	Power Distribution	10^7	Watts	Characteristic	90% Greater Than
	Threshold	10^7	Watts	Goal	50% Prob. Detection
Statistics	Detection Efficiency	90	Percent	Goal	of <u>All</u> Events
	False Alarm Rate	<10	Percent	Goal	of Total Events
	Pulse Duration	<1	Milsec	Characteristic	
Other	Wavelength	8683 7774	Angstroms Angstroms	Characteristic Characteristic	NI (1) OI (1)
	Data Dissemination	<5	Minutes	Goal	Near Real Time
	Risk-Cost/Schedule	.		Goal	Keep as low as Possible
Output	LITMAP	Location Intensity Time		Goal	Map of L, I, T.

scattering from clouds; and the dynamic range of events. These factors are interrelated and must be weighed carefully when



optimizing the system. The overall objective of the system trades and concept definition is to show that daytime lightning detection can be accomplished.

2.2 DESIGN PARAMETERS

The primary focal point for a systems analysis of an optical/detector system performance capability is the signal to noise ratio (SNR). This SNR relationship relates the various parameters of the detection system through which system optimization can be pursued via parametric analysis and performance trades. The SNR is defined as follows.

The number of optical signal generated carriers, N_s , in one sensor element (pixel) is given by:

$$N_s = \frac{\pi \delta_s^2}{4 (f/\lambda)^2} K Q \eta \frac{E_s}{E_{PHOT}} \nu \xi$$

The terms are defined in Table 2.2. Two factors have been added to accommodate the statistical lightning event splitting: spatial (ν) and temporal (ξ). These factors will be discussed later.

The noise generated carriers come from several sources including those due to the signal (N_s) and the background (N_b), (e.g. solar illuminated clouds). The detector also provides several contributions including amplifier ($N_{amp,rms}$), and dark noise ($N_{dn,rms}$). These sources are assumed to be uncorrelated, hence will add in quadrature to give the total rms noise N_n of:

$$\begin{aligned} N_n &= \sqrt{N_s + N_B + N_{AMP}^2 + N_{dn}^2} = \sqrt{N_B} \sqrt{1 + (N_s + N_{AMP}^2 + N_{dn}^2)/N_B} \\ &= \sqrt{N_B} \sqrt{1 + \epsilon} \end{aligned}$$

where the latter form is useful during parametric analysis

whenever $\ll 1$. The number of carriers created by the solar background irradiance is given by:

$$N_B = \frac{\pi \delta_p^2}{4 (f/No)^2} K Q I_B T_i \frac{\Delta\lambda}{E_{PHOT}} Alb$$

TABLE 2.2 Definition of Terms

SYMBOL	BASILINE	OPTIMISTIC (CHANGES)	UNITS	DESCRIPTOR
Alb	0.7		--	Albedo (scene reflectance)
A_s	121×10^6		m^2	Lightning Source Area
A_b	121×10^6		m^2	Background Area
C	3.00×10^8		m/s	Vacuum Speed of Light
E_s	4×10^{-6}		$J/m^2\text{-sr}$	Source Radiance (goal)
E_{phot}	2.29×10^{-19}		J	Energy per Photon = hc/λ
f/No	1		--	Effective F/#
h	6.63×10^{-34}		Js	Planks Constant
I_B	300		$W/m^2\text{-sr-}\mu m$	Background (solar) Irradiance
K	0.4	0.6		Optical Transmission
Q	0.35	0.5		Detector Quantum Efficiency
T_i	4×10^{-3}		sec	Integration Time
T_L	5.4×10^{-4}		sec	Event Width FWHM
δ_s	3×10^{-5}		m	Source Image Size
δ_p	3×10^{-5}	4×10^{-5}	m	Detector Pixel Size
η	0.15			Lightning Spectral Efficiency at λ
λ	8.683×10^{-7}		m	Center Wavelength
$\Delta\lambda$	5×10^{-4}		μm	Spectral Bandpass
v	0.62		--	Geometric Split Factor
ϵ	$(1 - \eta / 3T_i)$		--	Temporal Split Factor
N_{amp}	150		e's	Readout Noise
R	3.56×10^7		m	Sensor Altitude

The signal to noise ratio is defined as the peak signal to the rms noise and is given as:

$$SNR = \frac{N_s}{N_N} = \frac{N_s}{\sqrt{N_B (1 + \epsilon)}}$$

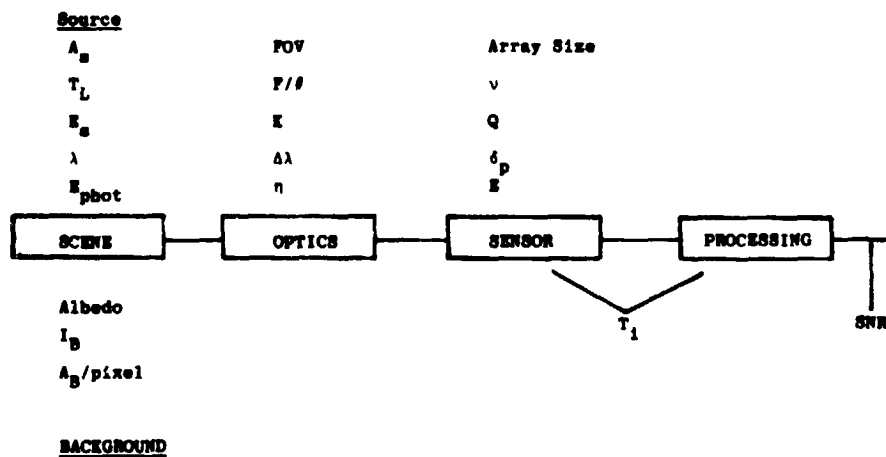
which upon rearranging becomes

$$SNR = \underbrace{\left(\frac{A_s}{A_b} v\right)}_{\textcircled{1} \text{ SOURCE FILL FACTOR}} \underbrace{\sqrt{\frac{\pi K}{\Delta\lambda}} \frac{\eta}{2(f/No)}}_{\textcircled{3} \text{ OPTICS/FILTER}} \underbrace{\sqrt{Q}}_{\textcircled{4} \text{ SENSOR}} \underbrace{\frac{E_s}{\sqrt{E_{PHOT} I_B Alb}}}_{\textcircled{2} \text{ SOURCE/BACKGROUND STRENGTH IN PHOTONS}} \underbrace{\frac{(1 - T_L / 3T_i)}{\sqrt{T_i}}}_{\textcircled{6} \text{ TIME}} \underbrace{\frac{1}{\sqrt{1 + \epsilon}}}_{\textcircled{5} \text{ OTHER NOISE SOURCES}}$$

ORIGINAL PAGE IS
OF POOR QUALITY

The factors in the SNR expression can be grouped in a number of ways, one of which is illustrated above with the segregation being based on the physical origin of each term (c.f. Figure 2.1). Factors 1,2 and part of 6 are source/object related. Item 3 is primarily optics/filter related; and 4 and 5 are dictated by sensor characteristics. Items 6 along with the total pixel count

FIGURE 2.1 PRIMARY SYSTEM ELEMENTS AND ASSOCIATED PARAMETERS



and sensor array partitioning quantifies the post detection electronic processing bandwidth.

Each term in the SNR relationship is discussed and quantified in Appendix A and summarized in Table 2.2. With the practical constraints defined, performance trades can be made with the objective of optimizing the design based on a given set of criteria (c.f. Table 2.1).

Since a desired SNR is a priori known, i.e., it is derivable from the desired average false alarm rate (FAR) and event pulse duration (T_L), the chosen approach was to solve the SNR equation for the equivalent attainable threshold energy. The parametric trades then focused on determining the practical combination of

parameters which will satisfy as many of the requirements in Table 2.1 as possible.

The following section summarizes the results of these parametric trades.

2.3 SUMMARY

Table A.4 summarizes the results of each parameter evaluated in Appendix A. This set of data provided the baseline configuration input to Table 2.2 as well as the "optimistic" data set. Two (often neglected) terms, geometric and time splitting, have been included in this analysis. As shown in Section 3 and Appendices A and B, these factors can influence the threshold performance capability by a factor of two or three, a very significant consideration when the total system is pushing the technology limits as LITMAP is.

~~PREVIOUS PAGE BLANK NOT FILMED~~

3. SYSTEMS ANALYSIS

3.1 DAYTIME OPERATIONS

As stated in Section 2, the SNR is determined by the FAR specification. Thus the approach used for the parametric study was that of determining the attainable spectral threshold energy for each set of parameters. The SNR relationship can be inverted to give the threshold energy, NE_{st} , for a discrete spectral line providing:

$$NE_{st} \equiv SNR \left(\frac{A_B}{A_S} \right) \sqrt{\frac{\Delta\lambda}{\pi K}} 2(f/No) \frac{1}{\sqrt{Q}} \epsilon_p \sqrt{E_{PHOT} I_B A_{lb}} \frac{\sqrt{T_i}}{(1-T_i/3T_i)} \sqrt{1+\epsilon}$$

Section 2 and Appendix A discuss and define the limits for each of the terms in this relationship. The above form of the expression is most useful when the sensor system noise is dominated by solar irradiance for which case $\epsilon \rightarrow 0$. As amplifier noise becomes more prominent, the threshold value is modulated by the ϵ term. A practical worse case condition would be when the non-solar noise sources equal the solar contribution for which $\epsilon=1$ and $\sqrt{1+\epsilon} = 1.41$, i.e., a forty-one percent rise in the lower threshold limit relative to the condition where solar is the only major "noise" contributor.

Two groups of variables appear in the E_s relationship: the linear more influential parameters (SNR, $f/No.$) and the those whose influence is somewhat suppressed via the square root dependency. Background/source area (modified by the geometric splitting factor) and the time (with time splitting) lie somewhere between these two groups.

3.2 NIGHT OPERATION

By definition of SNR

$$\text{Day: } \text{SNR}_d = N_{sd} / \sqrt{N_{AMP}^2 + N_{SOL} + N_s}$$

$$\text{Night: } \text{SNR}_N = N_{sn} / \sqrt{N_{AMP}^2 + N_s}$$

The relative day-to-night signal electrons (for constant SNR) is given by:

$$\begin{aligned} N_{sd}/N_{sn} &= \sqrt{N_{AMP}^2 + N_{SOL} + N_s} / \sqrt{N_{AMP}^2 + N_s} \\ &\equiv \sqrt{N_{SOL}} \sqrt{1 + \epsilon} \end{aligned}$$

But near threshold $N_s \ll N_{amp}^2 + N_{sol}$ in day
and $N_s \ll N_{amp}^2$ at night, hence

$$N_{sd}/N_{sn} \approx \sqrt{N_{AMP}^2 + N_{sol}} / N_{AMP}$$

If $N_{amp} \leq \sqrt{N_{sol}}/3$ then

$$N_{sd}/N_{sn} \approx \sqrt{N_{sol}^{(int)}}/N_{AMP} \quad (\text{rms}) \cdot$$

If $N_{amp}^2 = N_{sol}$ (a probable worse case design condition)

$$N_{SD}/N_{SN} \approx \sqrt{2} = 1.41.$$

As indicated previously, the nighttime threshold would be about 41% lower than the daytime. This small improvement is due to the large magnitude of the amplifier noise contribution.

If $N_{amp}^2 \leq N_{sol}/10$ then

$$N_{SD}/N_{SN} \approx \sqrt{N_{sol}}/N_{amp} = 3$$

that is, the nighttime threshold would be a factor of three lower

than the daytime value. For a value of $N_{s01} = 500K$, the amplifier noise would have to be less than 236 electrons rms. This noise level appears to be attainable. An upper limit of 500 e rms has been projected (Hughes, 5 MHz operation, custom device) and would give a $N_{SD}/N_{SN} = 1.73$, i.e., a 73% improvement for nighttime performance over daytime operation.

If a significant improvement in nighttime operation is desired, the non-solar background contributions to the overall noise must be minimized and an automatic threshold adjustment incorporated into the electronics.

3.3 ADJUSTABLE THRESHOLD

The results of the system analysis of available technology against LITMAP requirements indicate that the solar background will be a severe limitation during the daytime. Reaching the goal of $4 \mu J/m^2\text{-sr}$ at the 90% probability of detection with less than 10% FAR is very demanding. An array designed with large pixel size (hence large aperture) and large full well (FW) (hence longer integration time) will drive the system capability in the right direction.

There is another technique which would help optimize the threshold setting versus data output rate. The average sensor array threshold can be adjusted based on event throughput rate. The throughput rate would be set at a value which would be compatible with system constraints such as the down-link rate, onboard storage capability, etc. As the background energy decreases the throughput event rate will decrease for a fixed threshold setting. The threshold can be lowered until the event rate is back up again (a lower limit may also be desirable). When the storm activity increases, the threshold would be automatically adjusted to avoid overloading the down-link, etc. In this way, maximum sensitivity can be maintained which, under some conditions, may not meet the false alarm (FAR) or probability (P_d) specifications but would provide the maximum amount of data consistent with the systems constraints. The data could be further reduced on the ground using sophisticated

ORIGINAL PAGE IS
OF POOR QUALITY

analysis techniques. For scientific purposes this may prove to be very beneficial in that aspects of the FOV nonuniformities could be further suppressed, hence permitting extracting information which may have been lost if a fixed threshold had been utilized. This type of threshold adjustment is being used on a pixel by pixel basis for the newer satellite surveillance systems. A combination of fixed minimum plus an adjustable threshold level would contribute toward optimization of the LITMAP sensor system.

3.4 PARAMETRIC TRADES

The primary functional dependency of the detector threshold setting on most of the parameters can be deduced from the E_S relationship given in Section 3.1. Once an absolute baseline value is established, effects of other parameters such as $F/No.$, $\Delta\lambda$, and SNR can be determined by direct scaling (linear,

TABLE 3.1 Parametric Analysis Summary

	<u>DAY</u>	<u>NIGHT</u>	<u>COMBINED</u>	<u>CONCLUSION SUMMARY</u>
Baseline			X	
Ideal (Baseline)			X	Event splitting (time/spectral) is important.
Optimistic			X	Increased performance can be attained at some increase in risk and possible cost.
τ_L	X			Pulse duration and time splitting drives the integration time towards several milliseconds.
Fill Factor	X	X		Off nadir viewing will have a threshold degradation of up to a factor of about 3.
Pixel Size	X	X		Large pixel size is necessary ($>20 \mu m$).
N_{AMP}	X	X		Amplifier noise must be kept significantly below the solar contribution if enhanced night performance is (i.e., $N_{AMP} (rms) < N_{sol} (rms)/2$).
λ	X			Relative magnitudes of these spectral lines are needed.
$\Delta\lambda$	X			Narrow bandpass is necessary ($\leq 5\text{\AA}$).
Source Size	X	X		Event source size <u>must</u> be better quantified.
Commercial Devices	X			Existing commercial devices can approach the LITMAP baseline performance. Optimization and partitioning are required.

square root etc.). For parameters such as time and spatial splitting, the effects are not as easily visualized, hence parametric computations, graphically presented, become very useful. Table 3.1 summarizes some of the parametric analyses performed and Appendix B contains further discussions.

3.5 KEY SENSOR PARAMETERS

Although a number of parameters can be varied (e.g., F/No., SNR), the two primary adjustable parameters for the sensor array are pixel size and full well capacity. As indicated in Appendix A, these two parameters are somewhat related in that the larger pixel sizes have larger full well capacities. The relationship between these parameters and the minimum resolvable lightning threshold setting is given by:

$$FW(\min) = B_p^2(\min) = \underbrace{(DR N_s(\min))}_{\text{max signal}} + \underbrace{N_s^2(\min)/SNR^2}_{\text{max noise}}$$

$$\delta p(\min) = B^{-1} (DR N_s(\min) + N_s(\min)^2/SNR^2)$$

$$N_s = SNR^2 Z/2 + SNR \sqrt{SNR^2 Z^2/4 + N_{amp}^2}$$

$$Z = (1 + \Delta\lambda I_B t A l b/n E_s)$$

$$B = 1.1 \cdot 10^{15}(\max), 0.37 \cdot 10^{15}(\min)$$

Figure 3.1 provides ηE_s versus pixel size and full well requirements for several dynamic ranges. The shaded area for a 100:1 dynamic range accounts for the variability of existing devices. This variation is primarily related to device geometry and can be varied by design for a given configuration. The dashed lines illustrate that for a given threshold, larger pixel sizes (and FW capabilities) are required for larger dynamic ranges. Between 30 to 50 micron pixel dimensions with a full well (FW) capacity of 10^6 electrons are required to permit a source of $4 \cdot 10^{-6} \text{J/m}^2\text{-sr}$ to be detected from geosynchronous orbit using the baseline system specifications in Section 2. Smaller

ORIGINAL PAGE IS
OF POOR QUALITY

FW capacities result in high thresholds. This figure illustrates that the NASA/Galileo 15 micron pixel configuration is not compatible with the baseline LITMAP full disc requirements. Existing Westinghouse, Texas Instruments (TI) and RCA devices come closer to the desired specifications but still require partitioning to accommodate the short frame time requirement.

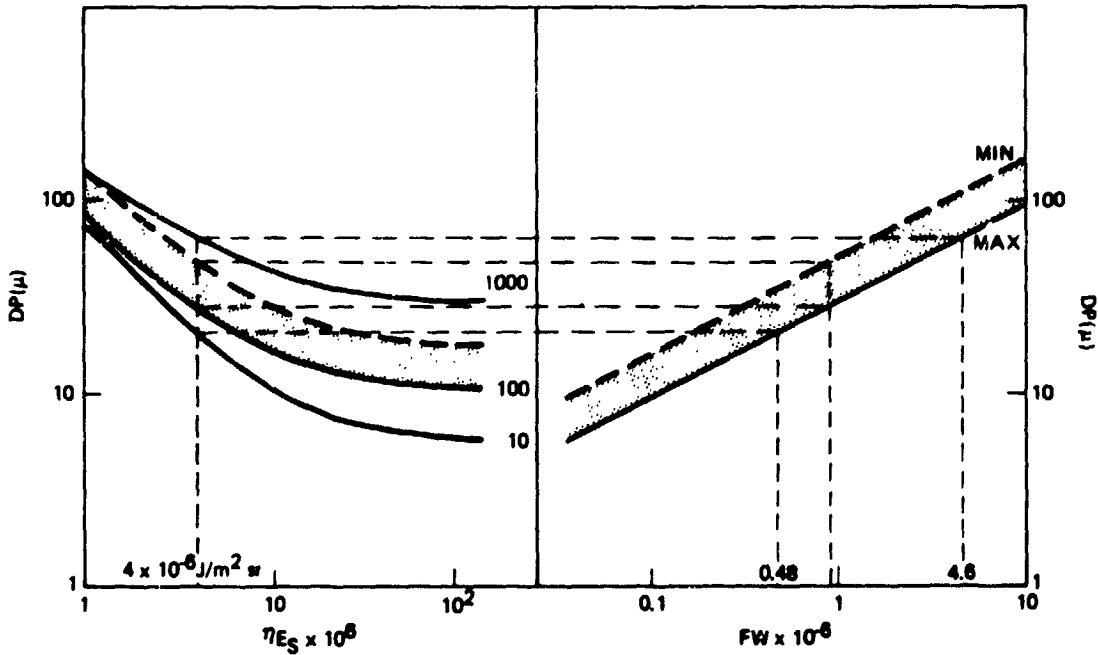


FIGURE 3.1 BASELINE DEVICE PIXEL AND FULL WELL REQUIREMENTS

3.6 SOLUTIONS TO SYSTEM DRIVERS

The parametric trades indicate that the system drivers can be eased by implementing some or all of the following (full disc, geosynchronous orbit assumed):

Background Clutter

- o Narrow band optical filter → less background noise: <5A
- o Large aperture → gain in SNR: Pixel > 20 μ m
- o Larger full well capacity → permits larger aperture: >5 10^5 e's
- o Smaller ground resolution → larger aperture, lower background: < 7 km
- o Background removal → eases dynamic range: frame subtraction

Dynamic Range

- o Larger pixel → larger full well: >>20 μ m

Data Rate

- o Device selection → high clock frequency: >5 MHz
- o Partitioning → lower rate per port: >16 ports
- o Larger integration time → longer frame time: >4 msec
- o Tailored output amplifier → lower readout noise: <300 e/pixel

These factors are discussed in this report

The degree to which the full potential of the imaging CCD technology can be realized depends on a number of factors. The main sensor factors are pixel size coupled with total pixel count. Other subsystem constraints include wide FOV coupled with narrowband filter and large pixel count coupled with short framing time.

As discussed in this report, there are a number of acceptable approaches which can be taken to implement the LITMAP instrument with minor modifications to existing devices. Table 3.2 summarizes some of these configurations. The first entry is the baselined approach discussed in this report from which all parametric trades were made. It provides the full disc coverage with the best performance/cost ratio with the large-FOV/narrow-bandwidth-filter combination being a key driver.

TABLE 3.2 Summary of Sensor Configurations

MULT.	OPTICS		FILTER		SENSOR		FOV		COMMENTS
	SINGLE	INTERFERENCE	BIREFRINGENT	EXISTING	SPECIAL	DISC	PARTIAL		
4,6		4,6		4,6 MODIFIED		X		<ul style="list-style-type: none"> BEST PERFORMANCE/COST RATIO, LARGER OPTICS ENVELOPE LOWEST COST/RISK IN OPTICS/FILTER/SENSOR LIMITED ARRAY SIZES AVAILABLE PARTITION TO ATTAIN FRAME TIME 	
4,6		4,6		4,6 MODIFIED			X	<ul style="list-style-type: none"> IMPROVE PERFORMANCE WITH SMALLER FOV/ELEMENT COVERAGE OF MOST OF DISC OR CONUS WITH IMPROVED RESOLUTION PARTITION TO ATTAIN FRAME TIME 	
	X	1		1 2X(100x100)			X	<ul style="list-style-type: none"> SINGLE UNIT COMPATIBLE WITH A SHUTTLE MISSION 	
4		4			4	X		<ul style="list-style-type: none"> HIGHER DEVELOPMENT COST, MODERATE RISK FOR SENSOR (X2 TO X3) 	
	X		1		4 2X(400x400)	X		<ul style="list-style-type: none"> AT LIMIT OF TECHNOLOGY SOLC AND 4 LARGE ARRAYS ARE HIGHER DEVELOPMENT AND RECURRING COST AND RISK (SENSOR & FILTER X2 TO X3) 	
	X	1	(1)		MOSAIC	X		<ul style="list-style-type: none"> LOWER PERFORMANCE WITH INTERF. FILTER } 1-2 PIXEL LOST BETWEEN MOSAIC ELEMENTS HIGHER COST WITH SOLC FILTER 	
	SPLIT FOCAL PLANE	X			4	X		<ul style="list-style-type: none"> VERY COMPLEX OPTICALLY POSSIBLE USE OF FIBER OPTICS 	
	X	X			2X(800x600) DUAL	X		<ul style="list-style-type: none"> NOT PRACTICAL DUE TO LARGE PIXEL AND LARGE ARRAY COMBINATION LOWER FILTER PERFORMANCE DUE TO LARGE FOV 	
	X	X		2X(800x600) DUAL MODIFIED		X		<ul style="list-style-type: none"> PARTITION TO ATTAIN FRAME TIME WILL NOT PROVIDE PERFORMANCE FOR FULL DISC DUE TO SMALL PIXEL DIMENSIONS AND LARGE FOV POSSIBLE USE FOR CONUS COVERAGE 	
4,6		4,6		4,6		X		<ul style="list-style-type: none"> FOCAL PLANE TIME SAMPLING (C.F. SECTION 4.3.3.C) LOW SENSOR COST (0.1) WITH GOOD PERFORMANCE 	
	X	X		X		X		<ul style="list-style-type: none"> MECHANICAL STEP/STARE (C.F. SECTION 4.3.3.d) LOWEST SENSOR COST (X0.01) EXCELLENT RESOLUTION POTENTIAL 	

BEST COST/PERFORMANCE WITH EXISTING TECH.

WITHIN TECHNOLOGY

NOT PRACTICAL

ALTERNATIVES

Custom imaging CCD arrays with single optical trains are covered in the second group of configurations. Although this group is within the present technology, the costs and risks are higher due to the requirement for larger CCD arrays which are not now in production and also due to the requirement for a SOLC birefringent filter to handle the large FOV and narrow bandwidth requirements. The sensor and filter can cost a factor of 2 to 3 above the corresponding baseline items. This cost/risk penalty may be deemed warranted by the ultimate users.

The third group contains two approaches which are not deemed suitable or practical for the full disc LITMAP application. The last group does not provide continuous full coverage but can provide near continuous coverage of specific storm areas using unmodified existing devices with a considerable decrease in electronics.

Section B.11 evaluates a few existing commercial imaging CCD devices which contain the necessary on focal plane frame storage. The results for a 4 millisecond integration time are:

<u>Device</u>	<u>uJ/m²-sr</u>	<u>Device</u>	<u>uJ/m²-sr</u>
RCA	9 (x2)	RCA	11 (x3)
TI 201	12 (x3)	Westinghouse	12 (x3)
Westinghouse	14 (x3+)	TI 201	17 (x4)
		TI 202 } Hughes }	20 (x5)

The (x2) refers to a threshold which is about a factor of two above the NASA measured 4 uJ/m²-sr. A (x2) to (x3) would be tolerable if the signal dynamic range is 100:1 or greater.

The large pixel, RCA device gave the best daytime sensitivity. Array partitioning and tailoring of the output amplifier for high speed operation are needed. The TI devices operate at TV rates (> 5 MHz) but array partitioning is still required to get the desired framing time. The Westinghouse unit is small (100 x 100 x 2) and would require a mosaic of 64 to 100

units to handle full disc coverage from geosynchronous orbit. This unit would be suitable for a Shuttle or U2 operation.

The RCA or TI sensor devices would provide the minimum risk and cost (< 1M) for implementing the LITMAP instrument using multiple optics.

Special larger imaging array devices can be produced which match the LITMAP requirements more closely with an increase in development risk and cost (> 2M + risk). For a single optical train, the large FOV may require a birefringent narrowband filter which may approach a million dollar development cost.

TI has had experience in producing the larger imaging CCD arrays followed by RCA. Both of these companies are preparing arrays for the commercial TV market. Hughes, Fairchild and Westinghouse also produce imaging CCDs. Hughes has provided a preliminary estimate to TRW for the development of sensor arrays which are compatible with the baseline configuration discussed in this report (c.f. fourth entry in Table 3.2).

3.7 SUMMARY

The primary conclusion based on a) 90% of the above cloud data is above $4 \mu \text{J}/\text{m}^2\text{-sr}$ and b) the intensity dynamic range between 10%-90% is at least 100:1 is that significant lightning data can be collected from geosynchronous orbit. Existing commercial devices can approach the LITMAP performance requirements of sensitivity (pixel size/aperture) and dynamic range (full well capacity). The integration and cycle time can only be attained within the present technology via securing partitioned sensor arrays with the total elements per port on the order of 10,000 to 40,000 pixels. This partitioning is quite doable but requires custom devices.

4. CONCEPT DESCRIPTION

4.1 GENERAL

This section deals with baseline hardware selection and concept definition. Trade discussions are briefly repeated to support the selection of a given hardware implementation approach. The details leading to the selection of the baseline set and the parametric trade results are summarized in Sections 2 and 3 with the bulk of the data given in Appendices A and B respectively.

The previous discussion of lightning characteristics, scientific requirements and signal/noise considerations have illustrated the challenge surrounding the design of an instrument to map lightning from synchronous orbit over the full disk of the Earth. The following sections discuss a proposed concept which satisfies the lightning mapper objectives.

The four major considerations are:

- o The optics, including the telescope, bandpass filter, any possible image splitting, and the detector at the focal plane. In the following section on optics, the issue of interference versus birefringent filters is discussed and three schemes for partitioning the image among multiple detectors will be weighed.
- o The detector. This section is primarily devoted to possible CCD formats with alternatives discussed briefly. The emphasis will be on creating a device which satisfies the requirements with minimal modification to existing designs. An argument is made for using multiple sensors to cover the full earth disk.
- o Signal processing includes that part of the instrument which takes the raw signal from the detector, decides when a lightning event has occurred and returns a digital signal proportional to lightning intensity. The discussion will cover the background suppression technique, choice of analog or digital background memory, and a method of adaptively setting the lightning detection threshold to allow improved nighttime performance.
- o Data formatting. For every lightning event, a data word is created into which is packed the lightning intensity, location, and time of occurrence. These data are saved in a small local memory for telemetry at a low data rate.

4.2 OPTICAL CONCEPT

The LITMAP performance criteria impose significant design requirements on the optical subsystem. Thus the optimization of the total sensor system requires an interactive trade between the optical and sensor constraints. The optical design effort was not a part of this NASA study but was evaluated under a separate IR&D activity. The following provides an overview of this effort.

4.2.1 Requirements

The desired field-of-view is a square 17.4 degrees on a side covering the entire earth disk. For a subsatellite ground resolution of about 13.6 km, an instantaneous angular FOV of 3.8×10^{-4} rad is required. This roughly corresponds to 800 x 800 elements.

Use of existing arrays limit the size of the focal plane to 2.4 cm with a pixel size of 30 μ m. The effective focal length of the system must then be 7.8 cm. Concurrently, the radiometric calculations for the system indicate that an entrance pupil of 15.2 cm is necessary. The resultant system has an F/No of 0.5. Although computer simulations indicate that such a design is possible for monochromatic light, in practice it would be prohibitively expensive. Section 2 defines some of the optics parameters which provide a workable compromise between scientific requirements and technology constraints. The filter transmission bandwidth of the system must be less than 5A to obtain sufficient background suppression.

The table below summarizes the above ideal requirements and also the baseline specifications presented in Section 2. The following sections provide a description of some of the alternatives considered for the filter and optics.

<u>Parameter</u>	<u>Ideal</u>	<u>Baseline</u>
Aperture	15.2 cm	9.7 cm
Effective Focal Length	7.8 cm	9.7 cm
Total FOV	0.303 rad (17.4 deg)	0.256 (14.9 deg)
Instantaneous FOV	3.78×10^{-4} rad	3.21×10^{-4} rad
Spectral Bandwidth	< 5 A	5 A
Spectral Line Center	8682	8683

4.2.2 Telescope Concepts

A catadioptric front end telescope (c.f. Figure 4.1) is typically used for this type of application. Clear apertures up to 15 cm were evaluated via computer. The image from the telescope of Figure 4.1 was minified 1:4 using a lens cluster. All goals can be met except for the spectral bandwidth. The best that an interference filter could do in such systems is 30A bandpass which is a result of the large FOV requirements. The filter constraints are discussed later.

An all refractive approach to a wide field telescope was also designed (c.f. Figure 4.2) for which 80% of the energy falls within a blur diameter corresponding to approximately one half of a resolution element. This approach also provides most of the desired features except for the filters. Again the F/No of the internal telescope combined with the FOV limits the bandpass of interference filters to more than 20A.

To accommodate the filter bandwidth constraint, various schemes for splitting the FOV after the primary images were tried and are discussed later. In all the splitting schemes the relays were mounted on an axis of symmetry for the partial FOV resulting in angular shifts of the filter bandpass on the order of 5 A.

ORIGINAL PAGE IS
OF POOR QUALITY

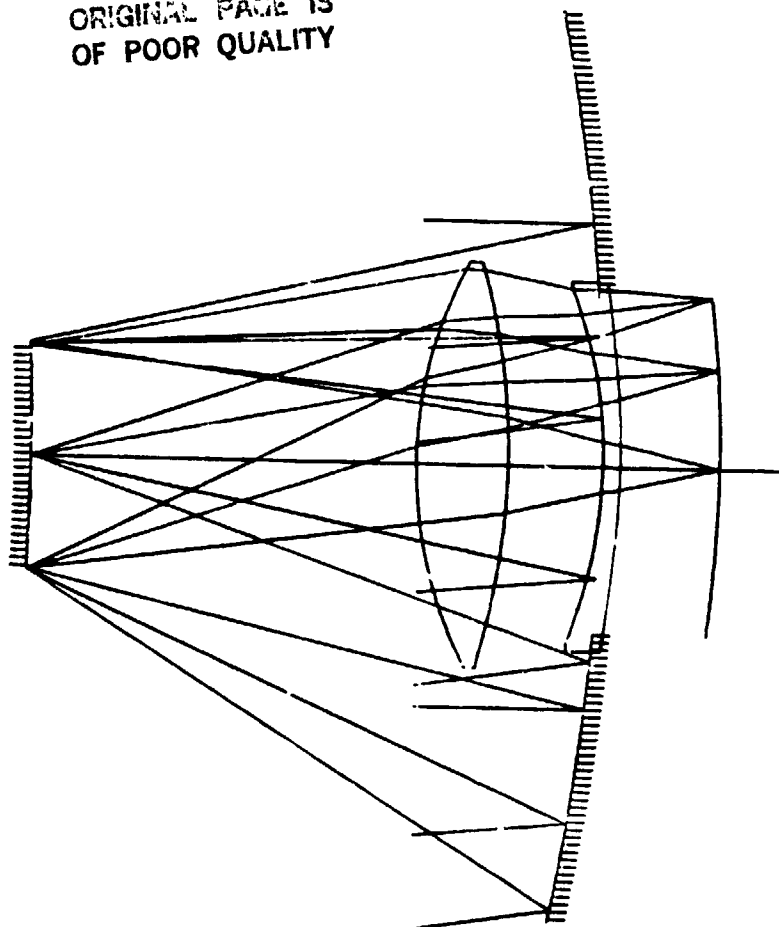


FIGURE 4.1 CASSEGRAIN



F/3 OBJECTIVE + 1/4.5 TRANSFER LENS

FIGURE 4.2 REFRACTIVE

The simplest approach to the FOV/bandwidth problem is to design a refracting telescope with 1.28 rad (7.4 deg) total FOV. Then a cluster of four of these 10 cm diameter telescopes would cover the entire FOV (c.f. Figure 4.3). Several advantages are apparent. First, existing 400 x 400 CCD arrays can be easily used at the four independent focal planes. Second, filters may

be placed over the apertures or at intermediate surfaces in the primary lens cluster and have maximum wavelength shifts of only 5 Å for a required bandpass of about 3 Å if the center wavelength and filter shape are placed properly. The design of the filter will be discussed in the section on filters. This latter approach (4-cluster) was selected as the baseline concept.

4.2.3 Optical Partitioning

The lightning mapper is a system in which the optical field splitting clearly improves performance and the feasibility of fabrication.

The three approaches selected for inclusion in the study were:

1. Four telescopes,
2. Knife edge image slicing, and
3. Fiber optics.

Each was shown to be completely feasible but possessed differing degrees of complexity and risk.

- o The four telescope approach was chosen as the baseline design as mentioned previously. The choice was based on minimizing the risk associated with system development.

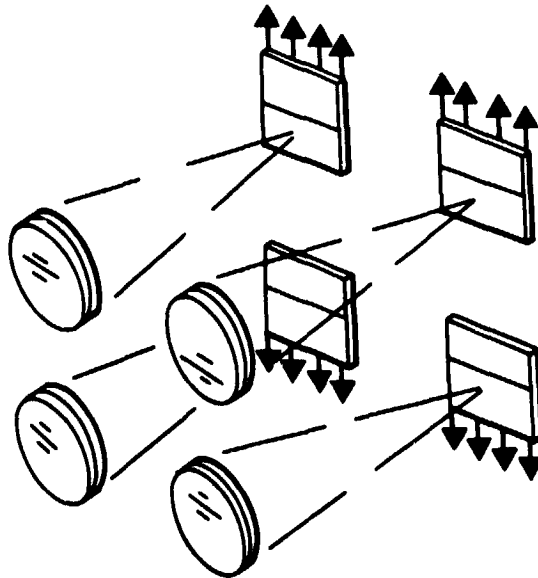


FIGURE 4.3 FOUR CCD'S WITH INDIVIDUAL OPTICS AND SPECTRAL FILTERS.

The alternate approaches are as follows.

- o Galileo Electrooptics indicated that a quadrifurcated image plane 10 x 10 cm could be fabricated with 20 micron spatial resolution. The primary image plane Figure 4.4 would be divided into four implemented focal planes each 4.8 cm on a side. Depending on signal processing needs each focal plane could be imaged onto an 800 x 800 array.

A further division into 16 separate channels would allow use of 16 600 x 400 arrays to fill the fiber optics area. This would achieve twice the ground resolution compared to the quad-telescope and hence enhance the threshold capability of the system. The alternative to using more detector arrays is to reimage the output from the fibers onto the 400 x 400 arrays with a 1:4 minification (Figure 4.5) as in the basic telescope. Only a single collector is required with either 4 filters or a single wide FOV filter.

- o The image slicer is a knife edge mirror in the focal plane of the primary optics (c.f. Figure 4.6). Since this only divides the images into two parts additional 1:1 relay lenses and knife edges are required for the final division into 4 fields (Figure 4.7). Each field must be minified and imaged as before and utilizing either 4 filters or a single wide FOV filter.

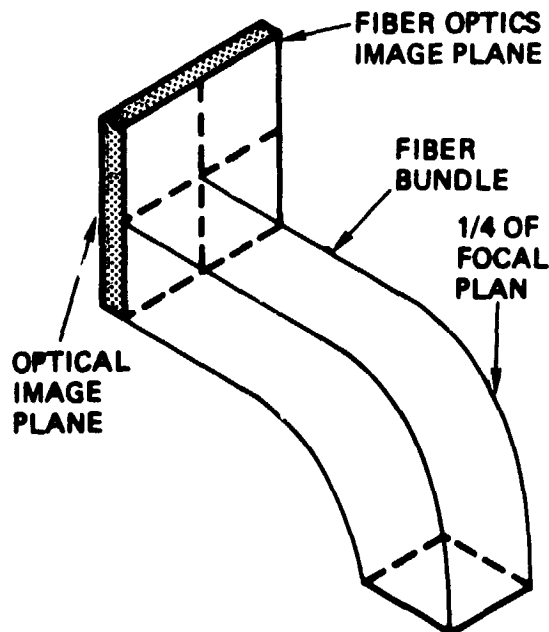


FIGURE 4.4 QUADRI-FURCATED FIBER OPTICS

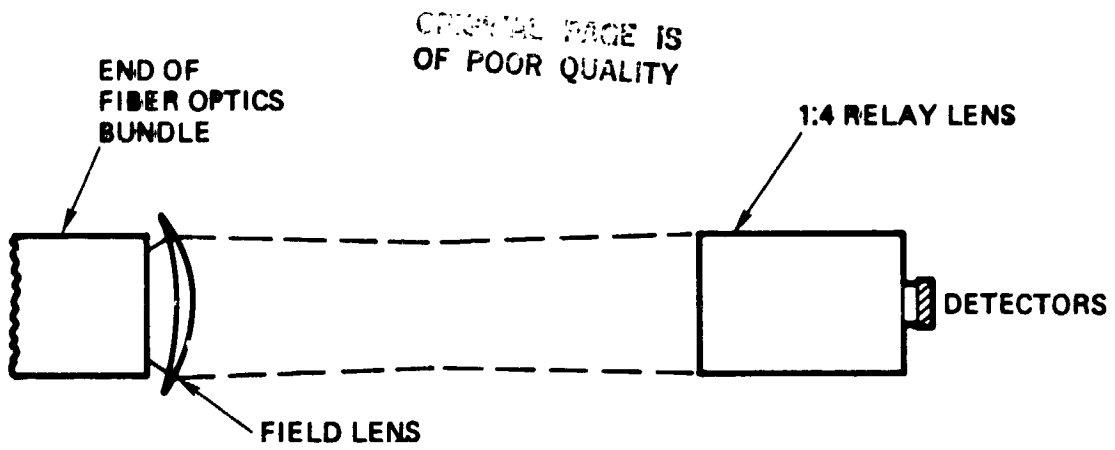


FIGURE 4.5 MINIFICATION OF FIBER OPTICS IMAGE

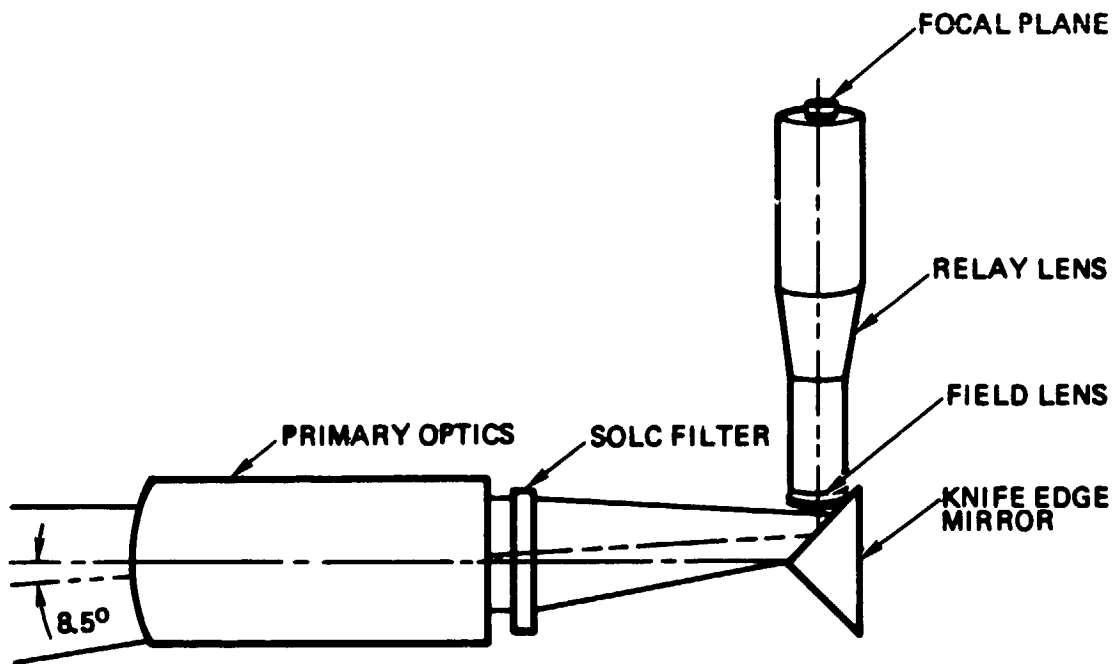


FIGURE 4.6 IMAGE SLICER, TWO WAY

ORIGINAL PAGE IS
OF POOR QUALITY

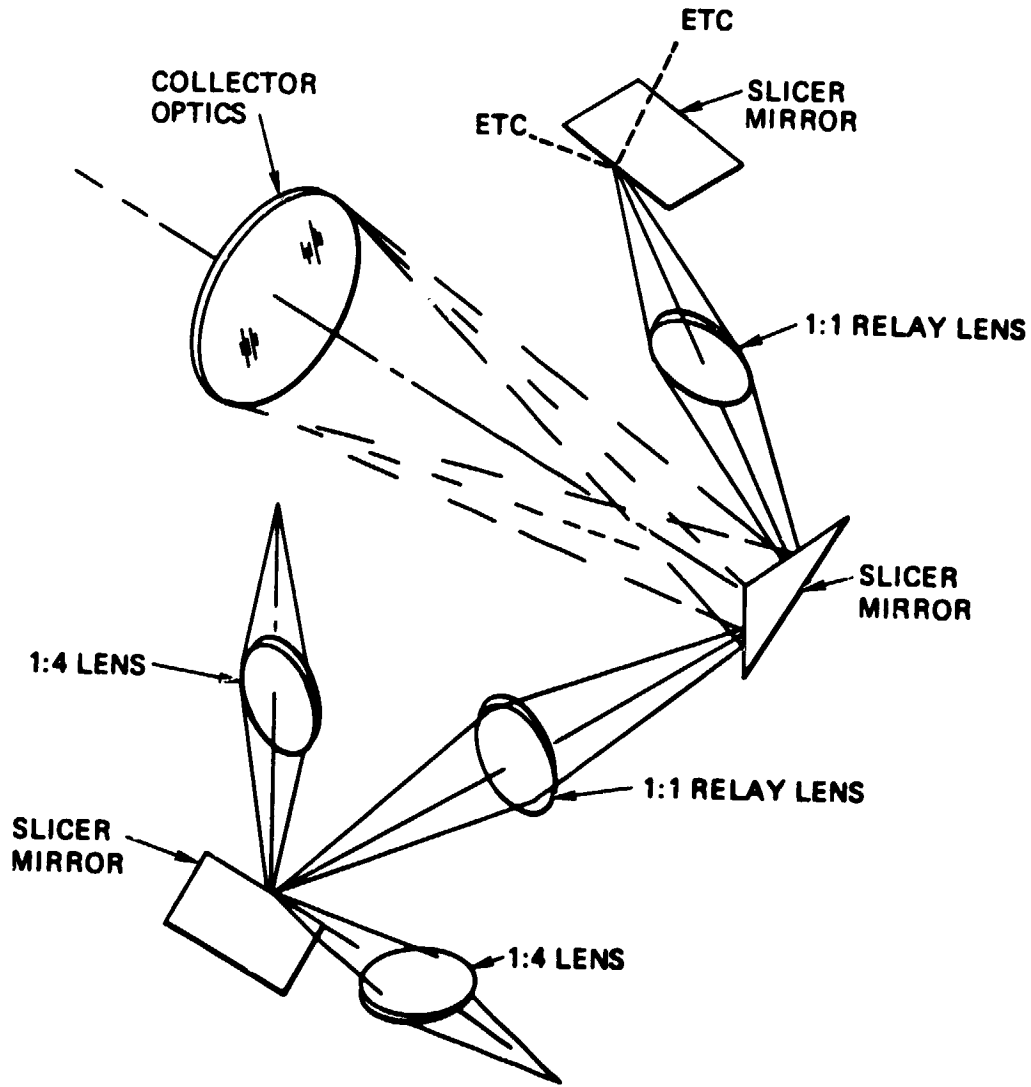


FIGURE 4.7 FOUR-WAY IMAGE SLICER CONCEPT

4.2.4 Filter

The threshold performance of the LIPMAP, when the scene is sunlit, pivots on background radiation rejection. Consequently, the spectral bandpass of the system must match the line shape of the Nitrogen line at 8683 A as closely as possible.

Unfortunately, with interference filters and birefringent filters an increase in the cone angle and/or field-of-view for a system increases the effective bandpass of the filter. The ideal situation would be to have all the light incident on the filter at a single angle. The limitations of the two filter types were investigated both theoretically and with potential manufacturers.

Multi-cavity Interference Filters The two cavity interference filters provide both a narrow spectral bandwidth with reasonably steep slopes and good out of band blocking. By shifting the filter toward the short wavelength side of the line (i.e., $< 8683 \text{ A}$) the filter bandwidth may be minimized. The filter will be designed for the specifics of the optical design. Figure 4.8 shows the wavelength shift as a function of angle and the approximately minimum filter bandpass attainable for the 4-cluster configuration.

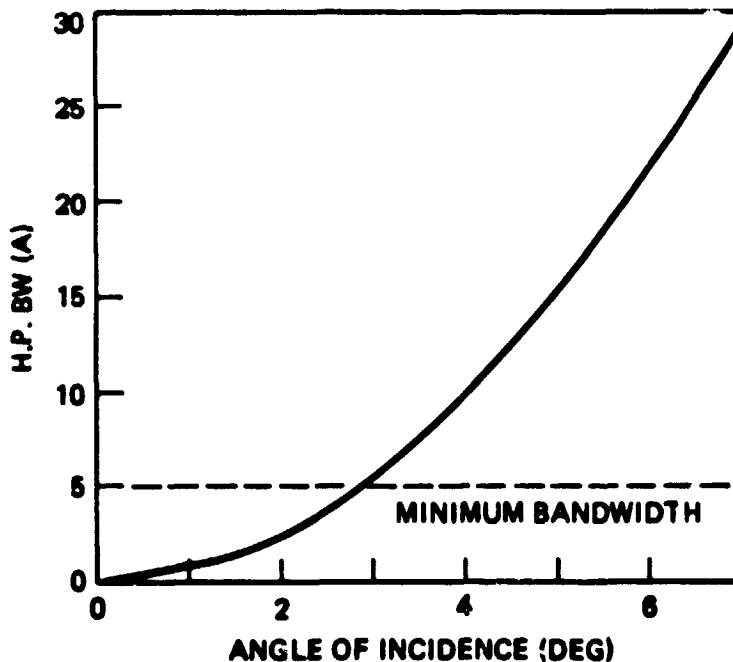


FIGURE 4.8 FILTER HALF POWER BANDWIDTH VERSUS MAXIMUM ANGLE OF INCIDENCE

ORIGINAL PAGE IS
OF POOR QUALITY

It is evident that mean angles of incidence greater than 4 deg will not allow the system bandpass requirements of 5 Å to be met. The peak transmission of the 5 Å filter may be as much as 40%. The interference filter was chosen for the baseline configuration.

Birefringent Filters The classic filters in this category are the Lyot-Ohman or Solc filters. A Solc filter was chosen for analysis since it is much more compact for the same FOV and bandwidth.

The Solc filter can easily achieve a bandpass from 1.5 to 3 Å over incidence angles of ± 10 deg. Consequently a single filter may be used even in a wide FOV collector optics train to suppress background radiation. The estimated peak transmission of a 5 Å filter for LITMAP is 25%. Figure 4.9 illustrates the design of a Solc filter. The use of Solc filters in a narrow FOV telescope is simplified since the filters are smaller and the angles of incidence are less. Under these conditions it would be relatively easy to achieve 1.5 Å bandpass.

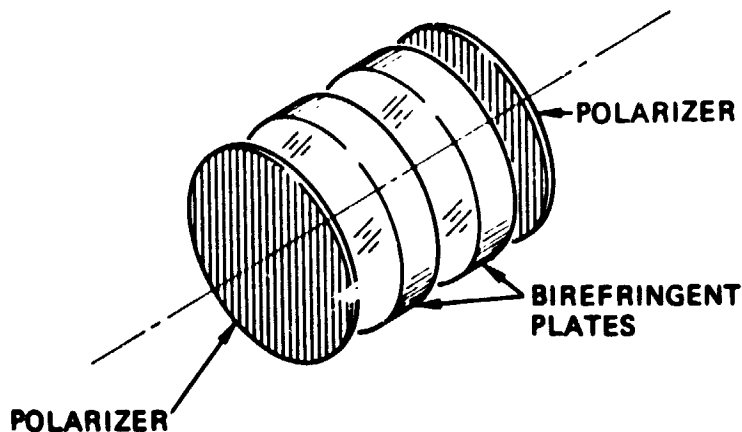


FIGURE 4.9 SOLC FILTER

4.2.5 Transmission

The optics will be antireflection coated with "V" coatings on each surface. These coatings will assure an inband transmission of 0.99 per surface. For the baseline design the overall transmission would be $(0.99)^{22} \approx 0.8$. When coupled with an interference filter transmission of 50%, the system transmission will be $\approx 40\%$. In the case of the Solc filter the transmission will be approximately 22%.

4.2.6 Baseline Performance Summary

The system performance of the baseline optics design is:

Clear Aperture	9.7 cm
Effective Focal Length	9.7 cm
Pixel Size	320 urad
Resolution	≤ 140 urad
Fields-of-View (4)	7.4 deg x 7.4 deg
Filter Bandwidth	≤ 5 A
Transmission	$\approx 40\%$
Filter	Interference
Configuration	Four cluster

4.3 DETECTOR

Detector selection is a key element of the LITMAP design process. It is here that the twin sets of constraints from the optical side and the electronic side converge, and it is from here that the logic of the design must flow, upstream towards the telescope and the physical appearance of the instrument and downstream to the signal processing and data formatting. There are some fairly general arguments that lead to the choice of a CCD as a detector, and some specific arguments that indicate the use of multiple CCD's to cover the full Earth disk. These are discussed in the following sections.

4.3.1 Selection of Detector Type

First, the minimum signal of interest, the worst case solar background, the size of a pixel on Earth and the satellite altitude are given. Selection of the pixel size at the detector fixes the focal length of the telescope. Placing a reasonable limit on the numerical aperture, say $f/1$, fixes the telescope diameter. Physical and manufacturing considerations described in Sections 2, 5, and Appendix A, constrain the optical filter bandwidth and losses. At this point in the logic the number of signal photons available to a detector that corresponds to the minimum lightning event is fixed as is the number of photons per second at a detector pixel due to the maximum solar background. For a detector pixel size of 30 μm , an optical bandwidth of 5A and an overall optics transmission of 0.4 these numbers are 3952 photons of signal and $1.5 \cdot 10^8$ photons/sec of background. It is the high magnitude of the photons per second for solar background that eliminates whole classes of detectors.

For a fixed telescope f /number, changing the detector pixel size changes the telescope size. The number of photons received, both of signal and background, is proportional to the square of the detector pixel size. For the LITMAP application, photon statistics are the limiting factor in attaining a useable signal/noise ratio and that in particular the instrument can be made to work with a pixel size of 30 micrometers and not with a

pixel size of 15 micrometers (c.f. Appendix B). This result will have important consequences later.

Figure 4.10 shows a family tree of detector alternatives. "FP" on this figure stands for focal plane. The first level of classification of sensors divides clocked or integrating detectors from random event or non-integrating detectors. Integrating detectors, e.g. CCD's or vidicons, have a definite frame time: incoming photons free charge carriers which accumulate until the next periodic readout time. Non-integrating or random event detectors read out only when an event occurs. A one-dimensional example of this would be a photomultiplier in a photon counting configuration or (to sense lightning events instead of photon arrivals) any single detector/preamp followed by a high pass filter and pulse discriminator.

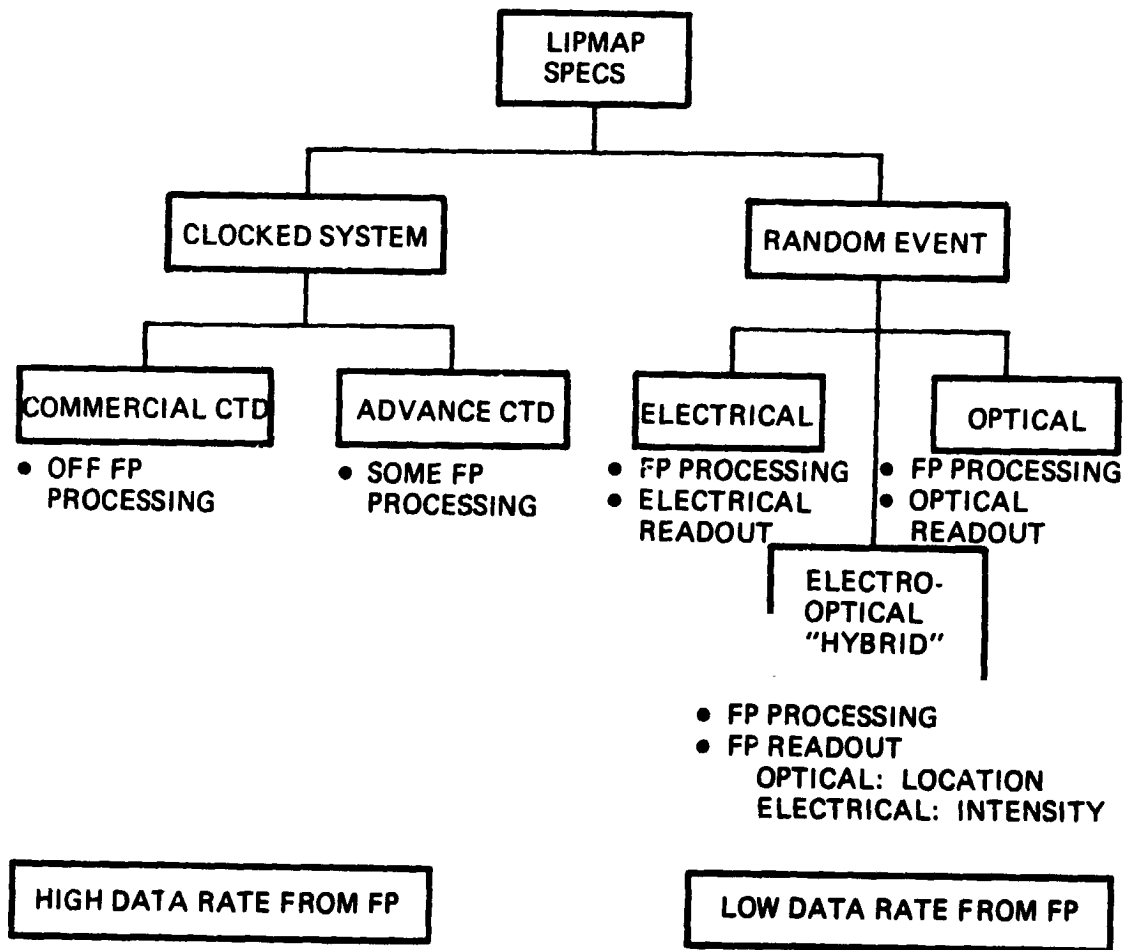


FIGURE 4.10 GENERIC DETECTOR ALTERNATIVES

A true two dimensional lightning event detector with the background/lightning separation performed on the focal plane, is not now available and a significant development effort would be required to provide it. Much effort is currently being expended on the background suppression problem, particularly for infrared arrays, but no devices are planned with the size and frame rate needed for LITMAP. The following detector concepts were evaluated for use with off-focal-plane background suppression.

CTD: Charge transfer devices (CTD's on the chart) and vidicon-like devices are integrating devices. Silicon target vidicons have similar optical and detector properties to CCD's but do not have the capability of multiple parallel readouts to keep the data rate down and are not in general suited to millisecond frame time applications. The only charge transfer device that might be considered for LITMAP besides a CCD is a CID, or charge injection device. A CID, with its ability to randomly access pixels, might be useful in a lightning mapper that only looked at a small, electrically steerable portion of the field of view, but its higher noise makes it inferior to a straight CCD for full time processing of the full Earth disk.

MAMA: A two-dimensional example of a photon counter is the Multi-Anode Microchannel (MAMA) system (Figure 4.11). It consists of a photocathode, a microchannel plate electron multiplier and two orthogonal sets of stripe anodes connected to coincidence logic. The MAMA system is an extremely effective 2D photon counter, but it counts photons, not lightning events and the maximum counting rate per pixel of less than 650 per second is many orders of magnitude short of the 220 million per second background rate.

ORIGINAL PAGE IS
OF POOR QUALITY

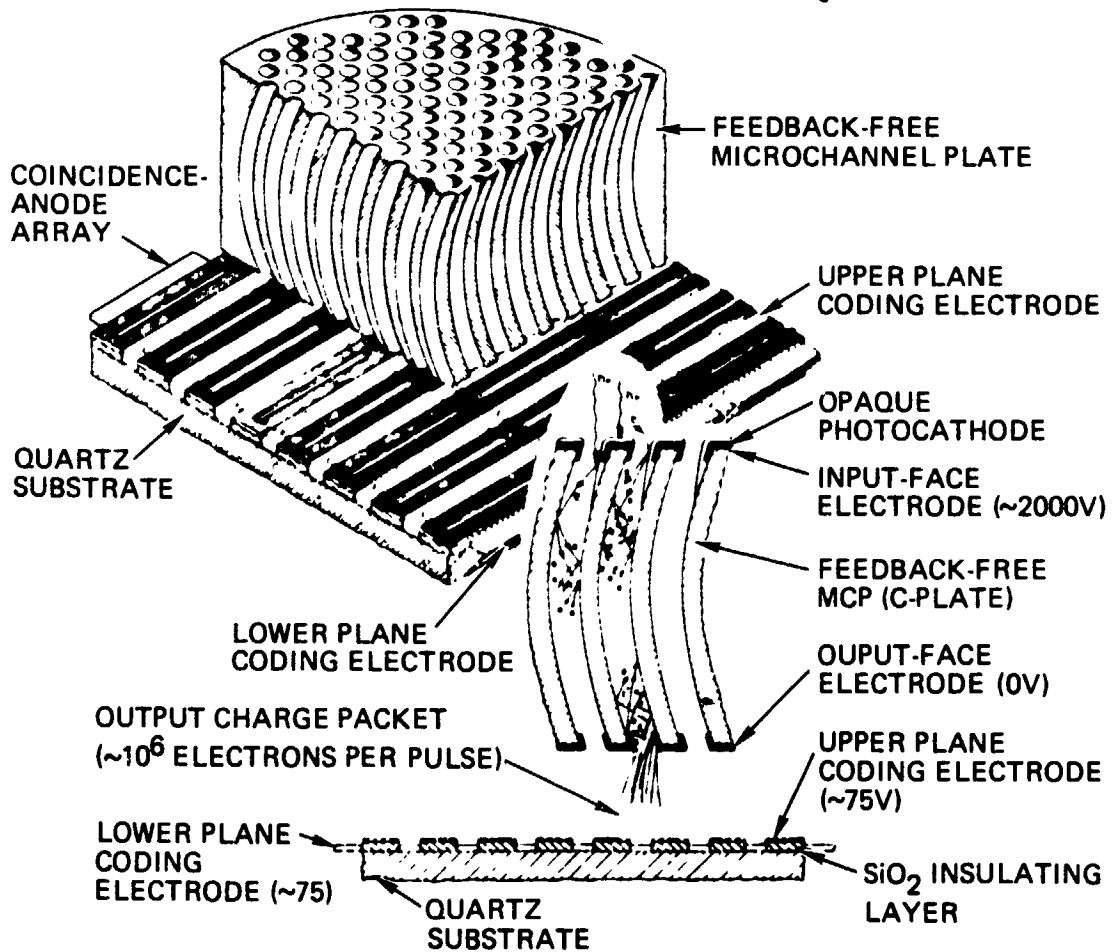


FIGURE 4.11 MULTI-ANODE MICROCHANNEL ARRAY

Anamorphic: The anamorphic concept has an appealing simplicity (Figure 4.12) and consists of two or possibly three linear arrays each with a cylindrical lens. A vertical or horizontal stripe from the field of view is focussed onto a single detector element. Each detector element has a preamp, high pass filter (to perform the background suppression) and threshold circuit. The (digital) signals from the two axes are correlated to sense the location of a lightning strike. Because each detector element sees a whole stripe's worth of solar background but only a pixel's worth of lightning, the

ORIGINAL PAGE IS
OF POOR QUALITY

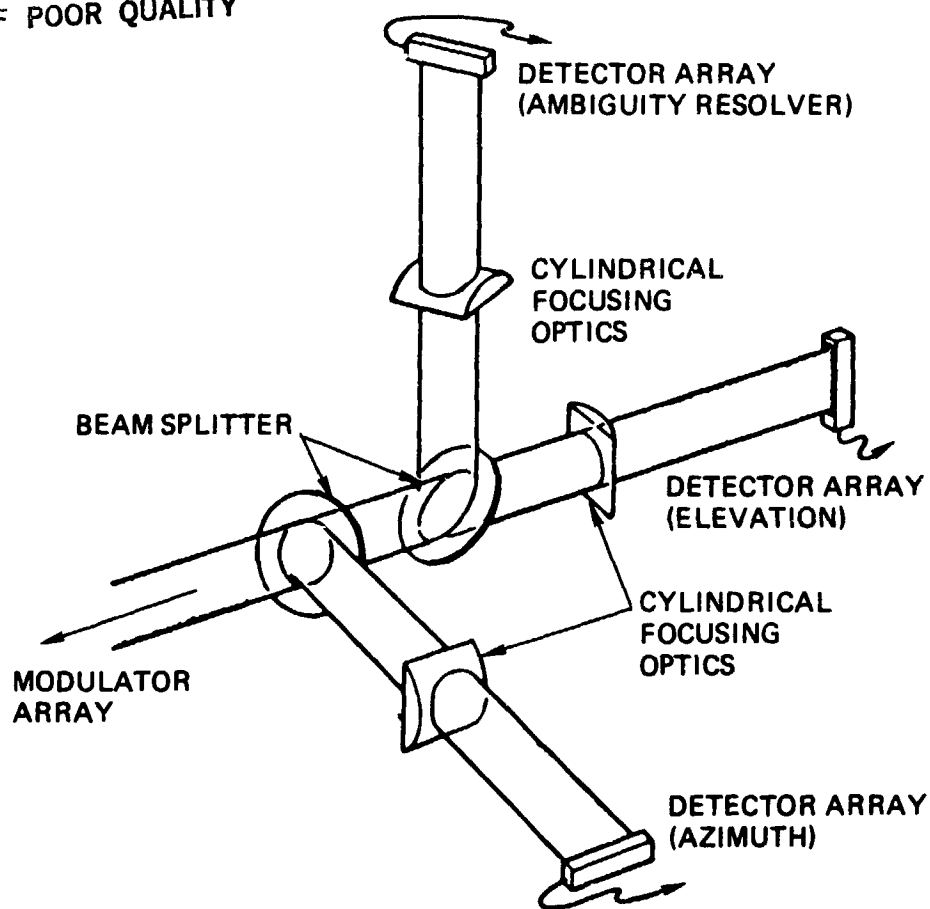


FIGURE 4.12 ANAMORPHIC OPTICAL SUBSYSTEM

signal/noise ratio required for this scheme to work is quite high. This high signal to noise ratio could be attained in a near earth (e.g., Shuttle) orbit but is not possible at synchronous orbit. It is difficult to suppress even one pixel's solar background from synchronous orbit, much less 800 times that.

- o From the above brief discussion, the most promising detector for full Earth daytime lightning coverage from geosynchronous orbit is a CCD. These devices are now discussed further.

4.3.2 Frame Transfer Methods

Frame Transfers Figure 4.13 shows schematically how a typical CCD is organized and Figure 4.14 is a photograph of a CCD. This CCD is a frame transfer device; there is an imaging area which is placed at the detector focal plane and there is a separate image storage area. Photoelectrons accumulate in the imaging area during an integration time, then the entire image (stored electrons) is rapidly shifted intact to the image storage

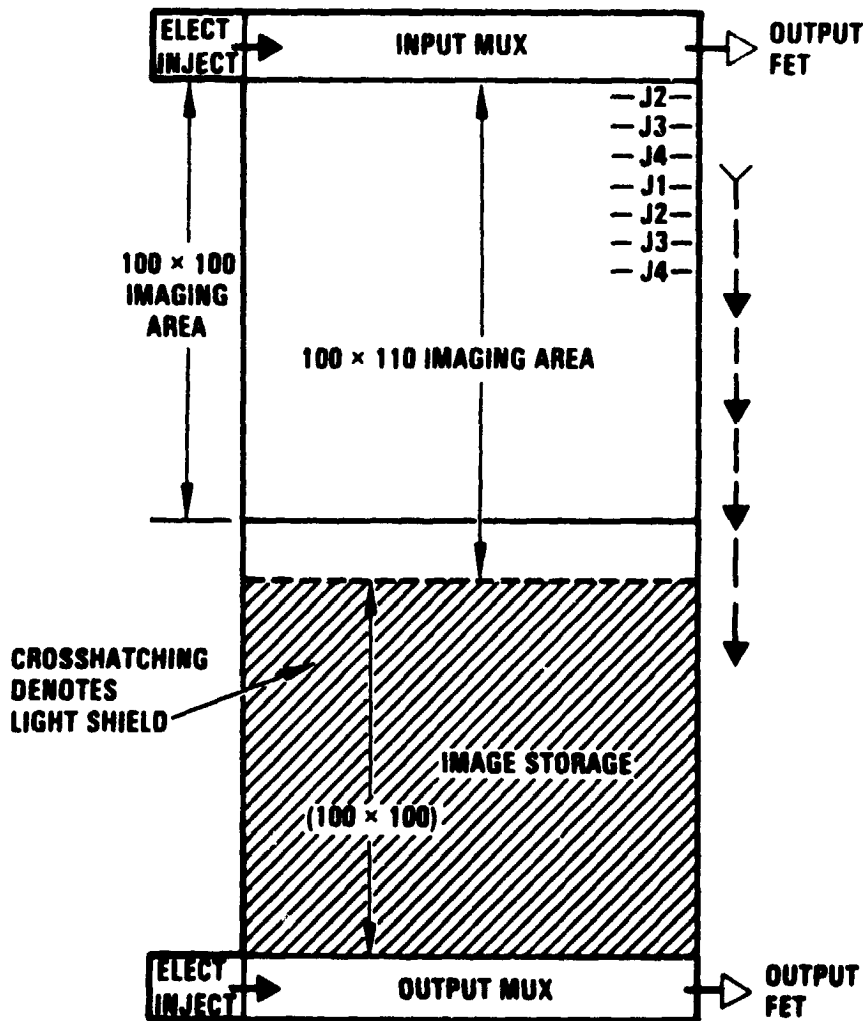


FIGURE 4.13 ORGANIZATION OF 5040 AREA ARRAY

ORIGINAL PAGE IS
OF POOR QUALITY

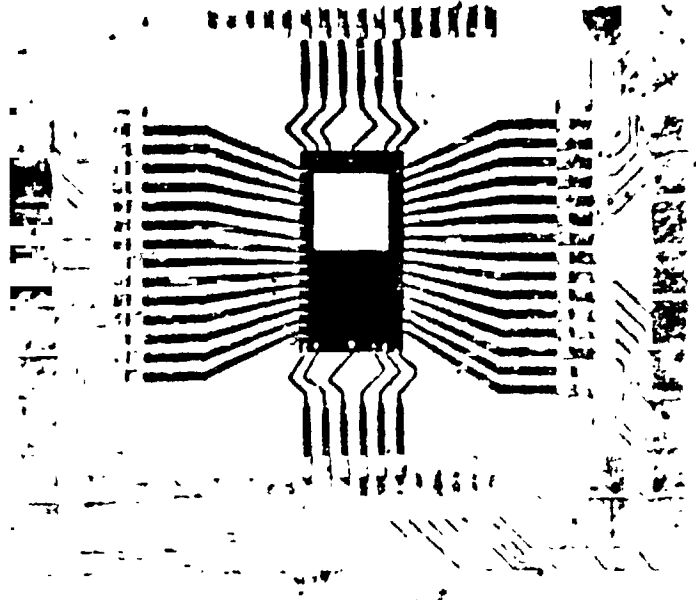


FIGURE 4.14 WESTINGHOUSE 5040

section. The image is then read out sequentially, pixel by pixel, a line at a time during the next integration time. Thus during an integration time one frame is being formed in the imaging section and the previous frame is being read out from the image storage section. A typical shift time for frame transfer devices is 0.3 milliseconds. This is an appreciable fraction of the 4 millisecond integration time needed for LITMAP and will cause some image smear of the stronger lightning flashes when they occur during the transfer interval.

Line Transfer - There are also line transfer and interline transfer CCDs. Line transfer devices have no on-chip memory and must use an external shutter to block the image while they are being read out. These are useful only in astronomical applications and the like where the significant readout time can be tolerated. Interline transfer devices have columns of opaque memory cells interleaved with columns of photosensitive cells. On command the accumulated electrons are shifted sideways one line into the interline memory columns where they are read out

during the next integration time. This type of CCD has much to recommend it for high frame rate applications: for frame transfer, the image moves over only one pixel instead of down a whole column and so transfers faster in the ratio of the number of pixels per column. The disadvantage of interline transfer devices is the lower effective quantum efficiency (0.12) resulting from having half the sensing area opaque for the frame storage function. Recently, rows of tiny cylindrical lenses have been manufactured with the sensor chip to redirect most of the focal plane light onto the optically sensitive portions resulting in increasing the effective detection quantum efficiency.

4.3.3 Focal Plane Configuration

Four CCD focal plane configurations were addressed to provide an assessment of alternate approaches for satisfying the LITMAP objective of obtaining lightning data over a full disc from geosynchronous orbit. These configurations ranged from severely pushing the existing technology to an approach which utilizes existing, unmodified hardware. Approach B is the baseline used for the concept definition and costing tasks of the study. Briefly these configurations are:

A: Two Chip - 800 X 800 Array - Modified

This is the most discussed approach using two sensor arrays such as the TI 800 X 800 array that is used by astronomers and by NASA for the Galileo project. A single simple prism split could be used to avoid any loss of information along the mating edge. No array exists which can handle the data rate required. Primary modification of existing devices would be array partitioning and the adding of output buffers and amplifiers to provide between 8 to 16 outputs per array, each operating in the 10 MHz regime to provide a two to four millisecond frame readout time. System analysis indicates that a pixel size considerably greater than the 15 microns of the existing 800 X 800 TI device is needed to handle the daytime background and to provide the dynamic range. TI has indicated that the yield for such a large device would be so low that its production could not be justified.

Mosaic: An alternative for the single focal

plane is to further sub-divide the focal plane and butt the arrays together into a single mosaic. Loss of significant information and the problem of getting a narrow band filter for the single wide FOV are significant added complications.

Itek/Bell Northern has been able to precisely cut and butt mount (along two opposite edges) sensor arrays to form a long continuous array. This technique has been extended to three sided buttability by several sensor manufacturers with RCA claiming that they should be able to do four sided butting with their PtSi sensor technology. In all cases to date, the dead space is at least 50 microns. For LITMAP this results in losing one to three pixels. The affect on a mosaic sensed image is the loss of information along strips which are between 10 to 30km wide at the sub-satellite point. Depending on the mosaic arrangement and satellite location, this loss of information could be intolerable. An operational approach could be used which slightly repositions the sensor FOV whenever coverage under the normally missed areas is desired.

Although the mosaic approach could be used to cover the full FOV with a single optical system with no auxiliary image splitting, there remains the problem of providing an optimum narrow band filter to cover the wide FOV as discussed elsewhere. The mosaic is a viable alternative and must be considered during detailed instrument design.

B: Four Chips - TI, RCA, Fairchild - Modified

Optically subdividing the total FOV into four sections relaxes the FOV and pixel cell size constraints to the point of being cost effective and compatible with the present optical and sensor technologies. Additional array partitioning is still required to accommodate the necessary data rate. Such partitioning, although fairly straight forward, will still require on the order of a million dollar development activity with about a year lead time. This is the baseline approach that is primarily focused upon in this final report.

The FOV splitting can be done with a single telescope coupled with four way prism image splitting or by using four independent telescopes for the four sub arrays. The required low F/No makes the prism splitting very difficult hence the four telescope approach is baselined. (A mosaic and single focal plane was discussed in the first configuration above.)

C: Four Chips - RCA - Unmodified

A RCA chip exists which can provide the required exposure time via the following procedure. The basic frame time through the existing output port is 17 milliseconds. The image section can be exposed for 13 milliseconds and then dumped to a drain at the opposite edge away from the output mux. The next 4 millisecond exposure is transferred to the on chip frame storage for output during the next 17 milliseconds. The dumping/output cycle can be repeated giving a 3 millisecond (or any other desired integration time) sample every 17 milliseconds.

This time sampling approach can provide statistics on total energy/stroke distribution but there will be no means of separating first return stroke data from other data. For an operational system such as a severe storm indicator, this mode of operation may be satisfactory. For scientific objectives, the relative roles of the strokes (first versus subsequent) will not be retrievable.

A potential variation of this time sampling approach would be to, during the readout cycle, rapidly transfer m rows (One or two MHz rate) to the output mux which will result in a loss of this data. The next n rows are transferred and processed at the normal rate (sub MHz row transfer). The remaining rows would be rapidly dumped, again with the total cycle time being the allowable 4 milliseconds (or whatever the selected integration time). The same n rows could be processed for a period of time (a few seconds would give hundreds of sampling cycles) then shifted to the next n rows. Repeat measurements over the same area would occur every few minutes providing a time sequence for each active area hence providing full coverage on a time-share basis. This approach would preserve the distinction between first and subsequent strokes which has scientific value.

D: Single (or two) Small Arrays With Mechanical Scan - Unmodified

A Westinghouse 2 X 100 x 100 chip exists which can provide the frame time required. Since only a few percent of the total field of view will contain active storms at any time, a smaller array combined with a mechanical scan mechanism can be used to cover the desired area. A given sub area can be observed for several seconds giving a few hundred frames and then another area is measured. On the order of 100 positions would cover the full field of view, hence a recycle over a given area can be done every few minutes. Alternately, a given storm can be fixed upon and followed over a period of time with only an occasional scan over the full area to determine if

other severe storm areas are developing.

The above summarized four focal plane concepts which can provide lightning data. Concept B will provide the best full time coverage at the expense of special sensor development. Approach D provides an off-the-shelf concept which can provide good storm coverage at the expense of an added mechanical tracking mechanism. Approach B was chosen for the baseline technology assessment.

- o Approach B was selected for the concept definition and costing tasks of this study.

4.3.4 Required Modifications

Table 4.1 illustrates a signal/noise calculation for a RCA CCD type SID 501D. The three left-most columns of the day and night tabulations on the bottom half of the page provide the minimum detectable and maximum non-saturating lightning intensity tabulated as a function of frame time. The units of the lightning intensity are $\mu\text{J}/\text{m}^2\text{-sr}$. These numbers can be compared with the MSFC NASA/U2 data taken in the summer of 1982:

Lightning Intensity (Max integrated radiance/event) $\mu\text{J}/\text{m}^2\text{ sr}$	Percent of Events Below this Intensity
1.8	1.6
4.2	7.2
5.6	12.0
7.5	22.3
13.3	50.9
42.2	80.2
56.2	89.7
100.0	98.4

A look at Table 4.1 shows that a frame time of two milliseconds gives excellent performance at night, losing only about 2 percent of lightning events at the low end and none at the high end. The daytime performance for the same integration time is adequate: a loss of 12 percent of lightning events at the low end and again, none at the high end.

The picture with a four millisecond frame time is a little less optimistic: the system performance is essentially unchanged

TABLE 4.1 RCA SID 501D Performance

*** LITMAP S/N ***

This is a calculation of the LITMAP minimum detectable signal and maximum non-saturating signal expressed in terms of lightning intensity at the cloud tops in ($\mu\text{J}/\text{m}^2 \text{ sr}$).

Required S/N ratio = 5.9
 Pixel size on Earth (edge of square) (km) = 10
 Effective source area (km^2) = 100
 Average stroke duration (as FWHM) = .54
 Satellite altitude (km) = 35600
 CCD type = RCA SID 501D
 Pixel size of CCD (μm) = 30
 Quantum efficiency = .28
 Readout noise (rms els) = 150
 Full well (electrons) = 250000
 Telescope f/number = 1
 Telescope focal length (cm) = 10.68
 Telescope diameter (cm) = 10.68
 Solar irradiance ($\text{W}/\text{m}^2 \text{ sr}$) = 301
 Cloud albedo = .8
 Optics transmission, including filter = .5
 Wavelength (nm) = 868.3
 Filter bandwidth (nm) = .6

Day (worst case sun):

Frame Time (ms)	Lightning Min ($\mu\text{J}/\text{m}^2 \text{ sr}$)	Lightning Max ($\mu\text{J}/\text{m}^2 \text{ sr}$)	Pulse Splitting Loss	Solar Bkgrnd (els)	Min Signal (els)	Bkgrnd Noise (rms electrons)	Readout Noise (rms electrons)	Total Noise
0.25	6.9	1385	0.39	15614	1169	125	150	198
0.50	5.0	791	0.64	31227	1385	177	150	235
1.00	4.9	529	0.82	62455	1737	250	150	294
2.00	5.8	318	0.91	124909	2283	353	150	387
4.00	7.5	0	0.96	249818	3096	500	150	525
8.00	10.1	*	0.98	499636	4281	707	150	726
16.00	14.0	*	0.99	999273	5981	1000	150	1014

* Solar background exceeds full well capacity.

Night:

Frame Time (ms)	Lightning Min ($\mu\text{J}/\text{m}^2 \text{ sr}$)	Lightning Max ($\mu\text{J}/\text{m}^2 \text{ sr}$)	Pulse Splitting Loss	Solar Bkgrnd (els)	Min Signal (els)	Bkgrnd Noise (rms electrons)	Readout Noise (rms electrons)	Total Noise
0.25	5.3	1477	0.39	0	903	0	150	153
0.50	3.3	903	0.64	0	903	0	150	153
1.00	2.5	705	0.82	0	903	0	150	153
2.00	2.3	636	0.91	0	903	0	150	153
4.00	2.2	606	0.96	0	903	0	150	153
8.00	2.1	592	0.98	0	903	0	150	153
16.00	2.1	585	0.99	0	903	0	150	153

at night, but in the daytime the CCD is saturated by the solar background. Even if the full well capacity were higher, the low end threshold has risen to the point of losing 20 percent of the lightning events. Hence the framing time needs to be kept as low as possible and the full well capacity as high as possible (see Appendix A for further analysis).

Commercial CCD's have frame rates appropriate to TV applications or slower, i.e. 50 or 60 per second or less, and can be driven less than a factor of two faster than that before significant performance degradation occurs. A frame rate of 250 frames per second (4 millisecond integration time) is required. The restriction is the speed at which a CCD can be read out which is limited primarily by the output amplifier. Image partitioning with the data sent to multiple output ports resolves this bottleneck. The manufacturers of the sensors have proposed various schemes for doing the partitioning (c.f. Technology Assessment, Section 5).

The electronics to deal with the multiple data streams emanating from the detector must be made in multiple parallel versions also. This electronics and how the background subtraction is to be implemented are discussed in the next section.

Table 4.2 is a signal/noise calculation for the device originally proposed by the Optical Science Center, University of Arizona, for a lightning mapper, the Texas Instruments 800 x 800 array. The threshold levels are above $25 \text{ uJ/m}^2 - \text{sr}$ due to the 5.4 cm aperture which is determined by the small 15 micron pixel size. Comparison of this 15 micron device results with the 30 micron device results above (c.f. Table 4.1) indicates that a large pixel size is required to meet the LITMAP requirements (c.f. Appendices A, B, and Sections 2 and 3 for further details).

- o Integration time must be kept low (4 millisecc nominal).
- o Array partitioning is required to keep the port operating frequency within technology limits.
- o Large pixel sizes are needed to attain low threshold capability.

ORIGINAL PAGE IS
OF POOR QUALITY

TABLE 4.2 TI 800 x 800 Performance

* * * LITMAP S/N * * *

This is a calculation of the LITMAP minimum detectable signal and maximum non-saturating signal expressed in terms of lightning intensity at the cloud tops in ($\mu\text{J}/\text{m}^2 \text{ sr}$).

Required S/N ratio = 5.9
 Pixel size on Earth (edge of square) (km) = 10
 Effective source area (km^2) = 100
 Average stroke duration (as FWHM) = .54
 Satellite altitude (km) = 35600
 CCD type = Texas Instruments 800 x 800
 Pixel size of CCD (μm) = 15.2
 Quantum efficiency = .13
 Readout noise (rms els) = 150
 Full well (electrons) = 109000
 Telescope f/number = 1
 Telescope focal length (cm) = 5.4112
 Telescope diameter (cm) = 5.4112
 Solar irradiance ($\text{W}/\text{m}^2 \text{ sr}$) = 301
 Cloud albedo = .8
 Optics transmission, including filter = .5
 Wavelength (nm) = 868.3
 Filter bandwidth (nm) = .6

Day (worst case sun):

Frame Time (ms)	Lightning Min ($\mu\text{J}/\text{m}^2 \text{ sr}$)	Lightning Max ($\mu\text{J}/\text{m}^2 \text{ sr}$)	Pulse Splitting Loss	Solar Bkgrnd (els)	Min Signal (els)	Bkgrnd Noise (rms electrons)	Readout Noise	Total Noise
0.25	46.5	5311	0.39	1861	938	43	150	159
0.50	29.5	3192	0.64	3722	973	61	150	165
1.00	24.6	2404	0.82	7444	1039	86	150	176
2.00	24.7	2007	0.91	14888	1158	122	150	196
4.00	27.8	1610	0.96	29775	1366	173	150	232
8.00	33.9	982	0.98	59550	1708	244	150	289
16.00	43.9	*	0.99	119101	2238	345	150	379

* Solar background exceeds full well capacity.

Night:

Frame Time (ms)	Lightning Min ($\mu\text{J}/\text{m}^2 \text{ sr}$)	Lightning Max ($\mu\text{J}/\text{m}^2 \text{ sr}$)	Pulse Splitting Loss	Solar Bkgrnd (els)	Min Signal (els)	Bkgrnd Noise (rms electrons)	Readout Noise	Total Noise
0.25	44.7	5404	0.39	0	903	0	150	153
0.50	27.4	3305	0.64	0	903	0	150	153
1.00	21.4	2380	0.82	0	903	0	150	153
2.00	19.3	2325	0.91	0	903	0	150	153
4.00	18.3	2215	0.96	0	903	0	150	153
8.00	17.9	2164	0.98	0	903	0	150	153
16.00	17.7	2140	0.99	0	903	0	150	153

4.4 SIGNAL PROCESSING

The signal content of each pixel consists of various components of which the desirable component is the lightning stroke intensity integrated over the sample time. The unwanted components consist of integrated background irradiance and the detector noise. Each pixel signal arriving from the detector must be tested for the presence of a lightning stroke. The detection, extraction and measurement of the lightning signal from the detector output data stream is the primary function of the data processor. The data processor will perform the following functions:

- a. Detect lightning stroke with time and location tag
- b. Measure lightning energy
- c. Format and return the data

The baselined 800 X 800 CCD imaging portion of the array consists of 6.4×10^5 pixels which must be individually integrated for the presence of lightning at the sampling rate of 4 milliseconds or less per frame. This transforms to a total data rate of at least 160 mega samples per second for the total detector array. This data rate through a simple port exceeds the present electronic processing as well as the CCD technologies. The data rate can be reduced to an acceptable level for processing by using multiple output ports from the detector array (see previous section). Table 4.3 gives the various combinations of array size, output port number, sampling time and the resulting sample rate. Each output port will then be serviced by a signal processor circuit. The extracted event data from each data processor, however, can be streamlined into a single data formatting circuit with reduced data handling rate capability because the lightning occurrence rate is sufficiently low. This parallel processing approach reduces the complexity of the system without sacrificing the performance.

4.4.1 Design Requirements

The data processor must be designed to perform the three

ORIGINAL PAGE IS
OF POOR QUALITY

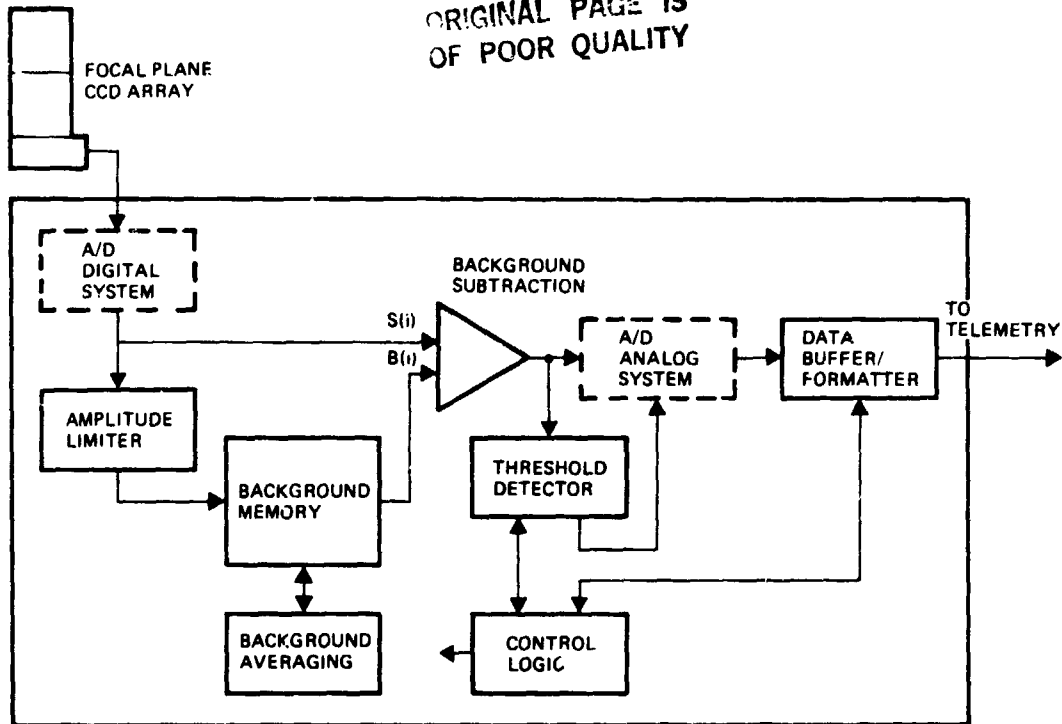


FIGURE 4.15 LITMAP SYSTEM CONCEPTUAL BLOCK DIAGRAM

primary functions listed in the previous section. In order to facilitate the evaluation of various design approaches and concepts, baseline design requirements were established. The baseline system block diagram in Figure 4.15 shows the primary functional blocks for a data processor servicing one of the output ports of the CCD. The total size and power requirement of the system is very much dependent on the number of output ports which results in the duplication of this data processor section. Based on past experience each data processor is estimated to occupy approximate half of a 7" X 7" circuit board with about eighty 16-pin dual-in-line packages. Therefore a system with 16 output ports can be fitted into less than one cubic foot volume which is comparable to other flight systems of similar complexity. From Table 4.3, a 16 channel system with an 800 X 800 CCD device at 4 ms sampling interval is equivalent to an effective data rate of 10 mega samples per second. A reasonable power budget based in similar flight hardware, is in the range of

TABLE 4.3 Array Size and Data Rate Trade.

ARRAY SIZE	SAMPLE INTERVAL (MSEC)	NO. OUTPUT PORTS	SAMPLE DATA RATE PER PORT (SPS)	BACKGROUND MEMORY SIZE PER PORT (SAMPLES)	PROCESSING TIME PER SAMPLE (MSEC)
800 X 800	3	16	13.3×10^6	40000	75
800 X 800	3	32	6.7×10^6	20000	150
800 X 800	4	16	10×10^6	40000	100
800 X 800	4	32	5×10^6	20000	200
300 X 800	5	16	8×10^6	40000	125
800 X 800	5	32	4×10^6	20000	250
800 X 800	3	16	10×10^6	30000	100
800 X 800	3	32	5×10^6	15000	200
800 X 800	5	16	6×10^6	30000	167
800 X 800	5	32	3×10^6	15000	333
100 X 100	3	1	3.3×10^6	10000	300
100 X 100	3	4	0.8×10^6	2500	1200
100 X 100	5	1	2×10^6	10000	500
100 X 100	5	4	0.5×10^6	25000	2000

30 to 50 watts.

In summary, the baseline electronic subsystem requirements are:

1. Data rate - 10 mega samples per second per output port
2. Power - 30 to 50 watts
3. Size - approximately 1 cubic feet
4. Weight - approximately 60 pounds

4.4.2 Background Subtraction

The lightning mapper system is required to detect lightning flashes during day and night. Since the background conditions vary drastically between day and night and over cloud top, land and sea, it is necessary to design the system to handle the worst

case background illumination conditions.

There are essentially three methods for extracting weak signals from a strong background. These are spectral, temporal, and spatial filtering. The spectral and temporal filtering may be implemented at the optical and analog signal stages of the process. They may be considered predetection processing techniques. Spectral filtering is essential to the performance of the system when the clouds are sunlit. The use of an optical filter has been discussed in detail in an earlier section and will not be presented here.

Spatial filtering uses an averaged background level from some adjacent pixels which is subtracted from the incoming signal in order to isolate possible lightning signals. This technique requires that the background level be relatively uniform over adjacent areas which often is not a valid assumption. Therefore the use of spatial filtering for background subtraction will not be considered for the LITMAP application.

Temporal filtering depends on the background remaining static for two or more successive frames. Successive frames may be subtracted to eliminate the background signal from each pixel with the drawback that the overall noise will increase by a factor of $\sqrt{2}$. A running average technique for the background statistically can reduce the $\sqrt{2}$ factor significantly. Further discussion of this technique will be presented in a later section.

4.4.2.1 Analog vs Digital

The baseline conceptual block diagram of the lightning mapping system is shown in Figure 4.15. Temporal background subtraction is employed. The present frame pixel signal $S(i)$ is being fed into the background subtraction amplifier. The subtrahend $B(i)$ is equivalent to $S(i-1)$ ($S(i)$ from the previous frame) plus some contribution from the past due to averaging. This scheme can be realized by using analog or digital hardware, or a hybrid. These approaches will be analyzed against the technology and design requirements and then, a data processor system design concept will be discussed.

4.4.2.2 Digital Approach

The digital background subtraction system can be visualized from Figure 4.15 by installing the A/D converter for the digital system as shown. The input signals from the focal plane CCD detector are preprocessed by the A/D to provide digital data. Subsequent data processing such as multiplication and background subtraction is carried out in digital circuitry. The three important circuit components to be considered in this digital approach are: the A/D converter, the background memory and the associated logic circuitry that controls the processing. In order to develop a feasible flight system the critical factors that need to be considered are size, weight, power and technology availability.

The A/D converter is a very important component in this approach. Based on previous data and calculations, the background irradiance can occupy as much as 20% of the () full well capability. IF the minimum lightning signal is taken into account, the A/D converter will require better than nine bits of resolution and the background memory will require eight bits for background information storage. The A/D resolution and range requirement can only be satisfied simultaneously by flash type A/D converters which have rather high power requirements (on the order of one watt). Lower power devices are available with less bit resolution but would sacrifice resolution and therefore can only be considered as an alternative. Another way to reduce the A/D resolution is by front-end signal compression using a logarithmic amplifier. Application of the log amplifier at this point, however, will induce large inaccuracy in the system where background signal is a significant portion of the entire useful signal range. This inaccuracy is worse at low level lightning signals and consequently will tend to reduce the quantity and quality of useful data. The signal compression technique, however, will be useful after the background subtraction to reduce the required resolution of the A/D converter for the analog approach that is discussed in a following section.

The data processing technique that is proposed in this

system consists of background averaging, limiting, subtraction and adaptive threshold adjustment. In order to realize these functions digitally, high speed digital processing circuitry and components have to be utilized which tends to significantly increase the power consumption of the system.

The background storage memory is a digital storage device and can be a module made up of an array of random access memory devices (RAM) with the associated logic control circuitry. The proposed system requires that the signals derived from the pixels within one frame be processed within the next frame of time. This results in less than 100 nsec data time per pixel based on 10 MSPS data rate. In order to store the current digitized frame information, the background memory in a digital system will require a storage capacity of 40000 X 8 bits (for 8 bit A/D conversion) at an access time of much better than 100 nsec. Commercially available bipolar or highspeed MOS devices generally can operate with better than nsec access time for read or write cycles. A module of 40000 X 8 bit memory will typically consists of 20 4k X 4 bit RAM chips in addition to the associated logic circuit for addressing control, and signal processing. When translated into 16 parallel output channels the total electronics size, weight and power will exceed the proposed design requirement by a wide margin. Therefore, alternate methods or devices have to be sought.

One method of reducing the per channel power requirement is to use low power high density MOS type RAM memories. Static RAMS with 8k X 8 memory size and 1/4 watt per chip power dissipation are available but are generally slower. The most straight forward approach to overcome the slow speed is to increase the number of output ports along with the number of data processors. If the 10 MSPS data rate is reduced to 5 MSPS by increasing the number of output ports to 32 for a 800 X 800 CCD array, the processing time is increased to 200NS and the background memory size is reduced to 20000 elements per data processor. This translates into a total of 3 memory chips and 3/4 watts power requirement per data processor. The power reduction however, is

offset by an additional 6 data processor modules. An alternate way of utilizing these lower power, higher density devices is to multiplex the data to two or more memory modules per channel to increase the effective storage area at a slower speed. However, all of this will require additional logic control circuitry and will increase overall size and power.

To summarize, the digital approach is best if size and power are not constraints. Since the objective is to design a system possessing reasonable size and weight, digital method appears to be a questionable approach. The future trend is toward high speed, lower power and high density. It is possible that in the future a system based on a digital approach would be more compatible with the power constraints while providing the necessary processing speed.

4.4.2.3 Analog Approach

An analog approach to background subtraction can be realized by storing the previous frame pixel signals in a CCD memory. A CCD device developed for the focal plane can be used for this purpose by masking out the photo sensitive area. On chip input and output ports equal in number to the focal plane output ports can be implemented. In addition the approach is a cost effective way of utilizing existing technology. Analog approach involves preprocessing the time multiplexed analog signal with fast analog circuitry. This type of circuitry currently exists and therefore the approach represents a lower risk than the digital approach. The total size, weight and power requirements are also substantially lower than for the digital approach. Further discussion of this technique will be presented below as part of the baseline approach.

4.4.3 Baseline System

Figure 4.16 shows the proposed data processor system block diagram. The focal plane sensor array consists of one or several large array CCD detectors, each with built in multiple-output ports. The system will be operated in the staring mode with

ORIGINAL PAGE IS
OF POOR QUALITY

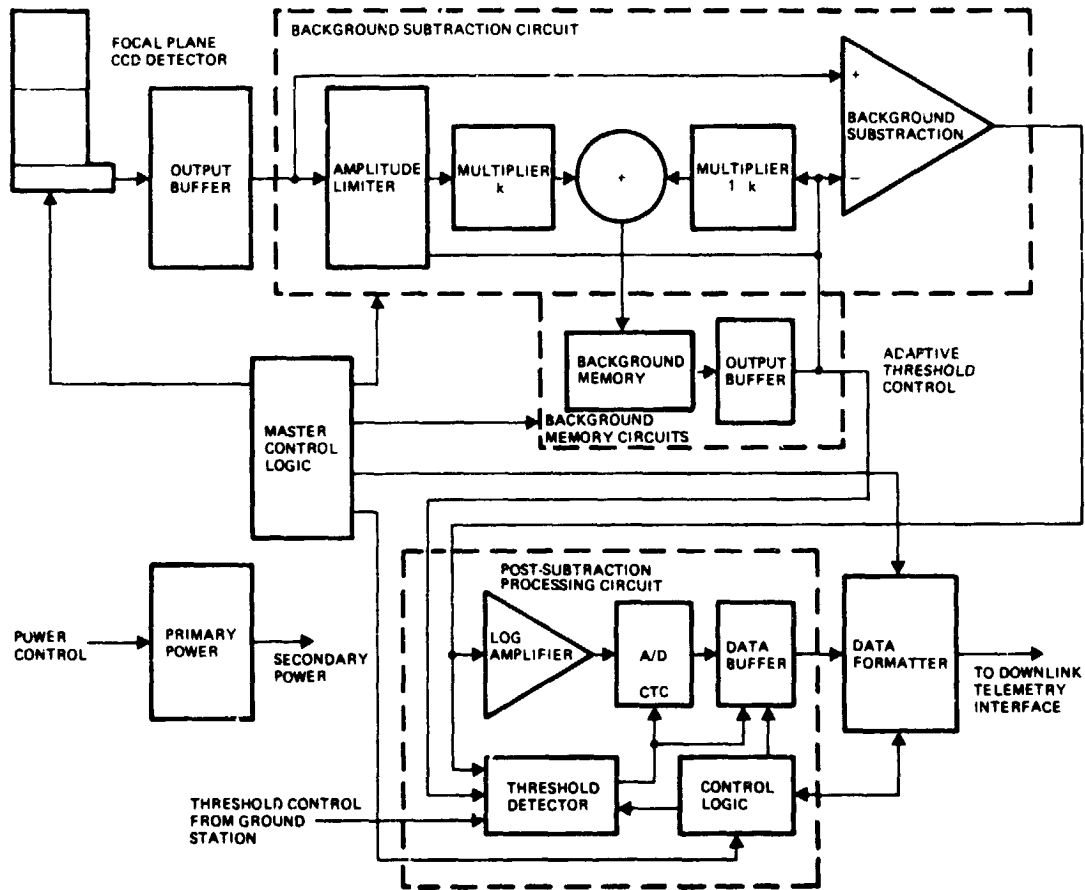


FIGURE 4.16 PROPOSED LITMAP ELECTRONICS SYSTEM BLOCK DIAGRAM

frame rate in the two to five milliseconds duration to optimize SNR. Detail discussion of the device and the SNR were presented in earlier sections and will not be repeated here. Each output port is serviced by its own analog data processor (DP). Background subtraction and threshold detection are carried out within the DP. The subsequent lightning intensity data, along with the time and location tags, will be fed to a single data formatter (DAF). The extremely low lightning occurrence rate allows the use of a single DAF approach without compromising system throughput while minimizing system complexity and

maximizes system efficiency. This multiple output-port approach also permits scaling the system (number of output ports) to match the array size with minimal modification of the baseline system. Example of this would be a small array focal plane lightning mapper system with a single DP that could be flown on Shuttle mission in lower earth orbit. A detailed description of the system is presented in the following sections. The resulting key features for the signal processing are:

1. Multi-port detector array
2. Multi-channel analog data processor
3. Background subtraction by temporal technique
4. Background smoothing by running average technique.
5. Post detection digitizing using A/D converter
6. Single data formatting circuit.

4.4.3.1 Data Processor

Output Buffer. The proposed data processor (DP) as described earlier is based on an analog approach. The CCD output signal is buffered and the data sampled and held. This S/H function is utilized to sample the data at the appropriate time to avoid transients and switching glitches. The buffer also serves to extract the signal from the DC bias voltage of the CCD output amplifier. Commercially available instrumentation and operational amplifiers and sample and hold amplifiers can be used to implement this circuit. However, at 100 ns processing time per pixel, the bandwidth requirement for these devices are well above 10 MHz. Commercially available devices which can operate to this specification generally have high power requirements relative to the total system power budget established in Section 4.4.1. Consequently, it is necessary to design circuitry based on discrete components or hybrid elements which also provides additional size savings.

The buffered signal is fed into the background averager and the background subtraction amplifier for further signal processing. The description and design approach of these

functional blocks will be discussed next.

Background Subtraction. The function of the background subtraction circuitry is to isolate lightning signals from the background and thus reduce the dynamic range required for the A/D converter. Averaging techniques are used to increase system responsitivity and performance. A simplified functional block diagram is shown in Figure 4.17. Subtraction is carried out in the subtraction amplifier with inputs $S(i)$ and $B(i)$. $S(i)$ is the buffered output from the detector and $B(i)$ is a conditioned derivative of $S(i)$ from previous frames.

The input signal $S(i)$ is fed to the amplitude limiter which prevents excessive lightning signal amplitude passing to and contaminating the background data. The limiter provides a coarse limiting of the signal pulse with further smoothing provided by time averaging the background samples. An adaptive feedback based on the average background is used to optimize for both day and night operations.

The background averager consists of the multipliers k and

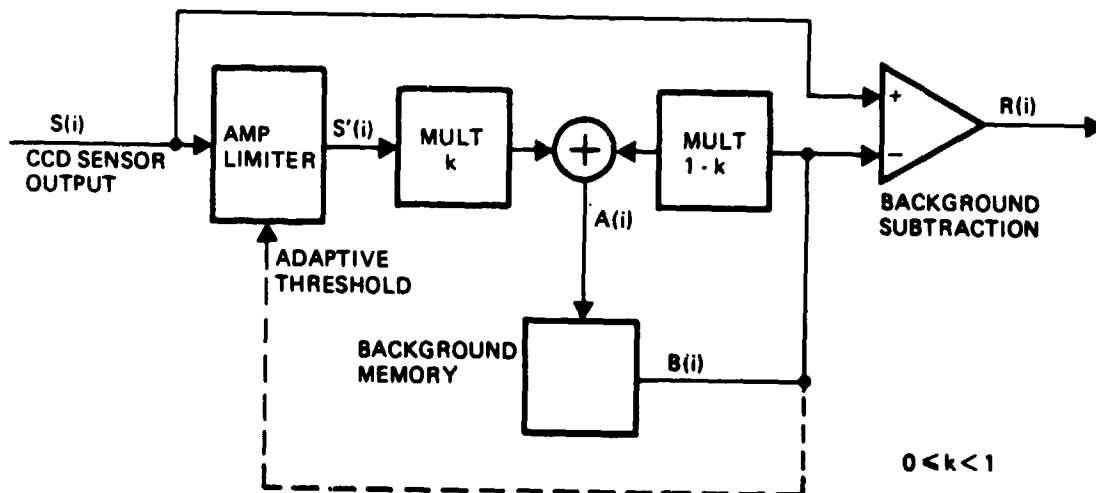


FIGURE 4.17 BACKGROUND SUBTRACTION WITH RUNNING AVERAGE

(1-k), the adder and the background memory. The background memory is essentially the same type of CCD device used in the focal plane detector. The function of this device is to store the analog data arriving from the adder, and to output on a first-in first-out (FIFO) basis the stored data for the background subtraction and for the averaging routine. The coefficient k is confined between zero and one. In general, the sum of the two multipliers k and (1-k) should be less than unity to prevent the system from saturating. The input to the background memory A (i) is

$$A (i) = K S (i) + (1-K) B (i)$$

$$\text{with } B (i) = A (i-1)$$

where i and i-1 refer to present and previous frames respectively.

If K=0, there is a straight throughput with no subtraction. On the other hand, k=1 corresponds to a simple frame-to-frame differencing. For $0 < k < 1$, the subtrahend S(i-1) is a "fading moving average". Frames are filtered with a time constant inversely proportional to k, i.e., the relative contribution of each sample decreases with age. Let S(i) contain some noise N_F . Then R(i) will contain some noise N_R also given by:

$$N_R/N_F = (2/(2-k))^{1/2}$$

Some representative values of N_R/N_F are:

<u>K</u>	<u>N_R/N_F</u>	<u>N</u>	
0	1.000	∞	No subtraction
0.001	1.000	1000	
0.125	1.033	7.49	Selected N
0.25	1.069	3.46	Another ADD for (1-k) = 3/4
0.5	1.155	1.44	Additional ADD
0.75	1.265	< 1	
1	1.414	< 1	FIFO simple two frame subtraction

where N is the effective number of frames being averaged as defined by

$$(1-k)^N = e^{-1} \quad \text{or} \quad N \approx 1 / \ln(1/(1-k)) .$$

Conversely

$$k = 1 - e^{-1/N} .$$

As the number of background frames being averaged increases the noise approaches that of the original frame (assuming incoherent noise). Simple frame to frame subtraction ($k=1$) will increase noise by $\sqrt{2}$, hence increasing the threshold setting. Background averaging (five to eight frames) permits the background to be removed while minimizing signal degradation.

The overall background subtraction circuitry can be realized in hardware by an integrated rather than a modular design. The multiplexers k , $k-1$ and adder can be implemented by a single summing OP AMP thus reducing the component count and therefore power requirements. Further size reduction can be achieved by hybridization of the entire background subtraction circuitry (excluding the background memory). It was mentioned earlier that the wide bandwidth requirement tends to drive up the power consumption of an OP AMP. It is therefore necessary to select the device with the best power to bandwidth trade but still be able to meet the performance specification. Commercial OP AMP components will be selected where available while transistor circuits using single supply source will be designed when necessary to minimize power consumption.

Another important design consideration is the circuit timing. The high data rate requirement provides very little excess processing time to allow for delay, transients and settling. Therefore, it is necessary to minimize these timing errors by optimally applying high speed circuit design techniques such as minimizing load capacitance, path and lead length, and transistor saturation.

Background Memory The background analog memory consists of several CCD devices similar to those used in the focal plane. The devices are opaque and have electrical input ports to accept the analog data. The background memory and supportive circuitry can be built on a single circuit card.

Input and output buffers are required for signal conditioning and signal level matching. On the input side of the memory a sample and hold (S/H) amplifier samples the output from the adder during the allowable time window to avoid transients. Amplification raises the background signal to a level which efficiently fills the full well capacity of the CCD memory to minimize the noise contribution from the analog memory. The output ports of the background memory have similar S/H amplifiers.

Post-Subtraction Processing. Post-subtraction processing consists of digitizing the lightning signal and buffering it with the appropriate location tag for distribution to the data formatter. Data compression using logarithmic amplifier may be implemented here to reduce the resolution requirement of the A/D converter. A threshold detector is utilized to establish the false alarm rate prior to digitization thus minimizing the load on the A/D. The functional block diagram of the post subtraction processing is shown in Fig. 4.16.

The primary function for an automatic background adaptive threshold control is to vary the threshold for day and night conditions, which occurs fairly slowly. The bandwidth requirement of this circuit is estimated to be much less than the focal plane data rate. Therefore, the design of this circuitry does not present any critical problems. Manual ground control circuitry can be implemented by feeding a digitized telemetry signal through a D/A converter and applying the analog voltage to the threshold detector circuitry.

The output of the background subtraction amplifier consists of pulses coinciding with the occurrence of lightning strokes. The average occurrence rate is extremely low. The maximum rate anticipated is in the order of several strokes per frame (entire

focal plane). The temporal spreading of a single stroke across several integration intervals is treated as two lightning events occurring in different sample frames and, therefore, poses no difficulty to the post-subtraction processing circuitry. The spatial straddling, however, will require the post-subtraction processing circuitry to be able to handle bursts of data packets associated with consecutive pixels. At 10 MSPS data rate the post-subtraction processing circuitry is required to complete each single event processing within 100 nsec. Hence, the bandwidth requirement on this circuitry is similar to the background subtraction circuitry except that it will be in a quiescent state most of the time due to the low average event rate. The low data rate also results in a lower power level than the similar circuitry used for the background subtraction.

Data Conversion. The output of the threshold detector is a one/zero signal to indicate the presence or absence of a lightning signal. This signal will be used to command the A/D converter to initiate conversion upon positive detection of a lightning signal, and to inform the control logic for timing and location tagging functions.

As mentioned earlier, the detected lightning stroke intensity is compressed by a logarithmic amplifier and a sample and hold amplifier freezes the output signal from the background subtraction amplifier. The bandwidth requirement of this circuit will still be dictated by the high event burst data rate as discussed in the last section, hence it will be implemented with operational amplifier technique using discrete components.

The A/D converter performs the final digitizing function on the log-compressed signal. The dynamic range requirement of the signal is 100:1. It is necessary to have adequate resolution in order to extract useful statistical data for the lower lightning intensities. The log amplifier compresses the intensity data without sacrificing the low level signal resolution. The lowest bit resolution of the A/D converter will depend on the log amplifier output level. In order to utilize the bit counts of

the A/D converter over the dynamic range efficiently, it is necessary to set a minimum bit resolution level. The minimum signal level based on a 4 msec frame time and 5A filter bandwidth is about 1800 electrons. Based on minimum bit resolution equal to 600 electrons and full well capacity of 250k electrons, a 6-bit A/D converter is capable of delivering an adequate performance. The table below lists the bit resolution for various compressed signal levels from 6, 7, and 8-bit A/D converters:

<u>SIGNAL LEVEL</u>	<u>RESOLUTION AT</u> <u>6-BIT</u>	<u>STATED</u> <u>7-BIT</u>	<u>SIGNAL LEVEL</u> <u>8-BIT</u>
250k el (Full well)	22828 el	11597 el	5845 el
110k el	10044 el	5103 el	2572 el
10k el	913 el	464 el	234 el
1830 el (Min. signal)	167 el	85	43 el

Each additional bit doubles the resolution capability of the output.

In order to have adequate slew rate capability, the A/D converter must have a sampling frequency double that of the data rate. Presently, off-the-shelf 6-BIT A/D converters capable of delivering this performance are available. RCA and Siemens are delivering devices requiring less than 1/2 watt. These devices (and their next generation spin-offs) will be the primary candidates selected to meet the design requirement.

Data Buffer. The function of the data buffer (Fig. 4.18) is to temporarily store the A/D output data and the location information from the control logic. This information will be extracted by the data formatter for downlink to the ground station.

As discussed earlier, each data processor (channel) will interface with some 40,000 pixels during each frame of sampling time. The location of these 40,000 pixels can be labelled by a 16-bit word. The proposed system will cycle through the 40,000 location labels in synchronization with the sequence of signal

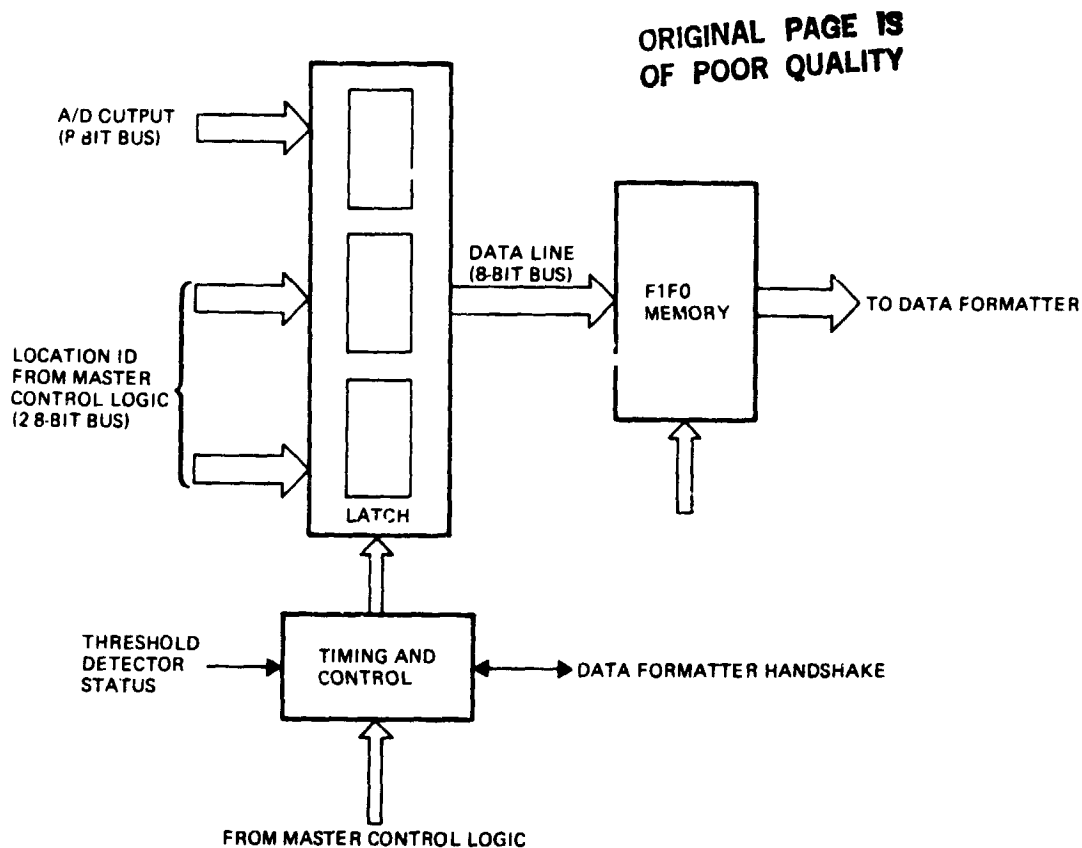


FIGURE 4.18 DATA BUFFER FUNCTIONAL BLOCK DIAGRAM

processing. When a lightning signal is detected by the threshold detector, its location label will be latched into the data buffer memory in 8-bit words, followed by the A/D output word. Thus, there will be three 8-bit data words to be stored in the data buffer for each pixel containing a lightning signal (Fig. 4.19). Based on the occurrence rate of lightning it is estimated that no more than four events will occur within the same 40,000 pixels in the same frame. Therefore, the size of the memory required is about 12 x 8 bit. The speed of the memory depends on the way the data words are latched into the memory. An 8-bit parallel data configuration will require an access time better than one third of the processing time, or better than 33 nsec. One method to implement this is to use two low power, high speed CMOS (such as

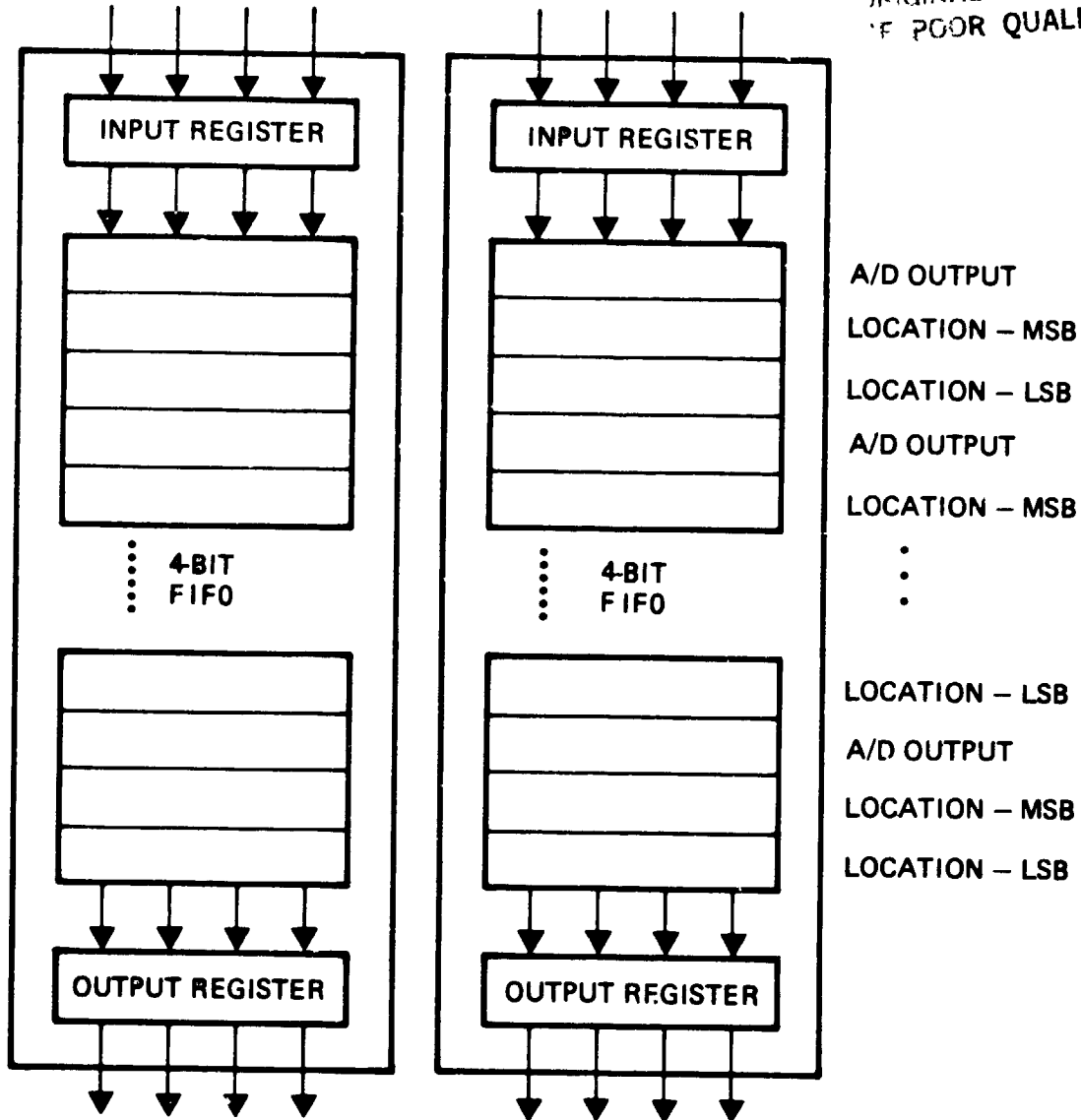


FIGURE 4.19 DATA BUFFER MEMORY STAGE FORMAT

QMOS) FIFO memories. Due to the low average occurrence rate, the FIFO will essentially be at low standby power. The data formatter will handle the channel tag and the time tag. Further discussion of the data formatter function will be presented in a later section.

4.4.3.2 Control Logic

The control logic consists of the master control logic (MCL) and the control logic (CL) circuits associated with the data processor. The MCL (Fig. 4.20) will perform the following functions:

1. Generate a high frequency clock pulse for sub-processing time synchronization
2. Generate clock pulses for frame transfer and output of the focal plane CCD detectors
3. Generate clock pulses for S/H actuation in the data processor
4. Generate clock pulses for input and output transfer of the background memory
5. Generate clock pulses to synchronize the data buffer
6. Generate clock pulses for data formatter
7. Interface with the ground-based threshold detector adjustment input.
8. Generate location labels to data buffer

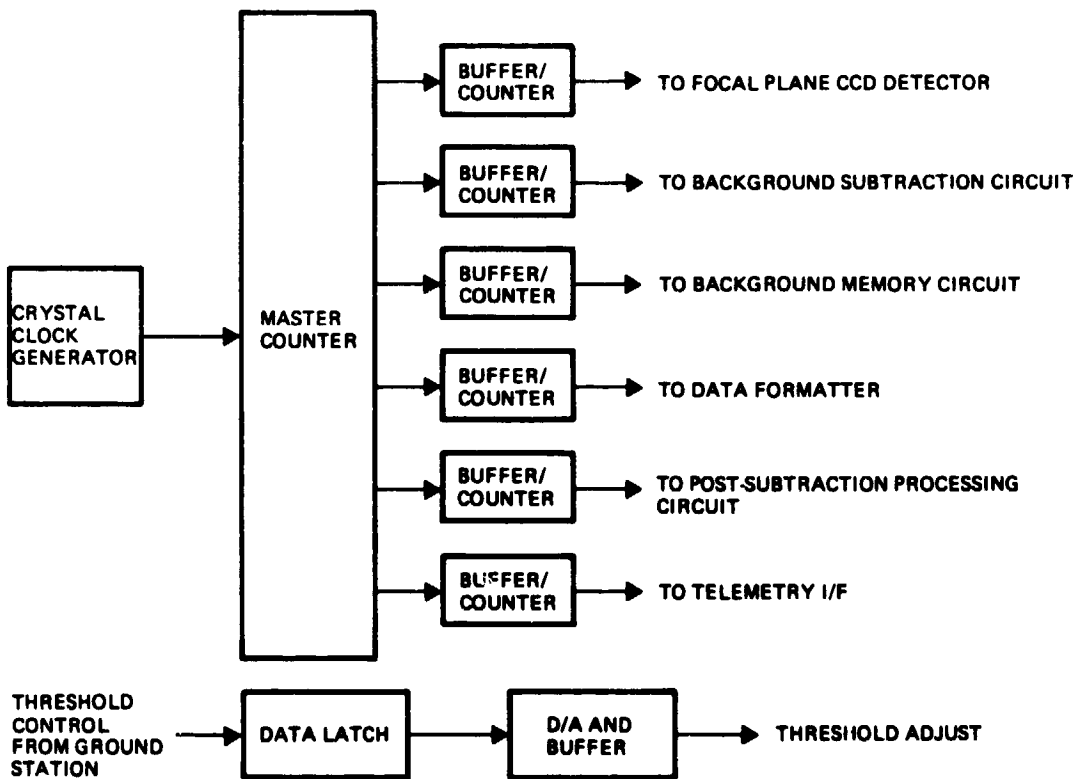


FIGURE 4.20 MASTER CONTROL LOGIC

The control logic circuits provide buffers for all the clock pulses and signals from the MCL to the appropriate destination. The MCL and control logic can be implemented using low power QMOS devices.

4.4.3.3 Data Formatter

The data buffer functions as a temporary storage of the lightning intensity and location data. The Data Formatter (DAF) (Fig. 4.21) will extract the data from all the data buffers. Due to the low lightning occurrence rate, the data formatter has a relatively low data rate requirement. It will have the frame sampling time (milliseconds) to extract data out from the buffers. A time tag for each frame sampling period will be generated by the MCL and latched into the DAF memory.

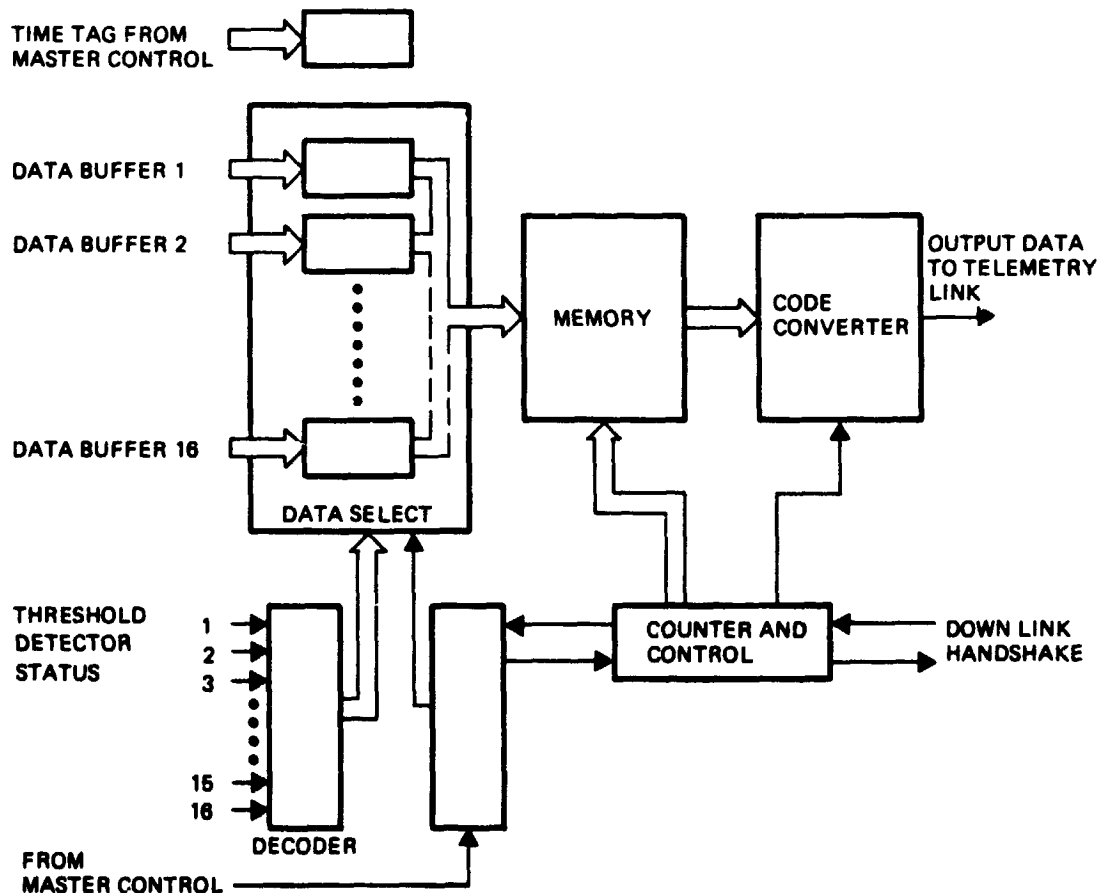


FIGURE 4.21 DATA FORMATTER FUNCTIONAL BLOCK DIAGRAM

Subsequently, all the data extracted into the DAF memory from the same time frame will be identified by this time tag. The segment or channel identification will be latched into the DAF along with its data. A 4-bit word representing 16 channels will be adequate to identify the channel numbers. Therefore, the total number of data bits allocated to location identification is equal to twenty (Fig. 4.22).

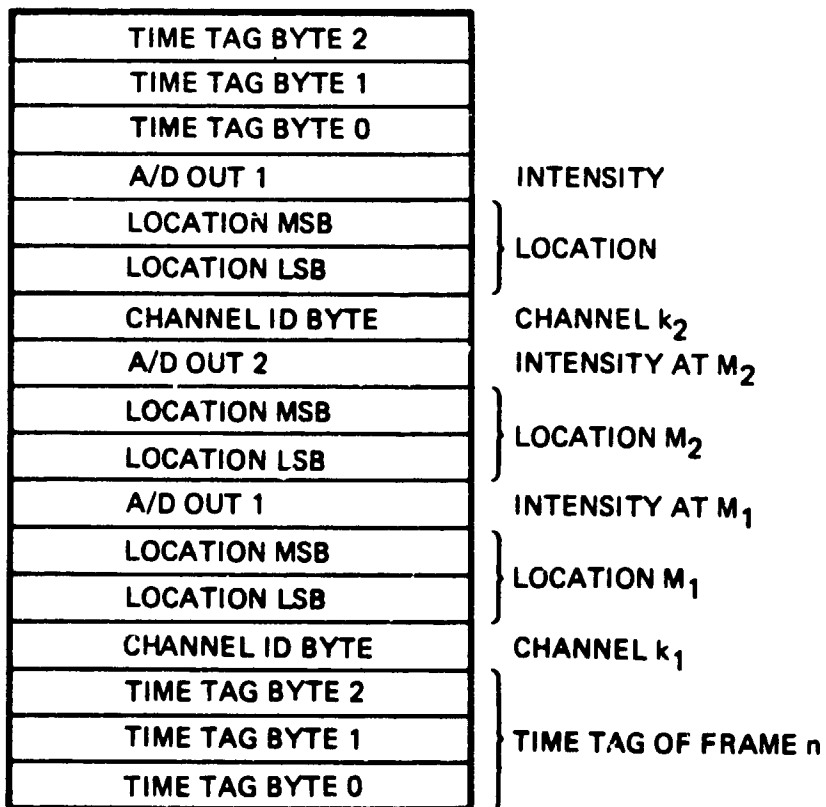


FIGURE 4.22 DATA FORMATTER MEMORY STORAGE FORMAT

The resolution of the time tag will be equivalent to the frame rate, which is 4 msec as indicated in the requirement section. The time tag for a 12 hour counter at 4 msec resolution will be equivalent to 10.8×10^6 counts or 24 bits. The DAF is interfacing with the down-link telemetry. At some time interval the DAF will perform a data dump to the telemetry link, and the cycle will repeat as commanded. During a high lightning occurrence interval, the data dump will speed up to avoid overflowing the DAF memory. The byte counter will perform this function by signaling the downlink interface when the DAF memory is filling up to a threshold level prior to the programmed data dump time.

The total capacity of the DAF memory will depend on the data dump rate and the lightning occurrence rate. However, since the occurrence rate is low the memory is not required to be a high speed device. Consequently, it is possible to use CMOS type RAM to conserve power.

4.4.3.4 Power Control

The power control circuit converts the bus raw power to secondary power sources for the electronics. Due to the low power allocation it is necessary to maximize the efficiency of the power control circuit. Commercial DC-DC converters qualified for flight generally have low efficiency (50 percent to 65 percent). Past experience with flight systems similar to LITMAP indicates that it is possible to design converters with more than 85 percent efficiency and will also provide fusing and transient protection for proper operation of the system.

4.4.4 Alternate Design Approaches

There are various design approaches based on the proposed

(+)

system described earlier that can offer some power and size advantages. These approaches, however, will require further study and analysis when more detailed and specific system requirements are specified. The following paragraphs summarize these approaches:

1. The effective data rate bandwidth and power requirement of the post-subtraction processing circuitry can be reduced by sharing their work load among themselves. All the outputs from the subtraction amplifiers can be fed into a multiplexing circuitry with proper sample and hold function and routed to several post-subtraction processing circuits. This approach will allow the reduction of the number of post-subtraction circuits as well as reducing their effective bandwidth requirement. This approach is feasible due to the low lightning occurrence rate. The trade-off is in the complexity of the multiplexing circuitry, the timing control and the location identification method.
2. A variation and subset of the above method is in multiplexing after the logarithmic compression to reduce the number of A/D converters. This method will allow the use of an A/D converter with higher resolution. This approach tends to increase resolution at the expense of reducing data rate handling capability. However, at low data rate this approach seems to offer advantages in lower part counts and size without compromising capability.
3. The background averaging technique can be treated as an option to provide improved system SNR and performance. There are alternate methods of arranging the various functional blocks to reduce part count and consequently reducing the power.
4. Methods to reduce average power consumption of the system can be implemented by operating the system during severe thunderstorm weather, or selected seasons and hours of the day only. The system can then be commanded to a power-off or standby mode during the quiescent and idling period.

4.4.5 Other Design Considerations

There are other design considerations for the LITMAP system in addition to the approach and the hardware realization discussed above.

4.4.5.1 Product Design

The packaging of this system is important in providing a

sound mechanical support and thermal as well as radiation protection. TRW has wide experience in designing flight systems operating under similar stringent requirements and as such the design approach will be given the most careful consideration.

4.4.5.2 Spacecraft Interface

The LITMAP system as a payload will be interfacing with the various capabilities of the bus. The interface design and system management will be an important design and development task. Detailed implementation and design will be carried out when specific design requirements are established.

4.5 RADIATION EFFECTS IN SILICON DEVICES

4.5.1 General

The synchronous orbit radiation environment can produce a number of effects/defects within silicon based components which can broadly be grouped into two categories:

<u>CATEGORY</u>	<u>PRIMARY EFFECT</u>	<u>SOURCE</u>	<u>RESULT</u>
soft	electronic ionization	e, p, gamma	free electrons
hard	atomic collision	fast neutrons	displaced atoms

References such as Chapter 6 of Barbe (1980), discuss these effects. Some brief comments can be made as follows.

4.5.2 Soft Damage

The soft damage is often transitory, but under certain conditions can result in a cumulative effect, e.g., trapped charge accumulation at a dielectric interface. Positive bias and surface devices are most susceptible to this trapped charge effect. Designs using negative bias and buried channels help minimize this effect. Gamma rays and a few MeV electrons can also sometimes cause hard damage referred to as point defects. The point defects usually are very limited in extent and are not of a major concern.

4.5.3 Transient Effects

A transient effect that must be considered is that of a soft event producing enough free charge within a given pixel which is accumulated and interpreted as a lightning event. A radiation dose γ at which the CCD pixel well will become saturated can be estimated by

$$\gamma = N_{FW}/g_{\gamma}(L + W)A$$

where

- N_{FW} = full well capacity in number of electrons
- g = electron/hole pair (ehp) generation rate
- A = surface area of pixel accumulation site

W = depth of pixel accumulation site

L = diffusion length

For a buried channel device with $N_{FW} = 5 \times 10^5$ electrons, $L = 50 \text{ um}$, $W = 12 \text{ um}$, $A = 90 \text{ um}^2$ and $g = 4.3 \times 10^{13} \text{ ehp cm}^{-3} \text{ rad (Si)}^{-1}$, a well is predicted to saturate after a dose of 0.2 rad (Si) . There are about 10^8 seconds in a five year period. For a 10^6 rad (Si) accumulated dose, this gives about 10^{-2} rad/sec , about $4 \times 10^{-5} \text{ rad/frame}$ or about $6 \times 10^{-11} \text{ rad/pixel-frame}$. Although a single alpha particle could generate 10^6 ehp or a cosmic ray event ($> 100 \text{ MeV}$) around 10^5 ehp , the event rates are so low as to be lost in the nominal background induced false alarm rate.

The CCD recovery time T_R after a transient pulse of ionizing radiation can be approximated by

$$T_R = g_{\gamma} V_{\text{coll}} / N_{FW} f_c$$

where V_{coll} is the well collection volume. For a 10^7 Hz clock rate, $T_R = 10^{-7} \text{ sec}$. Actual measurements on devices has indicated that recovery times vary from less the 0.1 milliseconds to over a second. Device design and selection (c.f., SIRTf, 1978) seems quite reasonable to hold the recovery time to below a single frame time for these soft effects.

4.5.4 Hard Damage

Hard damage is long lasting and results due to fast neutron collisions within the bulk material causing a displacement of atoms from their normal positions in the semiconductor crystal. This displacement damage leads to significant decreases in carrier concentration, carrier mobility and minority carrier lifetime. These effects become significant for greater than 10^{11} , 10^{13} , and $10^{15} \text{ neutrons/cm}^2$ respectively where about 50% of their energy goes into these "cluster (displacement) defects".

4.5.5 LITMAP Electronics Hardening Approaches

Two approaches can be taken in order to tolerate the radiation environment. One is to harden the devices so they can

withstand the exposure and the second is to shield the devices so that the effective exposure levels are dropped to a tolerable range.

Figure 4.23 (Space Systems and Technology Workshop II, 1982) shows the trapped particle dose as a function of aluminum shielding thickness with synchronous orbit solar particles contributing an additional few thousand rads. CMOS microprocessors, which are currently planned for future missions are able to withstand up to approximately 10^5 rads. Local shielding of 150 mils of aluminum will reduce the exposure to below this level, hence permitting 5-10 year missions.

Currently available unhardened CCD's with high sensitivity and low noise are available which can perform up to about 10^4 rads radiation exposure. Localized shielding of 300 mils of aluminum will reduce the expected dose to below this level. This will allow required performance for missions in the 5-10 year range.

TI and Hughes have been developing radiation hardened CCD structures. Presently Hughes has some multiphase, buried channel devices which perform fairly well up to 3.5×10^5 rad (Si) (Chang, 1980). The TI virtual phase devices have been tested (McGarth, 1981) and performed fairly well up to 10^6 rad (Si). If these hardened devices are available in LITMAP configurations, then the shielding requirements can be relaxed. For the synchronous equatorial orbit application, the spacecraft material plus a little shielding should provide the necessary reduction in radiation to permit five to ten year lifetimes. Hence, although the radiation environment must be considered, it does not appear to be a serious problem for the LITMAP application which does not have to survive a low, high inclination earth orbit or a thermonuclear event.

ORIGINAL PAGE IS
OF POOR QUALITY

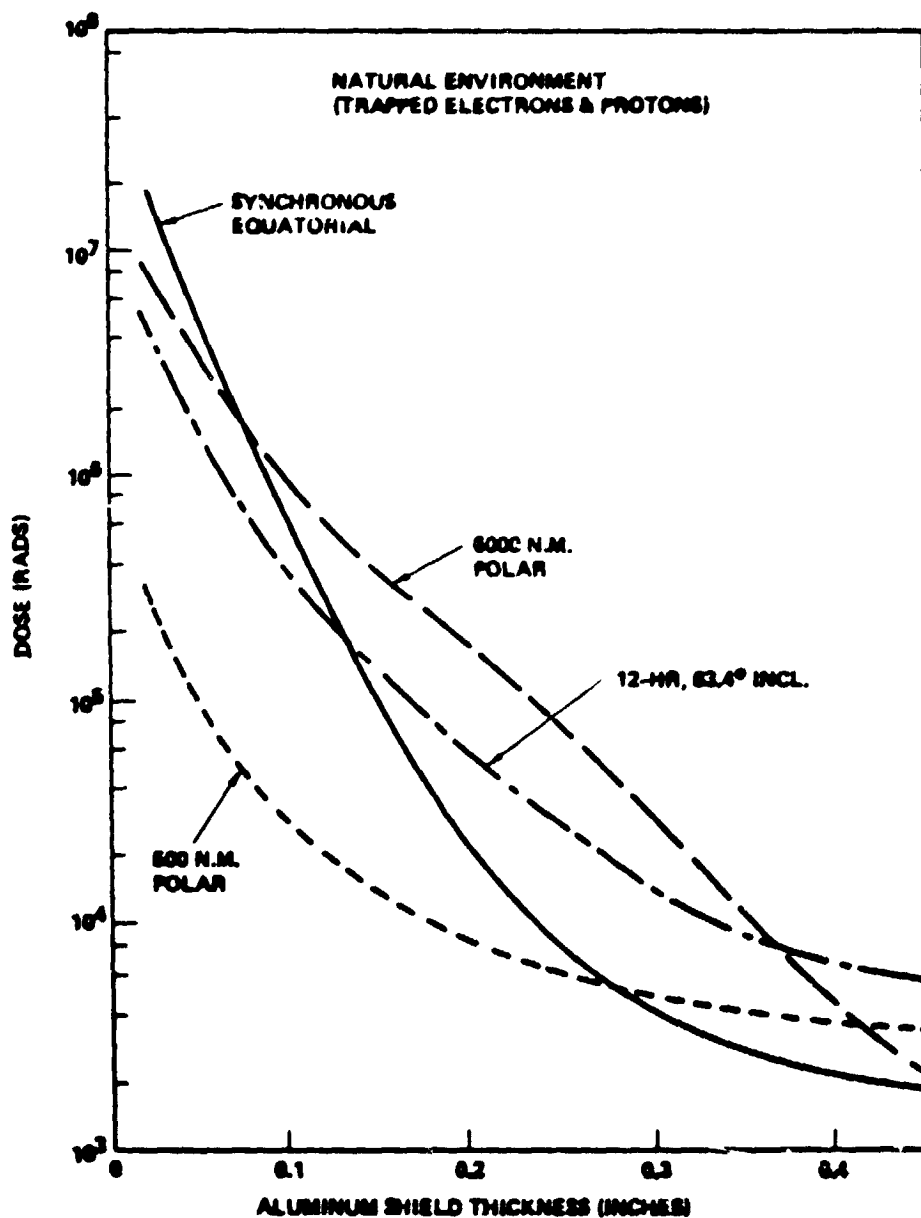


FIGURE 4.23 RADIATION DOSE VERSUS SHIELDING THICKNESS

5.0 IMAGING CHARGE-COUPLED DEVICE TECHNOLOGY ASSESSMENT

In considering suitable types of imaging charge-coupled devices for the Lightning Mapper application, discussions were held with domestic manufacturers to determine the applicability of currently available devices and also to determine the possibility of developing custom devices which would be optimized for this application.

Discussions were held with the following representatives of the manufacturers listed:

- a) Dr. Dean Collins, Texan Instruments, Central Research Laboratory
- b) Dr. E. D. Savoy, RCA Electro Optics and Devices Solid State Division.
- c) Dr. Garry W. Hughes, RCA David Sarnoff Research Laboratories
- d) Dr. David A. Robinson, Hughes Aircraft Co., Industrial Electronics Group Technology Center.
- e) Dr. Rudolph Dyck, Fairchild CCD Imaging

5.1 CCD REQUIREMENTS

The primary requirements of the CCD focal plane array for the Lightning Mapper sensor application are:

- a) Large format, to obtain wide angular coverage with high spatial resolution.
- b) Frame transfer configuration, to enable rapid transfer of induced electron charge from the imaging area of the CCD and thus almost continuous integration of radiation from the observed scene.
- c) High quantum efficiency in the near-infrared range of the spectrum, to permit observation of energy in either the 777 nm O₂ band or the 868 nm N₂ band.
- d) A high frame rate, in the order of 3 to 5 msec, to permit an optical time history of the lightning flashes to be obtained.
- e) Partitioning of the CCD to use multiple parallel output ports and preamplifiers to enable rapid readout of the on-chip storage section and high frame rate.
- f) A large pixel size, with large full well (electron

charge) capacity, permitting use of a large optical system for a given angular subtense of the pixel. The combination of the large optic and high full well capacity results in a high S/N ratio.

5.2 SENSOR CONCEPTS

As previously discussed in Section 4.3, the CCD focal plane array and sensor concepts which have been developed in this study consist of the following (Figure 5-1):

a) Two Large Format CCD'S

Two large format (800 X 800) pixel imaging CCD's modified to provide on-chip frame storage and multiple output ports and preamplifiers to enable fast (parallel) readout and thus a very high frame rate.

b) Four CCD's with One or Four Optics

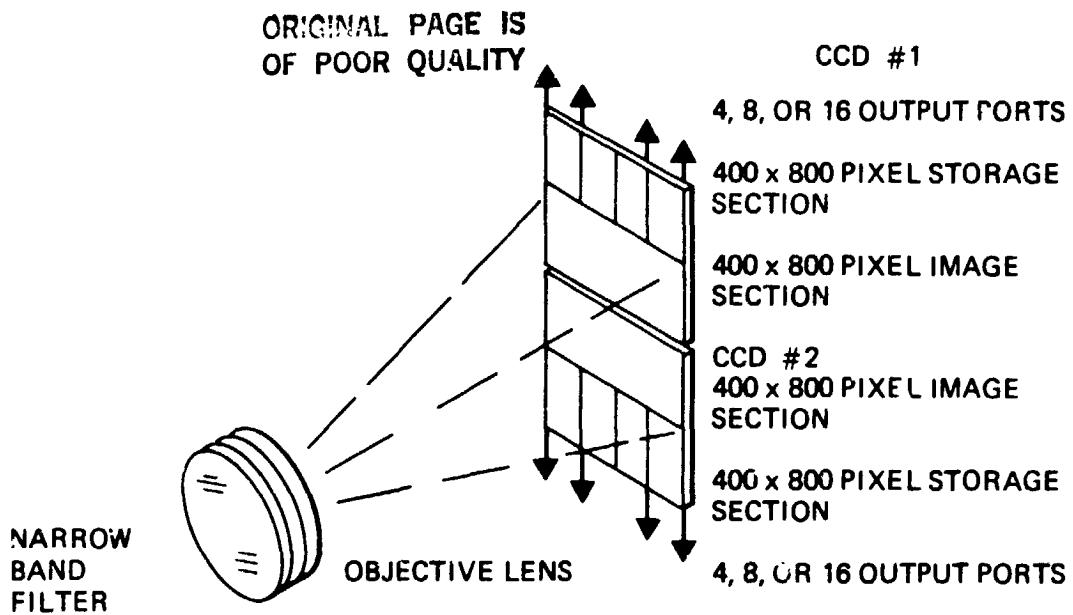
Four individual CCD's modified by partitioning to obtain multiple output ports and high frame rate. The optical fields of view might be combined by optical beam splitting, or individual optical systems could be used for each of the four CCD's. The former approach is difficult to accomplish using an optic with a low f-number and presents problems in design of the narrow-band spectral filters due to wide field of view of the 4-chip array. The latter approach eliminates optical beam splitting and results in a reasonable angular field of view for the narrow-band spectral filters.

c) Four CCD's with Intermittent Integration Sampling

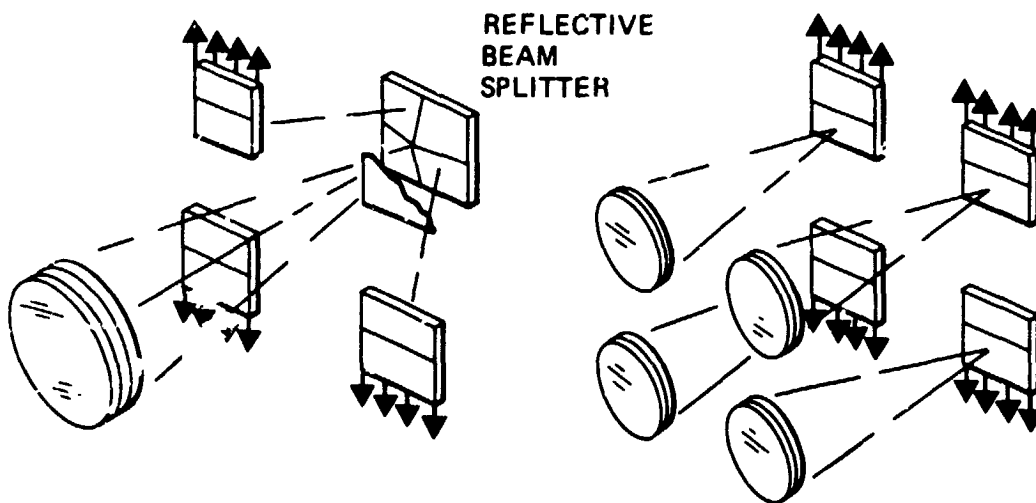
Four RCA frame transfer imaging CCD's, in either of two sensor configurations as discussed in b) (above), in which intermittent sampling of the incident optical radiation would be accomplished by the use of a short integration interval in conjunction with a longer readout time of the on-chip storage section. The short exposure time would be obtained by dumping most of the induced charge in the image section into a guard ring structure above the image section of the CCD, and using the remainder of the normal exposure interval for integration in the conventional manner. Thus, with operation at a frame rate of 60 Hz, a useable integration time of 4 msec out of the normal 17 msec integration time could be obtained.

d) One or Two Small CCD's With Small FOV

One or two CCD's with a single optical system covering only a small field of view. Here currently available CCD's would be used, but only very limited areal coverage would be obtained with a mechanical storm tracking mode being appropriate.

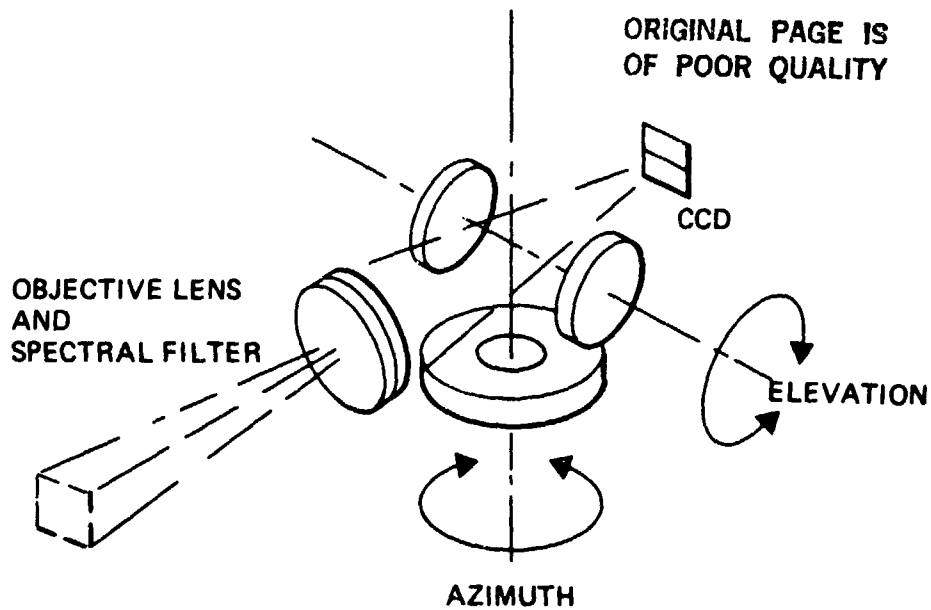


A) TWO LARGE FORMAT CCD'S



B) FOUR CCD'S WITH EITHER A COMMON OPTICAL SYSTEM AND SPECTRAL FILTER OR INDIVIDUAL OPTICS AND SPECTRAL FILTERS

C) SAME AS B) BUT WITH SHORT EXPOSURE TIME OF CCD



D) ONE SMALL CCD WITH A NARROW FIELD OF VIEW
GIMBALLED ON TWO AXES

FIGURE 5.1 SENSOR CONCEPTS

5.3 CURRENTLY AVAILABLE CHARGE-COUPLED DEVICES

Table 5.1 lists the characteristics of currently available imaging CCD's which can be considered for the Lightning Mapper application. These are indicative of the technological capability of the manufacturers listed in terms of CCD configuration and performance. Some of the devices can be directly applied to the LITMAP application, while others would require modification. Each device in Table 5.1 will be briefly discussed.

The largest format in a single CCD is that of the 800 X 800 pixel device from Texas Instruments. The device is in a line transfer configuration, and modification to a frame transfer configuration with multiple readout ports would be required. TI is also developing a 1024 X 1024 device for NASA, but this is still in the early developmental stage. A disadvantage of this

TABLE 5.1 Summary - Characteristics of Available Imaging CCD's

MANUFACTURER	TEXAS INSTRUMENTS	TEXAS INSTRUMENTS	TEXAS INSTRUMENTS	RCA	HUGHES AIRCRAFT	WESTINGHOUSE	FAIRCHILD
IDENTIFICATION	PROJECT GALILEO CCD	TC 201	TC 202	SID 501D	H 4068	5040	22.1
STATUS	IN PRODUCTION	IN PRODUCTION	IN PRODUCTION	IN PRODUCTION	DEVELOPED FOR USAF	DEVELOPED FOR NASA	IN PRODUCTION
PRIMARY APPLICATION	PLANETARY IMAGERY	TV (U.S. STD.)	TV (EUROPEAN)	SCIENTIFIC (ASTRONOMY)	STAR TRACKERS	GENERAL	CCTV
PHYSICAL CHARACTERISTICS	AREA IMAGER VIRTUAL PHASE LINE TRANSFER	AREA IMAGER VIRTUAL PHASE FRAME TRANSFER	AREA IMAGER VIRTUAL PHASE FRAME TRANSFER	AREA IMAGER 3-PHASE FRAME TRANSFER	AREA IMAGER 4-PHASE LINE TRANSFER	AREA IMAGER 4-PHASE FRAME TRANSFER	AREA IMAGFP 2-PHASE LINE TRANSFER
NUMBER OF PIXELS	800 X 800	328 X 245 X 2	390 X 292 X 2	320 X 256 X 2	324 X 324	100 X 100 X 2	488 X 380
PIXEL SIZE	15.2 X 15.2 μm	24.2 X 24.4 μm	22.4 X 22.4 μm	30 X 30 μm	25.4 X 25.4 μm	20 X 20 μm	12 X 18 μm
ACTIVE IMAGING AREA	+	+	+	+	+	+	+
ILLUMINATION	1.48 cm ²	0.48 cm ²	0.57 cm ²	1.47 cm ²	0.60 cm ²	0.08 cm ²	0.40 cm ²
NO. OF CLOCK PHASES	1	1	1	3	4	4	2
BLOOMING CONTROL	NO	NO	YES	NO	NO	NO	YES
PERFORMANCE CHARACTERISTICS							
QUANTUM EFFICIENCY	0.24 AT 777 mμ	0.40 AT 777 mμ	0.30 AT 777 mμ	0.47 AT 777 mμ	0.25 AT 777 mμ	0.50 AT 777 mμ	0.15 AT 777 mμ
OPERATING TEMPERATURE	0.13 AT 868 mμ	0.20 AT 868 mμ	0.20 AT 868 mμ	0.28 AT 868 mμ	0.16 AT 868 mμ	0.55 AT 868 mμ	0.13 AT 868 mμ
NOISE LEVEL	-70 C°	+25 C°	+25 C°	-40 C°	-40 C°	-25 C°	+25 C°
READOUT RATE	18 E RMS	150 E RMS	150 E RMS	50 E RMS	125 E RMS	75 E RMS	370 E RMS
FULL WELL CAPACITY	50 KHZ	6.3 MHZ	7.5 MHZ	50 KHZ	750 KHZ	300 KHZ	7.2 MHZ
DYNAMIC RANGE	109 KE	700 KE	190 VE	250 KE	10 ⁶ E	450 VE	370 KE
PIXEL UNIFORMITY	5777/1	4666/1	1266/1	5000/1	8000/1	6000/1	1000/1
DARK CURRENT	IX	IX	IX	2X	TBD	2.75*	17
RADIATION HARD	0.4 m A/cm ² @ 25 C°	5 mA @ 25 C°	5 mA @ 25 C°	4 mA @ 25 C°	0.3 mA/cm ² @ -40 C°	0.15 A/cm ² @ -25 C°	NOT SPEC.
RELATIVE COST	YES	YES	YES	NO	YES	NO	NO
AVAILABILITY	HIGH	LOW	LOW	LOW	HIGH	TBD	LOW
PROCUREMENT BASIS	TBP	1 MO.	1 MO.	3 MO.	TBD	TBD	1 MO
	DEVELOPMENT CONTRACT	COMPONENT PURCHASE	COMPONENT PURCHASE	COMPONENT PURCHASE	DEVELOPMENT CONTRACT	DEVELOPMENT CONTRACT	COMPONENT PURCHASE

■ MOST SUITED FOR LITMAP APPLICATIONS. MODIFICATION REQUIRED
 ▲ DEFICIENT FOR LITMAP APPLICATION (SEE APPENDIX A, B AND SECTION 2.3)
 □ COULD BE LARGER
 ○ UPGRADE WITH NEW OUTPUT AMP WITH SMALLER CAPACITANCE FOR HIGHER SPEED/LOWER NOISE READOUT
 + SENSITIVITY
 → DYNAMIC RANGE
 → PIXEL SIZE
 → FREQUENCY
 → READOUT TIME

CCD is the small pixel size, limited by the size of a device that can be produced with reasonable yield. Yield is limited by the degree of purity (number of defects) in the silicon base material.

Two CCD's are in development by TI for use in commercial television, the TC 201 (for U.S. standards) and the TC 202 (for European standards). The primary difference is that the U.S. version does not use blooming control, eliminating the need for anti-bloom drains within the imaging format, resulting in a more contiguous imaging area (higher packing density) and increasing the effective quantum efficiency. Pixel sizes of the two devices are comparable.

The SID 501D has recently been announced by RCA, replacing the previous SID 53612. The former has an overlapping gate structure and improved preamplifier, while the latter has a planar gate structure. This device is listed primarily to indicate the current capability of RCA in this field. This device uses a thinned substrate (laminated to glass and backside illumination to obtain high quantum efficiency. This sometimes causes problems in the near-infrared range of the spectrum due to interference fringe patterns occurring in both the glass laminate and silicon which result in high fixed pattern noise. Anti-reflection coatings and adjustment of substrate thickness may help resolve these problems. For the LITMAP application, frontside illumination and thick CCD substrate maybe preferable to eliminate the problems associated with deeply penetrating infrared radiation. RCA has previously manufactured such devices for use in CCTV cameras.

The salient characteristic of the Hughes H4068 CCD is that of radiation hardness, being processed to withstand both natural and weapon-induced radiation. This device has been developed for use by TRW in star trackers used for satellite attitude control under the MADAN contract to the USAF Space Division. The limitation of this device is that of the line transfer configuration, without on-chip data storage. However, it is feasible to add on-chip frame storage to this type of device.

The Westinghouse type 4068 was developed under NASA funding in 1977. Although small in format, the device has the advantage of high quantum efficiency due to the use of SnO gates, which are very transparent in the visual range of the spectrum. This device would be applicable for the LITMAP sensor configuration where only a limited optical field of view is used.

Fairchild is well advanced in development of the CCD 222. This device is used in both commercial CCTV cameras as well as in USAF military aircraft and helicopters. Considerable Navy funding has resulted in the development of integrated CCD logic and driver modules, as well as modules for video processing, resulting in versatility in available camera configurations. The primary limitation of the CCD for the LITMAP application is the use of opaque interline frame storage registers in the image section, which block out 50% of the imaging area. However, this limitation might be overcome by the use of a faceplate consisting of a series of miniature cylindrical lenses precisely registered to the CCD imaging area, similar to the method suggested by Cross et al (1982)

5.4 DISCUSSIONS WITH MANUFACTURERS REGARDING DEVICE OPTIMIZATION

5.4.1 Texas Instruments

The present 800 X 800 Galileo Project CCD uses an amplifier which is optimized for a slow readout rate (50 KHz) with the CCD at low temperature to reduce dark current. For the LITMAP application the preamplifier would be replaced with a wideband preamplifier of the type used on the TC 201 and TC 202 devices.

Partitioning the device for parallel readout with multiple preamplifiers presents no problem. Four, 8 or as many as 16 output ports could be used. Clocking can be performed at rates as high as 17 MHz without loss of charge transfer efficiency. However the use of correlated double sampling at this high readout rate is not feasible, as both sampling and transfer pulses must occur within the pixel readout interval. Without double sampling, a noise level in the order of 125 electrons

rms/sample should be realized with a readout of 6 MHz.

TI would want to maintain the small (0.6) mil pixel size, as the large format results in a large chip (2.4 cm² including I/O provisions) and yield is limited by chip size. Some reduction in spatial resolution would be expected due to the roll-off of the modulation transfer function in the near infrared range of the spectrum due to small pixel size. This would be more critical at the 868 nm wavelength than at the 777 nm wavelength.

For a CCD of this large size the cost of a new set of photomasks is in the order to \$100K, and total program cost would be in \$1M category. The duration of a development program of this type would be 1 to 2 years, depending upon requirements.

Interest of TI management in committing resources to the program would be based upon validity as a business proposition. TI would appreciate sharing in development of the total sensor design concept, rather than just accepting procurement specifications for CCD development, as previous related experience might be of benefit to the program.

Regarding the TC 201 and TC 202 types of devices, emphasis is being placed upon initiating production for use in commercial CCTV applications. Devices are available at relatively low cost with short delivery times. For this application the TC 201 would be preferred due to higher packing factor and quantum efficiency. These devices could be used in the four-chip focal plane array configuration with operation in a frame transfer mode if somewhat lower resolution is acceptable. Total format for four CCD's would be 648 X 490 pixels. The TC 202 would provide a total format of 780 X 584 for four CCD's

5.4.2. RCA Electro Optics and Devices Solid State Division

RCA has discontinued work on all frontside illuminated CCD's at the Lancaster, Pa. facility. All devices are thinned and backside illuminated. Major products are the SID 504 for CCTV applications, with small pixels (20 x 20 um) and the SID 501 with large pixels (30 x 30 um) for scientific applications. Both

would require special attention for this application due to the use of backside illumination with a very thin (10 um) substrate which results in severe fringing when observing near-infrared radiation. However, Dr. Savoy's group is considering development of a thicker scientific CCD with a substrate thickness of 30 um. In combination with a higher resistivity material, this type of device might be more suitable for use with red or near-IR radiation.

For this operation, Dr. Savoy suggested the following type of operation for the LITMAP application. The image and storage sections and output register of RCA CCD's are surrounded by a guard ring shaped like a picture frame which can be used as a drain to absorb unwanted photoelectrons from the image section. Assuming a normal integration time of 17 msec with a 60 fps field rate, the image section could be allowed to integrate optical radiation for 13 msec. Presumably a large amount of charge would be accumulated due to solar illumination incident on the earth. This could then be rapidly clocked upward into the guard ring (drain) and absorbed. The remaining 4 msec could be processed to obtain measurements of storm activity, and the induced electron charge in the image section would be clocked into the on-chip storage section and read out slowly in the usual frame processing manner. This method of operation would permit use of an on-the-shelf device in early feasibility tests of the LITMAP sensor.

In regard to accepting custom work in CCD development, Dr. Savoy stated that management at RCA is placing extreme emphasis on getting the SID 501 and SID 504 devices into production, and that the Lancaster facility could not accept custom work for the foreseeable future. This situation would probably change in a year or two.

5.4.3 RCA David Sarnoff Research Laboratories

Dr. Gary W. Hughes was quite familiar with the requirements for the LITMAP sensor, having previously worked with Dr. Wolfe of the University of Arizona on this application.

He agreed with the concept of using frame transfer CCD's

with multiple output ports. The parallel transfer rate (from image to storage sections) is limited to a maximum of 800 KHz by CCD capacitance and driver capacity. Output noise would be in the order of 200 electrons rms without correlated double sampling and 35 to 40 electrons rms with double sampling at a readout rate of 7.5 MHz. It may be possible to use double sampling at readout rates as high as 10 MHz.

He has been involved in the design and development of the SID 501 and 504 devices, currently in initial production at RCA Lancaster. These devices are representative of the largest format which has been developed by RCA.

If RCA were involved in development of a device for the LITMAP application, design would be performed at the research laboratories and fabrication would be accomplished at the Lancaster facility.

A rough order of magnitude estimate of cost of a development program of this type would be \$700K to \$1M, with schedule in the order of one year. Interest of RCA in bidding on a CCD development program would be based upon business potential.

5.4.4 Hughes Aircraft Co., Industrial Electronics Technology Center

Hughes Aircraft Co. has been involved in the development of radiation hard CCD's since 1975 under contract to NRL, DNA, and the Special Projects Office of the Navy. To date imaging CCD's have been developed for both the Navy and TRW (under the USAF MADAN project) with formats of 324 x 324 pixels in a line transfer configuration.

Hughes proposes development of a device with a 400 x 800 pixel format, with half of the area being used for on-chip frame storage. The storage section would have eight output ports, each operating at a rate of 5 MHz, resulting in a frame time of 4 msec. At this readout rate the noise level would be no larger than 500 electrons rms. As with the MADAN devices, the full well capacity would be at least 10^6 electrons. Pixel size would be 20 x 20 micrometers and quantum efficiency at 868 nm would be 30

percent or higher.

A budgetary and planning cost estimate was submitted by Hughes to TRW for development of both imaging CCD's and breadboard electronics.

5.4.5 Westinghouse Advanced Technology Laboratory

Westinghouse is currently under subcontract to TRW for development of an improved version of the 5040 imaging CCD. Details of the device are presented in Table 5.1. This device would be suitable for use in the sensor concepts described in Section 5.2 d. In conversation with Dr. James A. Hall, it was determined that Westinghouse has not developed CCD's with very large formats, although they would be interested in reviewing procurement specifications for such a program.

5.4.6 Fairchild CCD Imaging

The Fairchild 222 has a favorable frame transfer time due to its interline transfer and cylindrical lens arrays are being used to increase their detection quantum efficiency. The devices are used for a number of DoD applications. This device would be suitable for use in the sensor concepts in Section 5.2c but discussions for the development of a special device for LITMAP with multiple ports have not been made. The device is being considered for inhouse high frequency evaluation of the LITMAP frame subtraction concept.

5.5 CONCLUSIONS

Reviewing the requirements defined for the CCD in Section 5.1, we reach the following conclusions:

- a) Format Size - The largest format which has been developed to date is the 800 x 800 pixel device from Texas Instruments. However, in order to maintain a reasonable size of the chip to obtain an acceptable yield in wafer processing, the pixel size is small (0.6 x 0.6 mils). This results in the following:
 - o Small pixel size reduces the full well capacity, which due to the use of the virtual phase structure is 109,000 electrons for this device

- o For a given angular field of view for each pixel, a smaller pixel results in a shorter optical focal length and a smaller lens diameter. As less optical radiation is collected, a reduction in S/N ratio results
- o The smaller pixel size results in higher optical cross-talk when observing radiation in the near-infrared range of the spectrum. Due to the low absorption coefficient of the silicon, the near-IR photons generate carriers below the depletion region of the CCD, which migrate laterally to adjacent pixels. This results in loss of resolution which will be evident as broadening of point source images.

Thus the combination of small pixel size, low full well capacity, and increased optical cross-talk do not make a large format virtual phase CCD attractive for this application. None of the manufacturers surveyed were willing to consider development of a CCD with both a very large format and very large pixel size.

On the other hand, the TI TC 201 CCD looks attractive for this application due to large pixel size, large full well capacity, and high quantum efficiency. Format size when used in the frame storage mode is 328 x 245 pixels. This device will be applicable in a sensor configuration where multiple chips are used.

- b) Frame Transfer Configuration, Partitioning, and High Frame Rate - All of the manufacturers agreed that in order to operate in a frame transfer mode at a high frame rate, partitioning of the on-chip storage section of the CCD would be required. In the case of the 800 x 800 pixel TI CCD, partitioning into 4, 6, or as many as 16 sections with a corresponding number of output preamplifiers was suggested.
- c) Recommended Focal Plane Array Configuration - Only Texas Instruments has demonstrated the capability of producing very large CCD's (800 x 800 pixels). However, these have disadvantages as discussed in item (a) above. TI, RCA, and Fairchild have demonstrated the capability of producing devices with a format in the order of 250 x 300 to 400 x 500 pixels, with pixel sizes ranging from 12 x 18 to 30 x 30 micrometers. A practical approach to the focal plane array for the LITMAP sensor would be to use a mosaic of chips of this type with either a common or independent optical system.

6. REFERENCES

McGrath, R.D., J. L. Harris, M. M. Blouke, B. W. Keenan, H. H. Hosack
Final Technical Report for Draper Radiation Tolerance Imager Development,
CN N00030-79-C-0036 (for Charles Stark Draper Laboratory, Inc.),
Texas Instruments Incorporated, Central Research Laboratories, Dallas,
Texas, September 1981.

SIRTF, 1978: Shuttle Infrared Telescope Facility, Appendix A. Focal
Plane Instruments and Requirements Science Team, Ames Research Center,
April 1, 1978.

Chang, C.P.: CCD Radiation Hardening, CN N00173-78-C-0185 (for NRL).
Hughes Aircraft Company, Newport Beach, CA.

Barbe, D. F., Editor: Charge Coupled Devices (article by J. M.
Killiany), Springer-Verlag, New York, 1980.

Cross, E. F. et al: Optical Techniques for Increasing Fill Factor
of Mosaic Arrays, SPIE Proceedings, Vol 366, Modern Utilization of
Infrared Technology VIII, August 1982, pp 10-18.

A. PARAMETER SPECIFICATION

A.1 INTRODUCTION

This appendix contains some details and rationale for selecting the parameters for the baseline concept. The system analysis as summarized in Section 3 and Appendix B involved performing parametric trades about these baseline specifications. A summary of the results of this appendix is given in Section 2.

A.2 FIELD OF VIEW: FOV

One of the first parameters to be established is the field of view (FOV). Full disc (FD) and continental United States (CONUS) are given in Table 2.1 as design goals with emphasis being placed on FD. Geosynchronous orbit has also been specified in the SOW. From this vantage point (approximately 5.56 earth radii altitude) the absolute viewed disc will be less than the full earth diameter. This geometric viewing coverage is further restricted by the increasingly oblique line of sight (LOS) angle at the outer edges of the viewed region which is due primarily to the earth's curvature. These factors will now be quantified.

The earth latitude (θ), associated sensor viewing angle (ϕ) and distances in a projection plane ($\tan =$ tangent at the equator) are summarized in Figure A.1 with representative numerical values given in Table A.1.

For equal sensor pixel size over the full area, the incremental observation angle $\Delta\phi$, is constant. As ϕ increases the surface distance (S) (hence area) increases rapidly as illustrated in Figure A.2A. This normalized increase is illustrated in Figure A.3. For constant longitude, originating at the sub-satellite point, the area observed by a pixel will vary approximately linearly with the incremented change in the distance along the earth's surface, ΔS . Along a diagonal, both longitude and latitude are changing and the area increases in worse case as approximately ΔS^2 . This latter change is represented by the DA/DA_0 curve in Figure A.3. The relationship between ϕ and θ is shown in Figure A.4 which also

ORIGINAL IMAGE IS
OF POOR QUALITY

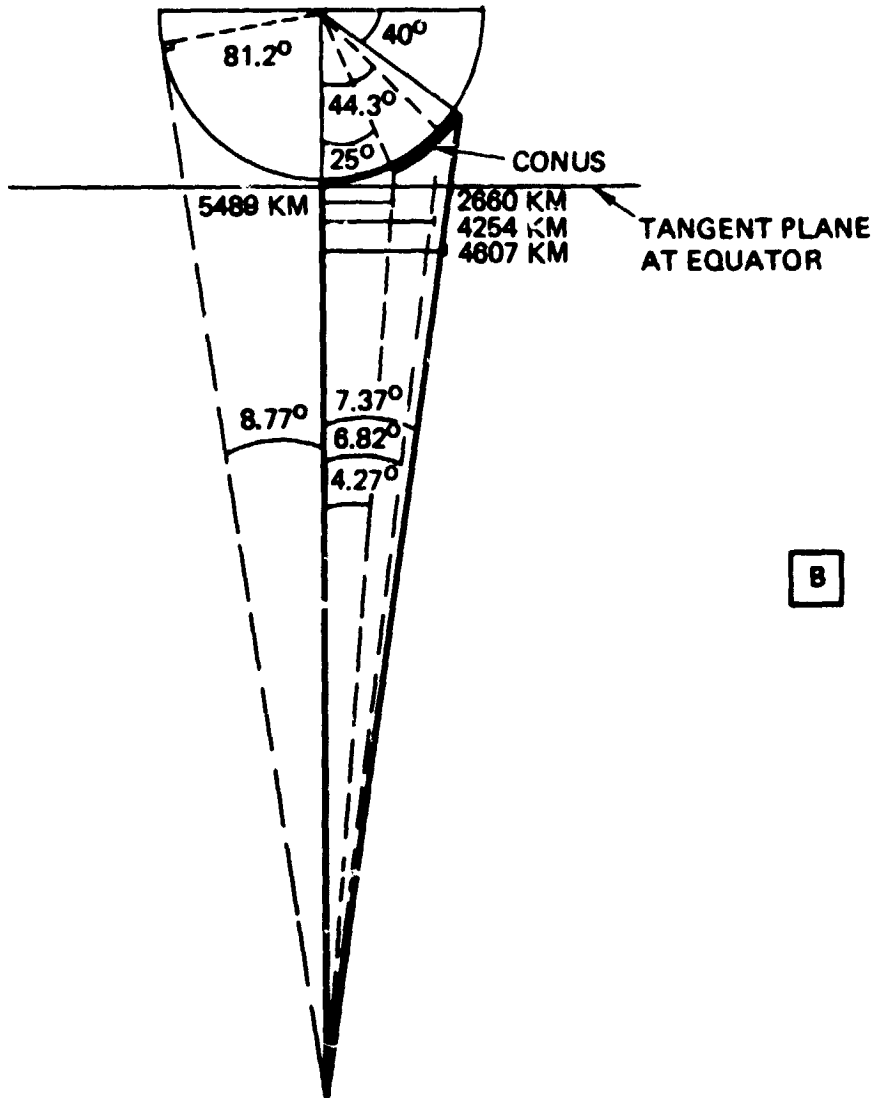
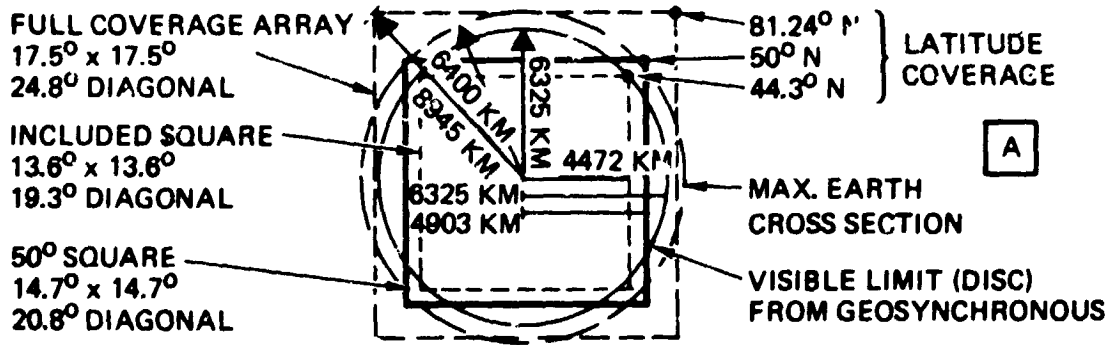


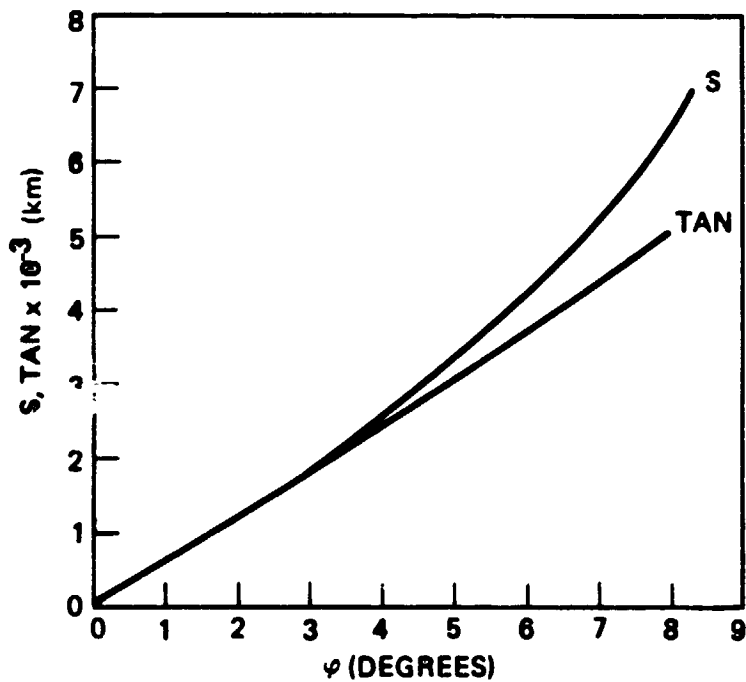
FIGURE A.1 Key Geometric Dimensions for a Geosynchronous Observation Vantage Point (B) and Geometric Overlay of Sensor Array onto Earth's Cross-section (A).

ORIGINAL PAGE IS
OF POOR QUALITY

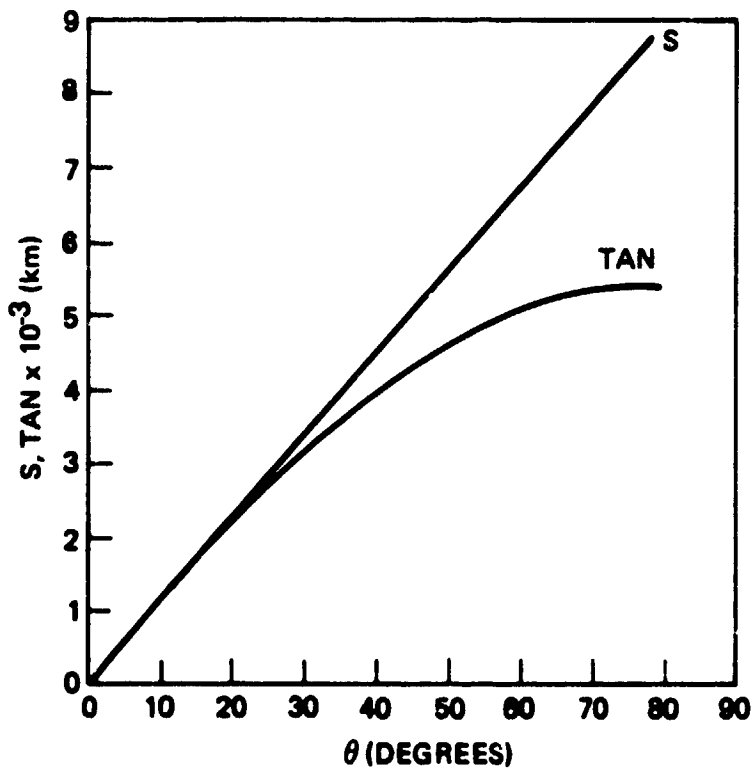
TABLE A.1 Observation Parameters from Geosynchronous Orbit

J	S (KM)	DL (KM)	(DEG)	Θ (RAD)	Y (KM)	Z (KM)	Φ (DEG)	(RAD)	TAN (KM)	DR	AR
0	12	12.1	.1	1.9E-01	12	6400	0	3.4E-04	12	1	1
10	115	12.1	1	.0179	115	6396	.2	3.22E-03	115	1	1
20	217	12.1	1.9	.0339	217	6396	.3	6.1E-03	217	1.001	1.001
30	320	12.1	2.9	.05	320	6392	.5	8.98E-03	320	1.002	1.003
40	423	12.1	3.8	.066	422	6386	.7	.01186	422	1.003	1.006
50	525	12.1	4.7	.0821	525	6378	.8	.01473	525	1.004	1.009
60	629	12.2	5.6	.0982	628	6369	1	.01761	627	1.006	1.017
70	732	12.2	6.6	.1144	730	6358	1.2	.02049	730	1.009	1.018
80	836	12.2	7.5	.1306	833	6346	1.3	.02337	832	1.011	1.023
90	940	12.3	8.4	.1469	937	6331	1.5	.02625	935	1.015	1.029
100	1044	12.3	9.3	.1632	1040	6315	1.7	.02913	1037	1.018	1.036
110	1149	12.4	10.3	.1796	1143	6297	1.8	.03201	1140	1.022	1.044
120	1255	12.4	11.2	.1961	1247	6277	2	.03489	1242	1.026	1.053
130	1361	12.5	12.2	.2126	1350	6256	2.2	.03776	1347	1.031	1.063
140	1467	12.5	13.1	.2293	1454	6233	2.3	.04064	1443	1.036	1.074
150	1575	12.6	14.1	.246	1559	6207	2.5	.04352	1550	1.042	1.086
160	1683	12.7	15.1	.2629	1663	6180	2.7	.0464	1653	1.048	1.099
170	1791	12.8	16	.2799	1768	6151	2.8	.04928	1756	1.055	1.113
180	1901	12.8	17	.297	1873	6120	3	.05216	1858	1.062	1.127
190	2011	12.9	18	.3143	1979	6087	3.2	.05504	1961	1.07	1.143
200	2123	13	19	.3317	2084	6051	3.3	.05791	2064	1.079	1.16
210	2236	13.1	20	.3493	2190	6014	3.5	.06079	2157	1.088	1.18
220	2349	13.3	21	.3671	2297	5974	3.6	.06367	2270	1.095	1.205
230	2464	13.4	22.1	.385	2404	5931	3.8	.06655	2373	1.108	1.228
240	2581	13.5	23.1	.4032	2511	5887	4	.06943	2476	1.12	1.25
250	2698	13.7	24.2	.4216	2619	5840	4.1	.0723	2579	1.132	1.281
260	2818	13.8	25.2	.4403	2727	5790	4.3	.07518	2682	1.145	1.311
270	2939	14	26.3	.4592	2836	5737	4.5	.07806	2785	1.159	1.344
280	3061	14.2	27.4	.4783	2946	5682	4.6	.08094	2888	1.175	1.38
290	3186	14.4	28.5	.4978	3056	5625	4.8	.08381	2991	1.191	1.419
300	3313	14.6	29.7	.5176	3167	5562	5	.08669	3094	1.209	1.462
310	3442	14.9	30.8	.5378	3278	5497	5.1	.08957	3197	1.229	1.51
320	3573	15.1	32	.5584	3391	5426	5.3	.09245	330	1.25	1.562
330	3708	15.4	33.2	.5793	3504	5356	5.5	.09532	3404	1.273	1.62
340	3845	15.7	34.4	.6007	3616	5279	5.6	.0982	3507	1.298	1.685
350	3985	16	35.7	.6227	3733	5199	5.8	.10108	3611	1.326	1.757
360	4129	16.4	37	.6451	3848	5114	6	.10396	3714	1.356	1.838
370	4277	16.8	38.3	.6682	3965	5024	6.1	.10683	3818	1.389	1.93
380	4429	17.2	39.6	.692	4084	4928	6.3	.10971	3921	1.426	2.034
390	4585	17.7	41	.7165	4203	4826	6.5	.11259	4025	1.468	2.154
400	4747	18.3	42.5	.7418	4324	4719	6.6	.11546	4129	1.514	2.292
410	4915	18.9	44	.768	4446	4603	6.8	.11834	4233	1.567	2.454
420	5090	19.7	45.6	.7954	4570	4480	6.9	.12121	4336	1.627	2.646
430	5273	20.5	47.2	.8239	4696	4348	7.1	.12409	4440	1.696	2.876
440	5465	21.3	48.9	.8539	4825	4205	7.3	.12696	4544	1.777	3.157
450	5667	22.6	50.7	.8853	4955	4050	7.4	.12984	4648	1.873	3.509
460	5883	24.1	52.7	.918	5089	3881	7.6	.13271	4753	1.99	3.96
470	6115	25.8	54.7	.9534	5226	3695	7.8	.13557	4857	2.133	4.56
480	6366	28.1	57	.9947	5367	3486	7.9	.13844	4961	2.323	5.396
490	6645	31.1	59.5	1.0382	5514	3250	8.1	.14134	5065	2.577	6.64
500	6961	35.6	62.3	1.0876	5667	2973	8.3	.14421	5170	2.947	8.685
510	7336	43	65.7	1.1442	5832	2636	8.4	.14708	5274	3.56	12.675
520	7823	59	70	1.2224	6015	2185	8.6	.14995	5379	4.886	23.864
530	8779	92.6	78.6	1.3717	6274	1266	8.8	.15281	5483	15.938	234.021

ORIGINAL PAGE IS
OF POOR QUALITY

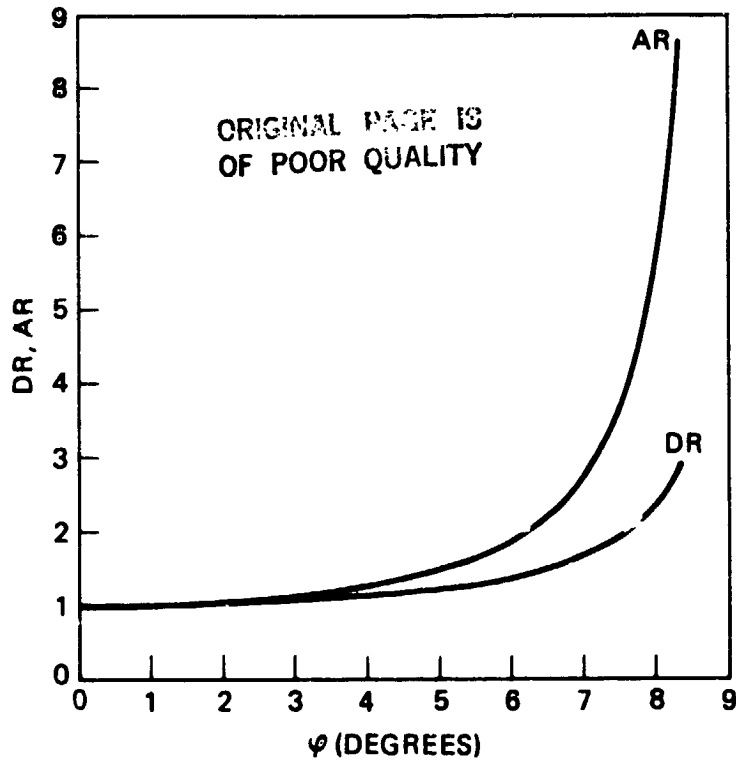


A

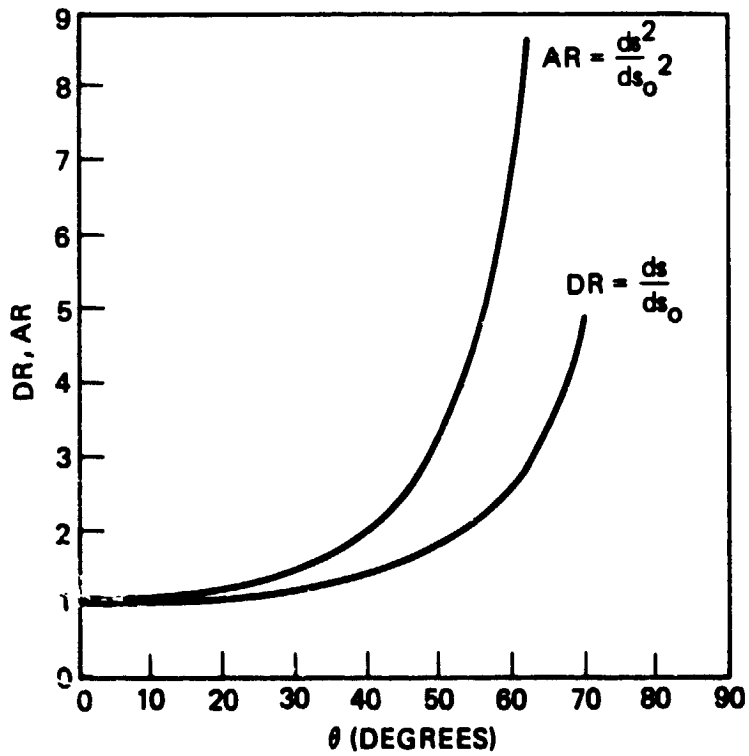


B

FIGURE A.2 Distance Along Earth's Surface as Function of Sensor Observation Angle (A) and Earth's Latitude (B).



A



B

FIGURE A.3 Linear and Area Variations (for equal steps) Normalized to the Respective Dimension at the Subsatellite Point Relative to Sensor Observation Angle (A) and Earth's Latitude (B).

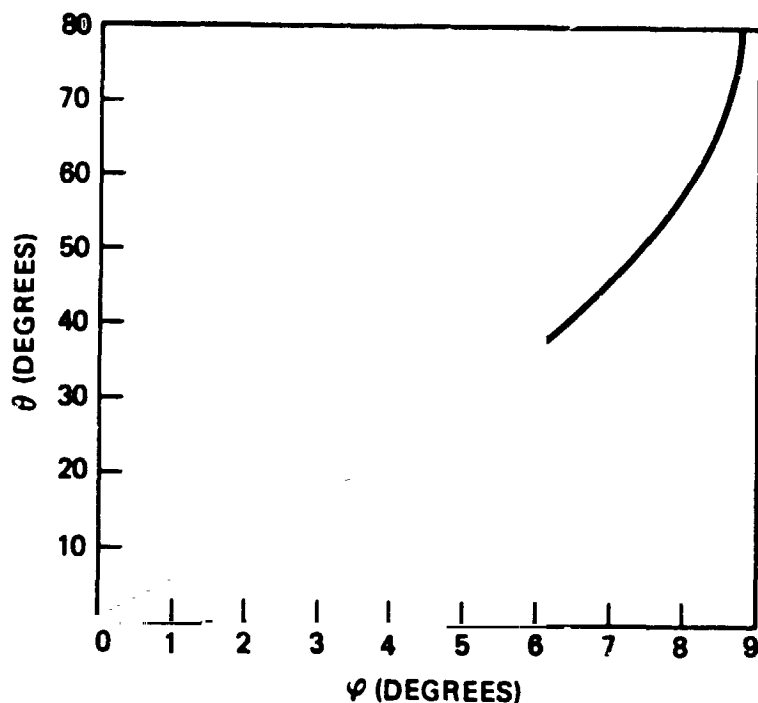


FIGURE A.4 Variation of Earth's Latitude (fixed longitude) with Observation Angle.

illustrates the rapid increase in earth's latitude as the observation angle increases.

The selection of the full FOV limits must be based on several factors which include such consideration as: desired surface coverage, SNR degradation and circular earth cross-section vs square sensor array. As seen in Figure A.1A, if the full disc is covered, a latitude coverage to approximately 81 degrees can be provided. For a nominal square sensor array, this choice would result in a significant number of pixels which will extend beyond the earth's surface, hence not contributing to the primary objective of lightning detection. Although circular arrays may not be out of the question, they would require complete new design with special processing circuits. Since, as seen in Figure A.3B, the high latitude areas will have rapid SNR degradation due to the observed area increase coupled with finite source size, a smaller FOV coverage would be a more practical choice.

If a square inscribed within the full disc is chosen, the coverage would be limited to about 44 N (the east-west can always be covered by an increase in number of satellites). This excludes a portion of the CONUS. Figure A.3B shows that the constant longitude linear dimension (hence area in this case) increases by a factor of 2 at about 52 degrees. The upper limit of the CONUS is at about 49°N. The selection of 50°N would be a reasonable compromise among the various factors mentioned previously.

FOV Selected : (half angle) -- 7.37° (50°N latitude)

A.3 AREA PER PIXEL: A_B

From Table 2.1 a nominal ground resolution goal of 5km is specified which for a 50°N FOV would result in a linear pixel count, N, of about $N = S/\Delta S_N = 5770\text{km} / 5\text{km} = 1,114$. The full disc FOV would require an array with twice this dimension of 2228 X 2228. As shown in the technology assessment section, single, double or quad arrays satisfying this criteria do not exist at this time.

Special sensor developments for DoD applications are directed at the 1250 square array category, some of which may be amenable to LITMAP requirements (submicron wavelengths). These (e.g., RCA PtSi and Pd₂Si technology) show promise (due to restricted image spreading) for future generations of LITMAP (post 1990).

Within the present technology, the most practical single array size would be a 400 X 400 (maybe 500 X 400) active sensor array with matching on chip frame storage. Chips with 390 X 292 active region with frame storage and moderate pixel size do exist which would require only the addition of parallel output ports to handle the LITMAP framing time.

Based on the technology assessment (see Section 5), a square arrangement of four 400 X 400 units was selected for the system trades. The average resolution for this array size is then given by the distance/number = $S/N = 5570/400 = 13.9 \text{ km/pixel}$. Using

Figure 2.4 this nominal pixel size translates into a Δs (subsattellite resolution) of 12.2 km and 10.3 km when the nominal 13.9 km resolution element is located at the center of the upper hemispheric FOV (25°N) or at the center of CONUS (37.5°N) respectively.

N- ARRAY SIZE SELECTED: N = 400 (North) plus frame storage

	Sub-Satellite	Central CONUS	50° due north Sub Satellite Point
Scaling	1.00	1.35	1.82
Resolution Selected (km)	11	14.9	20
$A_b = \text{Area/pixel (km}^2\text{)}$	121	163	220

A.4 SOURCE CHARACTERISTICS

The key source properties in the SNR relationship are: source area, lightning pulse length, energy distribution, detection wavelength, associated energy per photon and source/pixel fill factor. Each of these will now be quantified.

A.4.1 Source Area: A_s

The source area specified in Table 2.1 is that of the source illumination filling a representative cloud cell, given as 5km radius. The ideal situation is that the source fill the full pixel, that is keep the background area A_b as small as possible without dividing an lighting event between two or more pixels. This consideration is important when defining the true statistical threshold detection capability. For larger lightning events significantly above threshold, subdivided events can be post-detection summed to give the original even energy.

Data on effective source area is very limited. One approach is to assume that the source always fills the pixel FOV, but as the FOV increases, this assumption could cause significant error in assessing a design capability. Lopex (1977) has given some data as shown in Figure A.5. Fifty percent points range from below 0.1 km to 25 km for various parts of the world with most

DISTRIBUTION OF
OF POOR QUALITY

falling in the 2 to 10 km range. For baseline systems analysis, the filled pixel condition was assumed and a parametric analysis made about this baseline. Due to pixel geometry and considering the source size, a square geometry approximation was used.

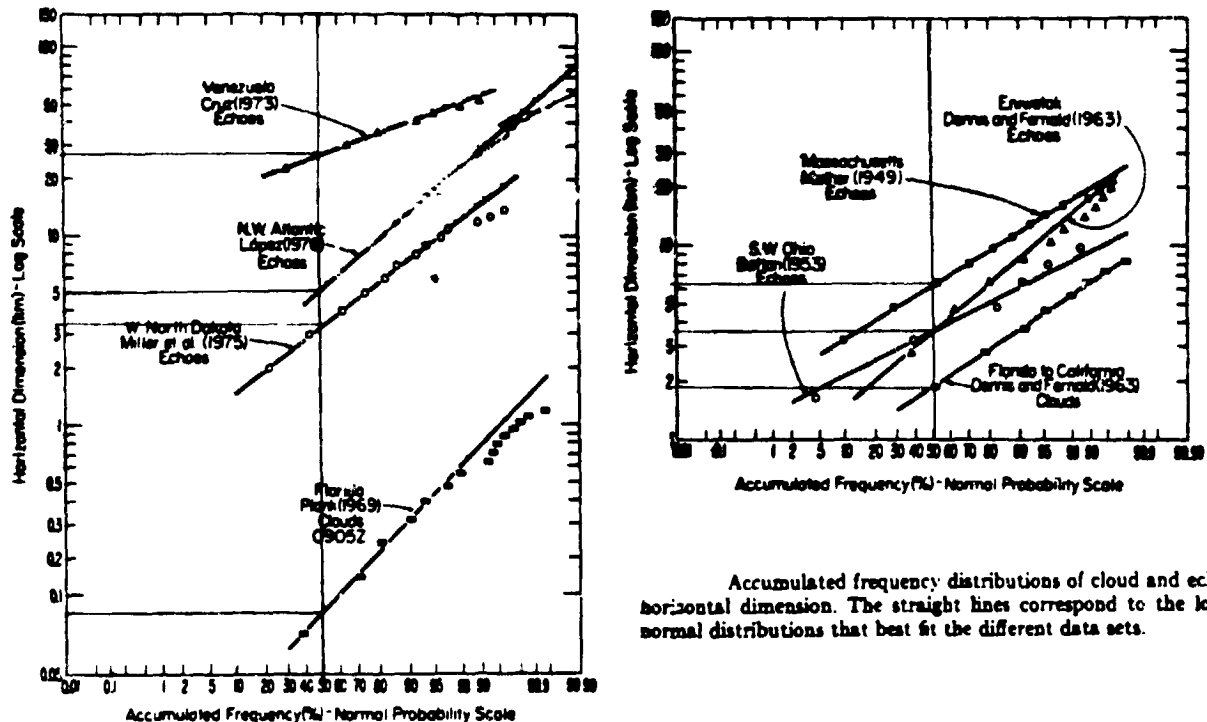
A_s = nominal source area: 121 km² at sub-satellite point

A.4.2 Geometric Splitting Factor: ν

In the ideal situation, the event is assumed to be centered on the detection pixel. In the lightning mapper application, the centroid of an event can fall randomly, anywhere with the sensing pixel area. Even if the event's area is smaller than the pixel's footprint at the source, there is still the probability that the event will straddle the boundary between two or more pixels. Streuber and Bailis (1980) has addressed this situation with the quantitative results shown in Figure A.6A. When the pixel size B is equal to the source size δ_s ($\delta_B/\delta_s = 1$ where

JULY 1977

RAUL ERLANDO LOPEZ



Accumulated frequency distributions of cloud and echo horizontal dimension. The straight lines correspond to the log-normal distributions that best fit the different data sets.

FIGURE A.5 Distribution of Horizontal Cloud Dimensions.

ORIGINAL PAGE IS
OF POOR QUALITY

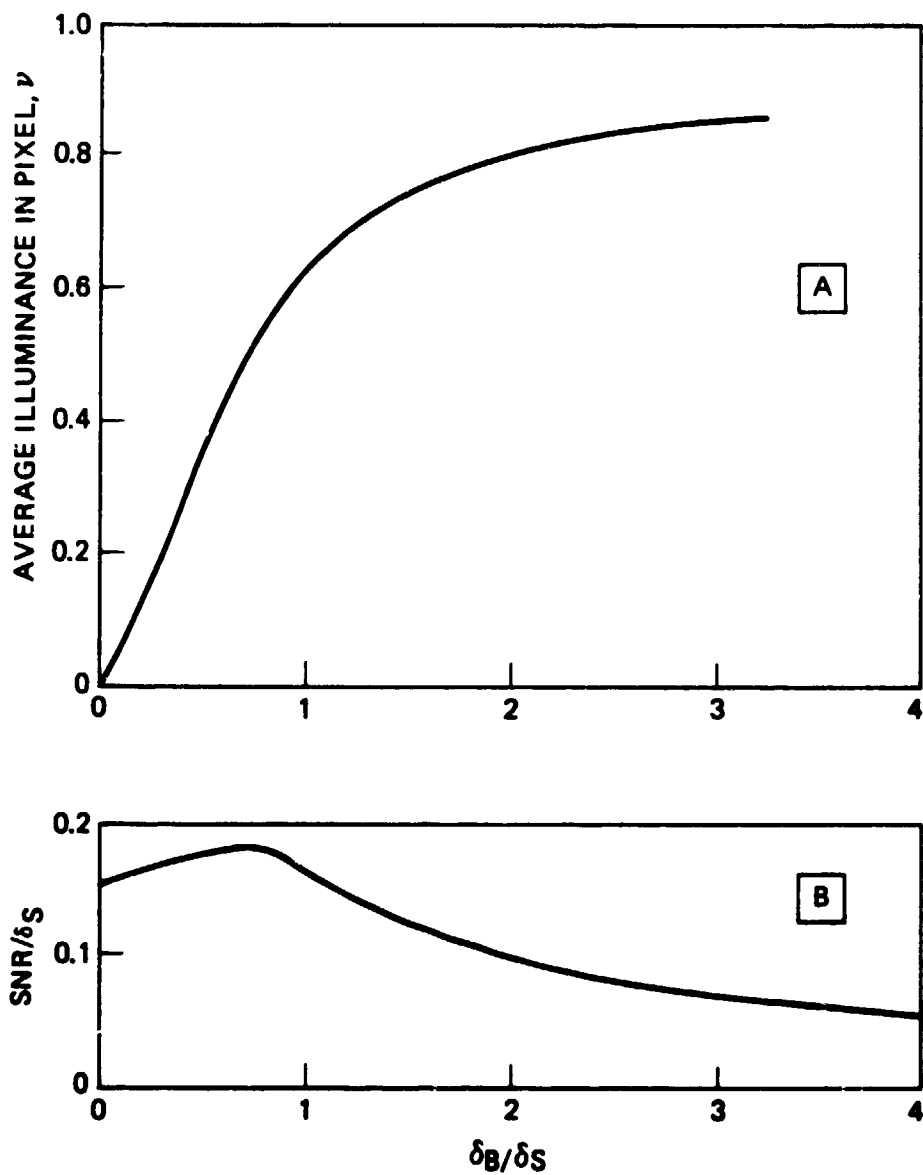


FIGURE A.6 Average Illuminance Within a Pixel as a Function of Pixel Size δ_B Normalized Relative to Event Size δ_S Pixel Focal Plane.

the source size has been chosen as the four sigma point) there will be on the average, about 62% of the source energy falling within a specific pixel bounds. The implication of Figure A.6A is that the larger the background area, the better the results, a condition which would be somewhat true for night time conditions.

But under daytime, solar background conditions, a larger background FOV means more noise, hence a decrease in the SNR. This overall factor is qualitatively illustrated in Figure A.6B for the situation where solar background noise predominates over all other noise sources. For background conditions where $\delta_B/\delta_S \gg 1$, the SNR does decrease. As the background FOV area is decreased however, there is a relative maximum in the SNR/ δ_S factor, after which the SNR decreased slightly until SNR/ δ_S becomes, in the limit, approximately $1/2 \pi$. This means, for a fixed source size and as the background area becomes significantly smaller than the source area, there is a point where the pixel will always be filled with equal area of background and the lightning source at which time the SNR will converge to a fixed value. In practice, noise sources other than background would result in a lower limit for the resolution size below which no SNR improvement will occur. In addition, sensor technology constrains the selection of the array pixel count.

As discussed previously the source dimension is likely to be smaller than the background FOV for attainable array configurations. For sub-satellite fill factors less than one, the δ_B/δ_S scales proportionally (for constant longitude). This fill factor correction is an important parameter in the parametric trades.

	δ_B/δ_S	ν	<u>LOCATION</u>
	0.63	0.44	optimum
Selected	1	0.62	at sub-satellite point
Values:	1.35	0.70	at 37.5 N
	1.82	0.78	at 50 N

A.4.3 Lightning Pulse Duration: T_L

Lightning pulse duration contributes to the definition of the shortest integration time that can be used if time splitting of the pulse is to be avoided or at best optimized. Figure A.7 summarizes the effective pulse width of lightning for some recent U-2 data (Gillapsy, 1/83) and for data from Turman (1976). Both imply an increase in pulse duration with an increase in total energy. Care must be excersized here, because the peak energy and peak power data were not necessarily from the same event. Subsequent data from NASA/ MSFC (Gillaspy 6/83) reproduced in Figure A.8A for maximum stroke per flash and Figure A.8B for all strokes indicates an interesting alternative. Even though there is a variance of effective pulse duration for any energy level, a constant average, effective pulse duration could be specified

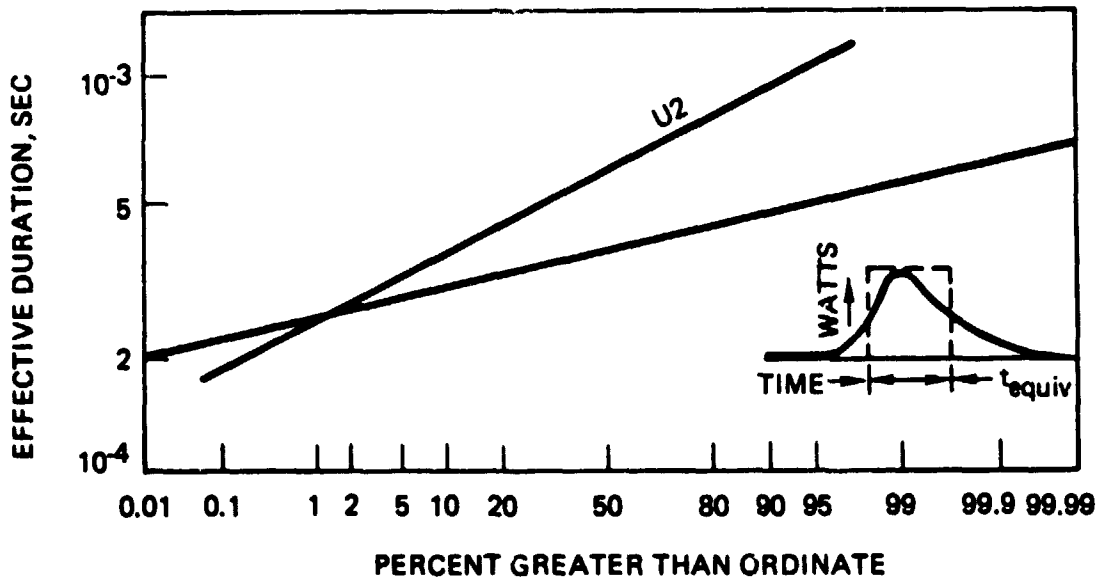


FIGURE A.7 Effective Pulse Duration (peak energy/integrated power)

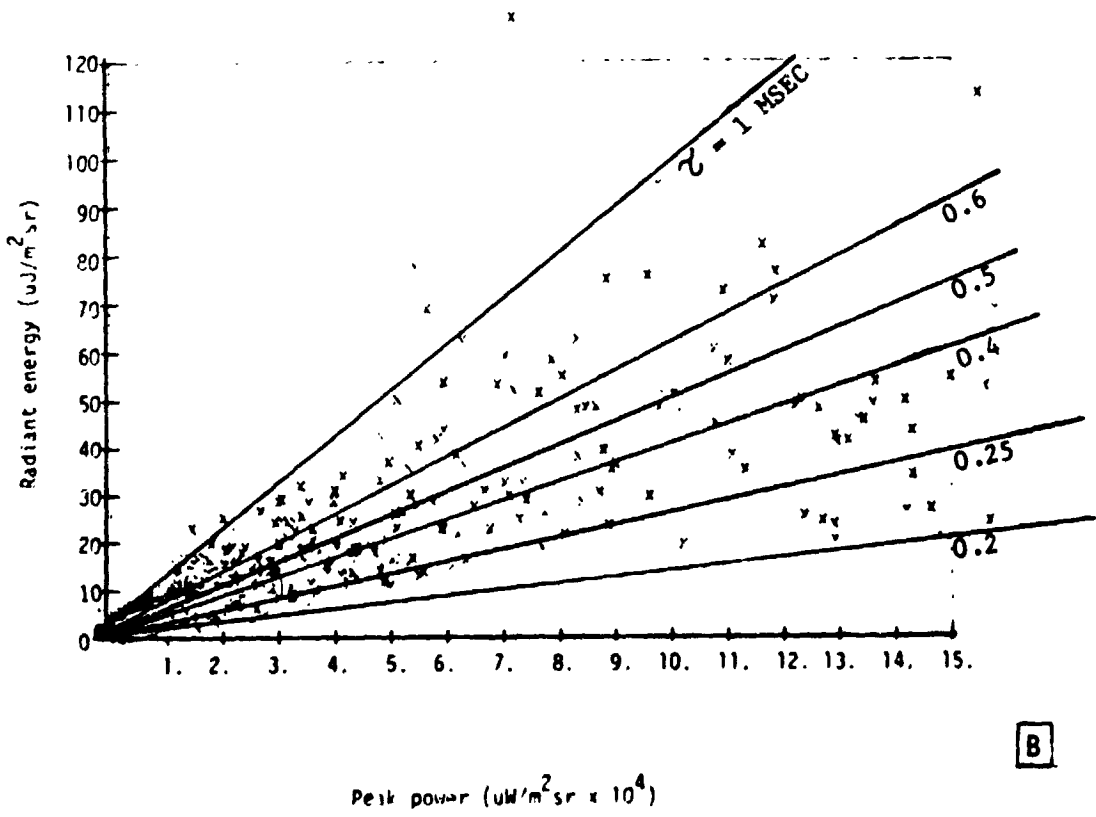
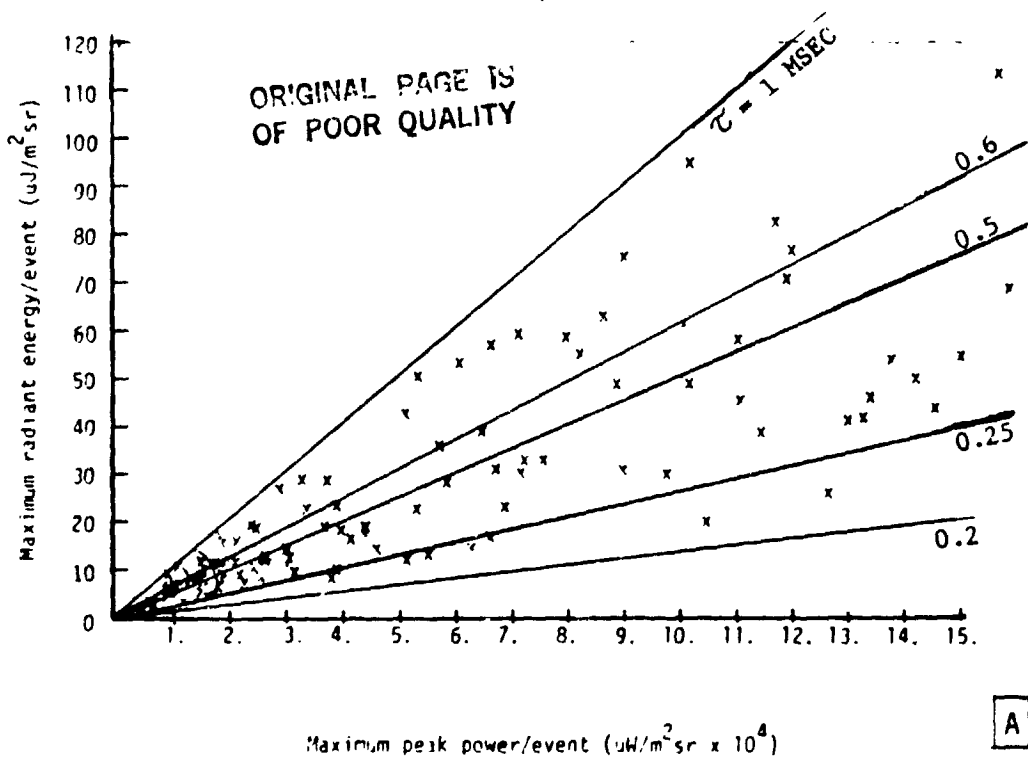


FIGURE A.8 Maximum Radiant Energy vs. Maximum Peak Power (A) and all Strokes (B).

which would apply to all maximum strokes independent of total energy involved. Figure A.8B indicates that this conclusion could be loosely applied to all strokes. An assessment of the NASA provided data for the full width at half maximum indicates a value of 0.54 milliseconds at the 50% point which is relatively close to previous data from Turman of 0.45 milliseconds.

T_L - selected value: 0.54 milliseconds

A.4.4 Pulse Splitting: ξ

Nagler (1981) addressed the fact that lighting events occur randomly in time relative to the frame sampling time, hence resulting in time splitting of strokes between two frames. The nearer the integration time is to the pulse duration, the more prominent this problem becomes. As mentioned for the spatial splitting, the occurrence of this phenomenon in most important near threshold where the loss of part of a pulse could result in a loss of an event with the consequence being an effectively higher threshold. Sensor dead time (e.g. during frame transfer) will also contribute to the loss of data. An assessment of some of the pulse waveforms provided by NASA/MSFC indicates a quasi-triangular waveform.

The time splitting factor for a triangular wave form is given by:

$$\begin{aligned} \xi &= T_1 / T_L - (T_1 / T_L)^2 / 3 & 0 \leq T_1 \leq T_L \\ \xi &= 1 - (T_L / T_1) / 3 & T_1 \geq T_L \end{aligned}$$

In the SNR relationship, the full time dependency is given by or $\xi/\sqrt{T_1}$ in normalized terms $\xi(T_L/T_1)^{1/2}/(T_L)^{1/2}$. The factor T_L is assumed constant and the normalized $\xi(T_L/T_1)^{1/2}$ is plotted in Figure A.9. For maximum SNR, $T_1=T_L$, but small variances in T_L would result in significant variation in pulse detectivity. The SNR falls off extremely rapidly for $T_1 < T_L$. To minimize a large variation in SNR as the event pulse width changes, a value of

ORIGINAL PAGE IS
OF POOR QUALITY

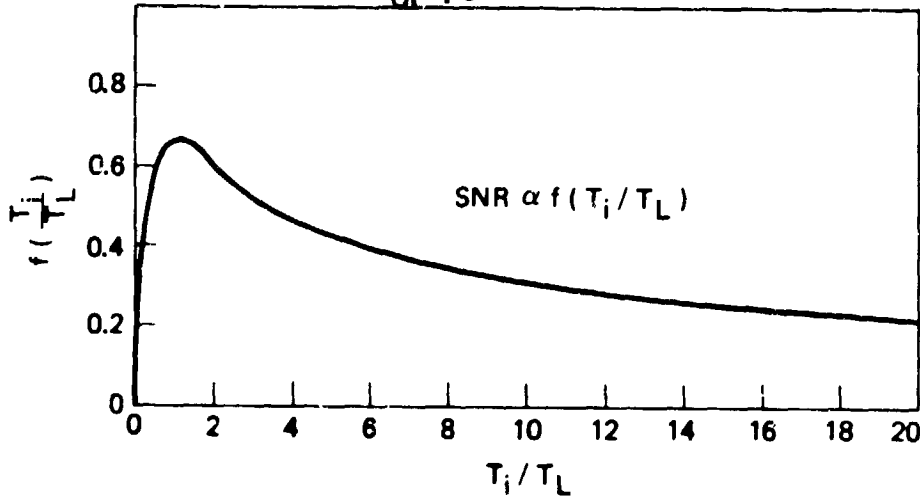


FIGURE A.9 Time Factor Effect on SNR

$T_i \gg T_L$ should be chosen, a factor greater than 5 would be recommended.

Other wave forms result in some variation of the constant $1/3$ in ξ , but the peak will still occur in the same place (at $T_i = T_L$). Change in steepness of the curve and a change in the absolute magnitude of this time splitting factor would occur, however, with no significant change in the conclusion.

ξ - Stroke time splitting factor: $(1 - T_L/3T_i)$

A.4.5 Energy Strength: E_s

Table 2.1 indicates two candidate wavelengths, 8683A and 7774A. A threshold of 10^7 watts (total optical power) is also given. NASA U-2 data (Gillaspy 1/83) indicates the following values near the 8683A line:

$\mu\text{J}/\text{m}^2\text{-sr}$	Probability Greater Than
4	90%
13	50%
24	mean
52	90%
100	Maximum Observed

The total optical energy values were derived by assuming that a

ORIGINAL PAGE IS
OF POOR QUALITY

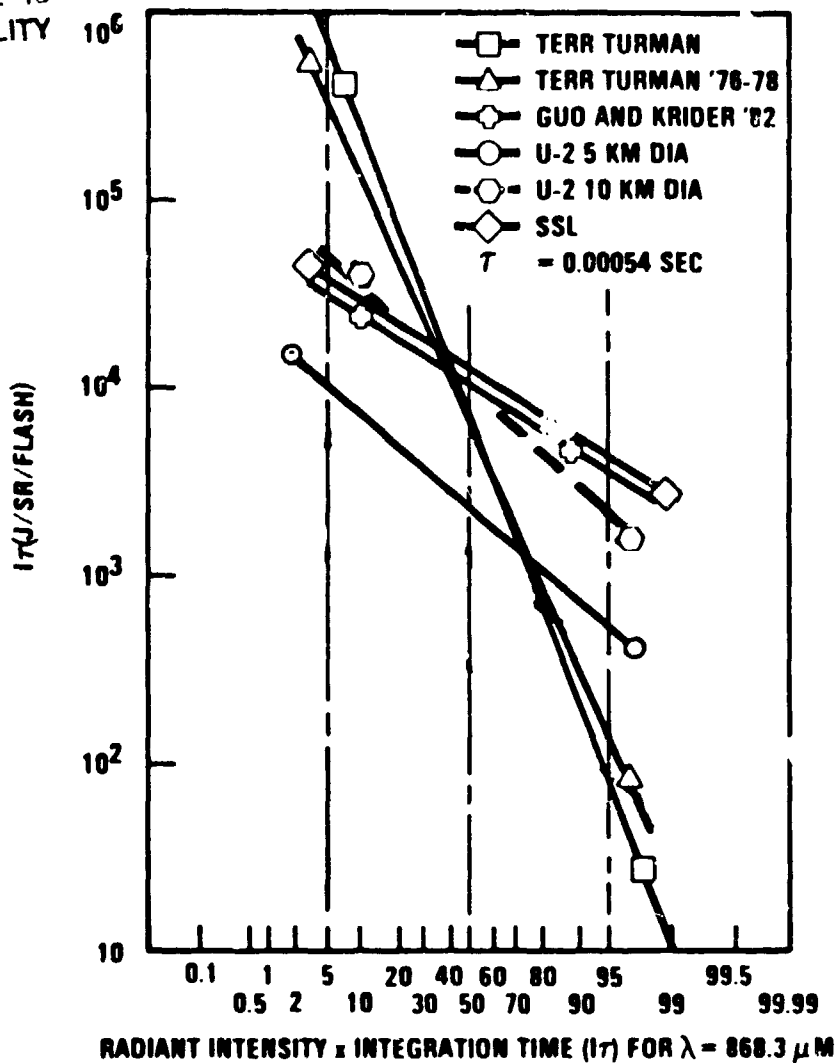


FIGURE A.10 Energy Distribution for Lightning.

nominal value of 15% of the optical energy is contained within the 8683A line region. Figure A.10 compares ground based lightning data with that collected by NASA/U-2 and that from space analyzed by Turman. Both above cloud collected data show a narrower dynamic range, a fact which may be real or due to a limited data base. Some of the U-2 data showed only a 12:1 dynamic range, but due to the limited data set, a minimum dynamic range of 100:1 should be used for the system analysis. A threshold goal of 10^7 watts is given in Table 2.1. This translates into (15 percent of energy in the line assumed)

ORIGINAL PAGE IS
OF POOR QUALITY

T_L Milliseconds	Source Area km ²	Energy in Single Line $\mu\text{J}/\text{m}^2\text{-sr}$
1	25	9.5
	100	2.4
0.5	25	4.7
	100	1.2

where a flat plate radiating from both surfaces has been taken as a typical cloud deck with an internal lightning stroke. The 0.5 millisecond, 5km square source area give a integrated source strength comparable to the U-2 measurements. This result must be reinforced by addition field data. Modelling by GUO and Krider (1982) indicates that the source may not be Lambertian, but could have preferential radiance in a cone about the vertical, a result due to multiple internal scattering. The 1982 NASA/U-2 data will be used as the baseline value for the threshold integrated energy.

nE_s - Radiant Energy: 4 $\mu\text{J}/\text{m}^2\text{-sr}$ NASA/U2 Data
 λ - Wavelength : 8683 A
 $E_{\text{PHOT}} = hc/\lambda$: 2.29 E-19 Energy/Photon
 J/photon

A.5 SIGNAL NOISE RATION: SNR

The average false alarm rate FAR is defined as the average number of times per second the output noise electrons exceeds the threshold setting of the detectors. This can also be expressed in terms of the SNR as:

$$FAR = \frac{e^{-\text{SNR}_T^2/2}}{2\sqrt{3} T_L}$$

This FAR rate decreases rapidly as the threshold value (SNR_T) is raised. The probability of detection P_d is approximately the

probability that the signal plus noise exceeds the threshold at the instand of signal peak, giving

$$P_d = (1/2) (1 + \text{erf} ((\text{SNR}_s - \text{SNR}_T) / \sqrt{2}))$$

where SNR_T is the threshold SNR setting and SNR_s is the SNR of a given signal (note that when $\text{SNR}_s = \text{SNR}_T$, $P_d = 0.5$, i.e, 50%). Figure A.11 graphically illustrates this relationship between FAR and SNR. For $\text{FAR} \ll 1$, the SNR requirement is not very sensitive to the absolute value of the pulse duration between 0.54 and 1.0 milliseconds.

A FAR design goal of less than 10% is given in Table 2.1. A.2 summarizes the SNR required on a pixel by pixel basis to provide this FAR. A nominal value of the threshold SNR is around 6.0. Note that the smaller the area which a pixel views, the more stringent the SNR value due to the lower lightning activity in

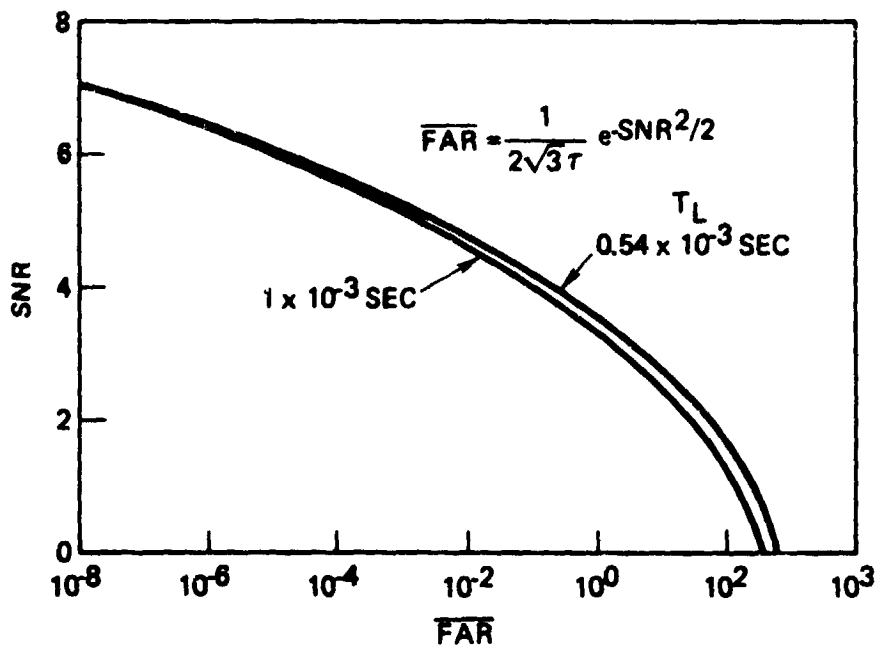


FIGURE A.11 FAR vs. SNR.

TABLE A.2 SNR vs. FAR

ORIGINAL PAGE IS
OF POOR QUALITY

	FLASH/km ² sec		EVENT RATE				S/N	
			FLASH/SEC PIXEL		FOR 10% FALSE EVENTS			
			(10 km)	(20 km)	(10 km)	(5 km)		
SPIE 245 - WOLFE/WAGLER								
GLOBAL	2	10 ⁻⁷	2	10 ⁻⁵	8	10 ⁻⁵	6.2	6.0
US	2.3	10 ⁻⁷	2.3	10 ⁻⁵	1.8	10 ⁻⁴	6.2	5.9
STORM COMPLEX	4	10 ⁻⁵	4	10 ⁻³	1.6	10 ⁻²	5.3	5.0
SEVERE STORM	1.7	10 ⁻³	1.7	10 ⁻¹	6.8	10 ⁻¹	4.6	4.2
NASA/MSFC (Hugh Christian)								
GLOBAL	2.9	10 ⁻⁷	2.9	10 ⁻⁵	1.2	10 ⁻⁴	6.2	5.9
(150/sec total)								

that reduced area. The respective values of SNR for footprints of 5,7,10,13, and 20km are 6.4,6.3,6.2, 6.1 and 6.0 for a nominal global rate of 2×10^{-7} flashes/km² sec. The higher the local activity, the lower the SNR can be set for the same FAR.

There is also a 90% probability of detection specification. Figure A.12 relates the probability of detection relative to the SNR threshold setting (i.e, SNR at $P_d = 50\%$). From Figure A.12, an event with a SNR greater than 45% above the threshold setting will have a probability of detection greater than 90%.

SNR - Baseline value: 6.0

A.6 BACKGROUND: I_B , ALBEDO

The solar spectral irradiance can be found from a number of handbooks. Approximate values for $I_B \pi$ (W/m² - um)

λ	m=0	m=2 (zenith = 60°)
8683	950	800 W/m ² -um
7776	1160	907 W/m ² -um

Most of the cloud tops are above a significant part of the atmospheric air mass, in particular, above much of the earth's water vapor (c.f. Figure A.13). Hence a worse case but realistic

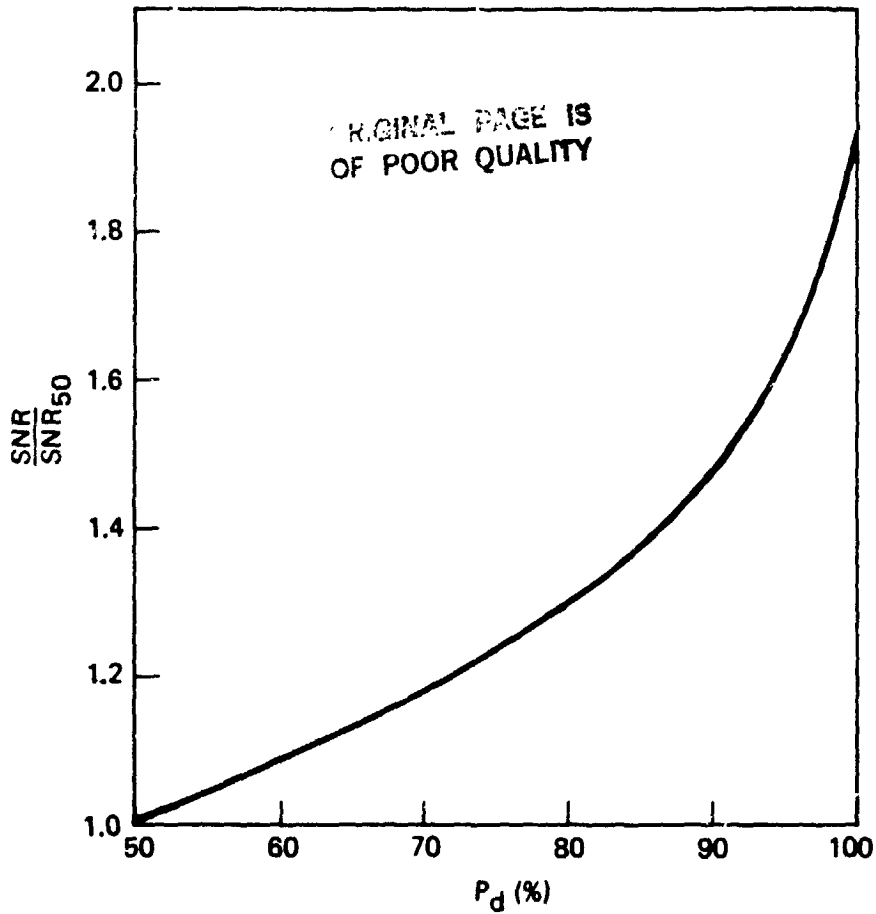
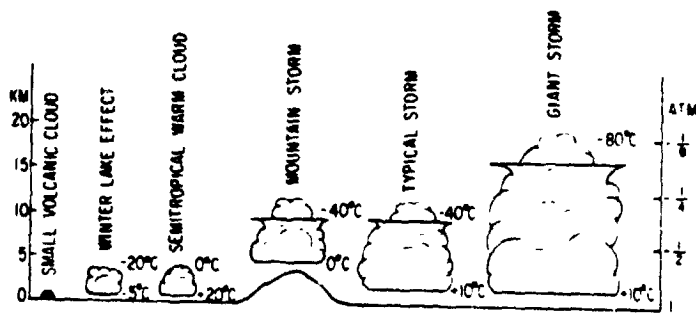


FIGURE A.12 Probability of Detection vs. SNR.



Approximate sizes of various lightning producing clouds

FIGURE A.13 Cloud Top Altitudes.

ORIGINAL PAGE IS
OF POOR QUALITY

solar condition would be $m = 0$ giving for 8683,

$$I_B = 302 \text{ W/m}^2\text{-um-sr.}$$

The albedo (solar reflectance) varies for different backgrounds. Of specific interest are clouds, but a pixel may view a broken cloud deck. Some albedo values are

<u>OBJECT</u>	$\lambda=7776$	8683A	
Winter snow/ice	0.85	0.8	worse case background
Clouds	0.7	0.67	normal cloud cover
Summer ice	0.5	0.45	} surface background
Vegetation	0.4	0.5	
Soil/Rocks	0.3	0.33	

A nominal baseline value of 0.7 was used for the system parametric analysis.

	8683A	7774A	Units
I_B - Selected Values:	300	396	$\text{W/m}^2 - \text{um-sr}$
Albedo - Selected Values:	0.7	0.7	

A.7 OPTICS: F/NO.,K

The two primary characteristics of the optics in the SNR relationship are the F/No (relating focal length and aperture diameter) and the optical throughput efficiency, K.

The preliminary analysis indicated that the F/No would need to be pushed to optimize the SNR. This is one of the few factors which contributes proportionally to the SNR rather than by the square root. Pushing the F/No. often means more glass, higher fabrication precision and mechanical limits. A F/1 is often considered the lower limit with F/1.5 being more practical. Separate design activities have indicated that an F/0.78 system might be doable for the LITMAP requirements. Refractive and reflective alternatives are possible. The requirements of the filter must be considered when defining the optics.

ORIGINAL PAGE IS
OF POOR QUALITY

The optics system will probably have many surfaces, hence appropriate coatings to maximize throughput must be used. Coatings with $K=0.98$ to 0.99 transmittance per surface should be attainable.

F/No-Baseline: 1.0
K-Selected value: 0.98

A.8 FILTER:

When considering the filter requirements, care must also be taken that the throughput of the filter is also considered. Although the optics and filter were not part of this study, their significant impact on the overall system trades necessitated a look at their impact during a related IR&D activity.

Table A.3 compares the overall effects of two filter types and several optical band passes. The interference filter must have a bandpass sufficient to handle the angular effects (c.f.

TABLE A.3 Filter/Optics Figure of Merit

FILTER TYPE	λ (Å)	K FILTER	K^{**} FILTER + OPTICS	Figure of Merit $\sqrt{K/\Delta\lambda}$
INTERFERENCE	25	0.90	0.57 - 0.72	0.15 - 0.17
	5 (rectangular)	0.70	0.56	(3) 0.43 (5) 0.31 - 0.33
	2.5 (gaussian)	0.40	0.25 - 0.32	0.31 - 0.35
BIREFRINGENCE (SOLC)	2	0.25	0.16 - 0.20	0.28 - 0.32
	1	0.25	0.16 - 0.20	0.4 - 0.44

* of optical line being isolated is assumed to be one or two angstroms.

** Assumed optics with 11 elements (22 surfaces): $(0.99)^{22} = 0.8$; $(0.98)^{22} = 0.64$

Figure A.14 while the SOLC filter can handle the larger FOV while maintaining a narrow bandpass.

ORIGINAL PAGE IS
OF POOR QUALITY

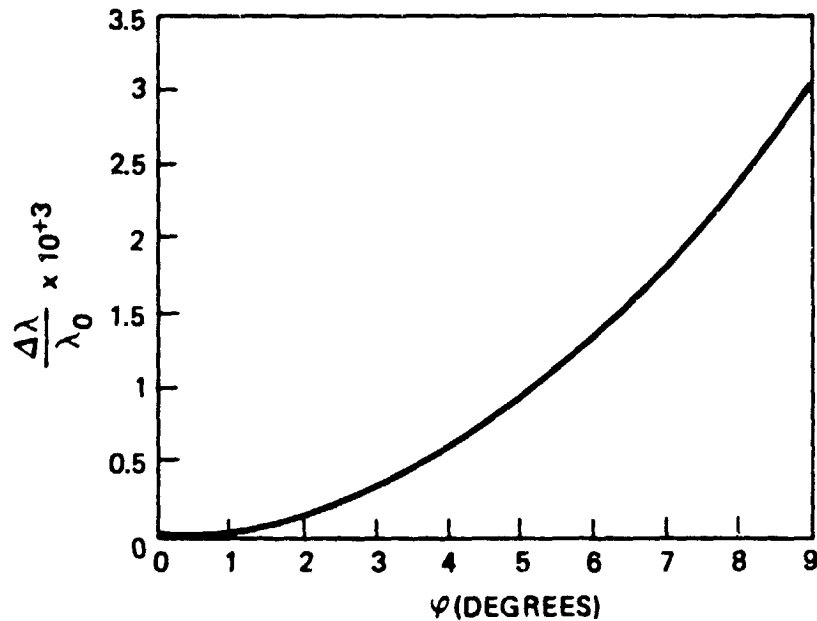


FIGURE A.14 Angular Shift for Interference Filters.

For wider FOV's (e.g., 18° full angle) the SOLC has a 2 to 3 advantage over the required 25A bandpass interference filter. For the narrower FOV (as exists when the full disc is split four ways with separate optics for each, see Section 4) both filters provide comparable performance with the development risk being larger with the SOLC filter. If more than 3 A bandpass is required, interference filters are the most cost effective approach.

For band passes of a few angstroms, a single line of the lightning spectra can be isolated. An approximate value of 15% of the total optical energy is associated with each of the candidate lines of 3683 and 7774 angstroms.

$\Delta\lambda$ - Selected: 5 A

η - Selected: 0.15

A.9 SENSOR CHARACTERISTICS

A.9.1 Quantum Efficiency; Q

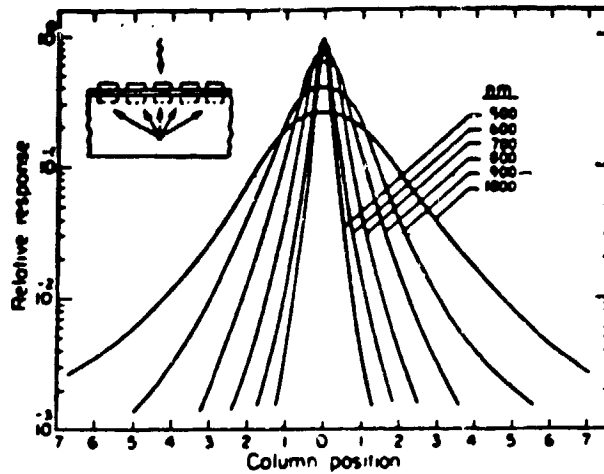
The quantum efficiency term includes the overall conversion of the total incoming photon flux to charge carries within the detector. This not only includes the absorption properties of the active region but also accounts for the optically obscured areas. This latter is very dependent on sensor fabrication techniques and overall sensor topography design.

The photon-to-charge carrier conversion efficiency is also wavelength dependent. One primary effect for silicon based detectors is that for wavelengths greater than 0.7 μm , the silicon starts to become transparent. Also when the thickness of the active region exceeds the pixel dimension, lateral charge carrier migration can occur resulting in image spreading (c.f. Figure A.15).

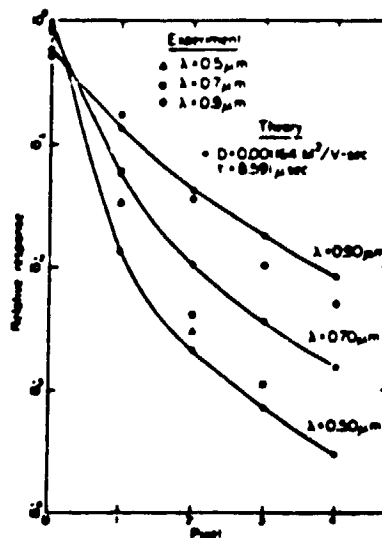
This spreading will divide the event amount two or more pixels resulting in an effective increase in the detection threshold. Shorter wavelength and/or special sensor material selection (e.g., Pt Si) can minimize these effects. Relative values of the total energy within the 7774 and 8683 angstrom lines must be obtained before this spreading effect can be fully assessed. Larger pixel dimension is one of the geometric trades which can be used to offset the image spreading factor.

Commerical device quantum efficiencies range from 0.12 to 0.6 with shorter wavelengths in the region of interest having higher values. Some isolated cases have claimed quantum efficiencies up to 0.8 for back illuminated devices but this does not appear to be consistant with the bulk of the 8683 angstrom wavelength devices.

	Typical	Goal
Q- Selected range:	0.35 - 0.45	(0.6)



Horizontal line-spread function measured at various wavelengths. Line of illumination with 6- μ m half-width was positioned at the center of central pixel.



Calculated and experimental line-spread functions at 500, 700, and 900 nm. The calculated points were obtained from a two-dimensional numerical solution of the diffusion equation by the method of conjugate gradients. The integrated flux for each pixel is normalized to the total flux over the central 9 pixels for both calculated and experimental values. The calculated points (open circles) are connected by a line, which serves only as a guide. The one-sigma error on the experimental points at low light levels corresponds to a relative response of 0.002. Peak illumination level was ~50 percent of saturation.

FIGURE A.15 Image Spreading in Array Detectors.

A.9.2 Pixel Dimensions: δ_p

The selection of pixel size is dependent on a number of parameters including resolution, aperture, effective F/No. and orbit altitude as well as manufacturability. When resolution is the driver, diffraction limits must be considered. As shown in Figure A.16, the approximate diffraction limited pixel size ($L \sim 2 \lambda R/D$) for a F/1 system is around 1.6 μm : over a decade below the pixel size required for the LITMAP application. Hence LITMAP is not diffraction limited for global coverage. This figure also relates aperture diameter to object resolution for various pixel sizes. These factors are related by the pixel angular FOV and is given by:

$$L = (R \delta_p) / ((f/No) D)$$

Where all values are in meters and for Figure A.16

$$R = 3.6 \cdot 10^7 \text{ m}$$

$$f/No = f/1$$

Each L vs D curve applies to all constant values of $\delta_p/(f/No)$.

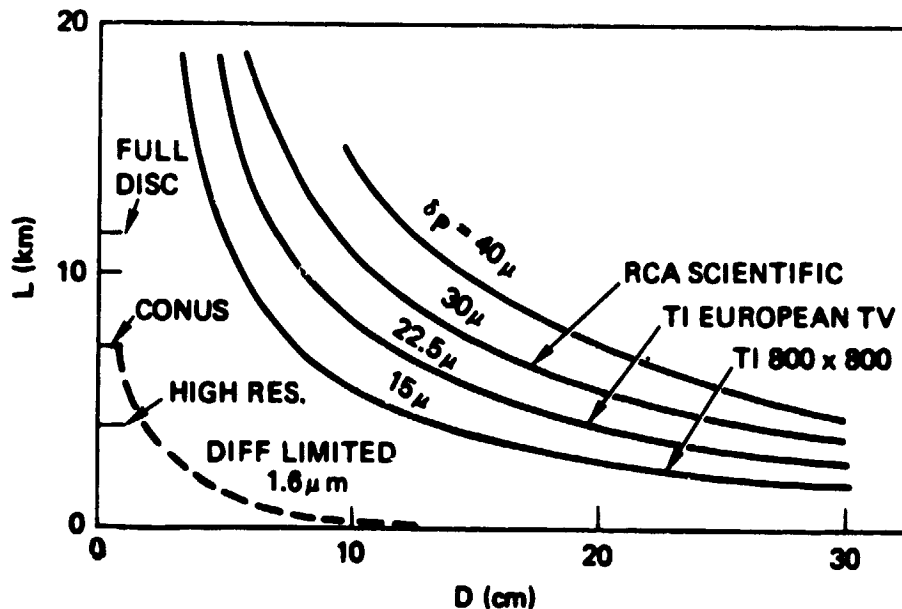


FIGURE A.16 Resolution vs. Aperture.

Hence an $f/1$, $40 \mu\text{m}$ δ_p gives the same curve as an $f/2$ and $80 \mu\text{m}$ pixel. Note that for a specific pixel size, there is a limit on the aperture size associated with a given resolution, e.g., 11 km imposes an aperture limit of about 5 cm for a $15 \mu\text{m}$ pixel. Larger pixels permit larger aperture. Figure A.17 replots this latter figure giving curves of constant resolution. The SNR relationship shows that a larger pixel size (hence larger aperture) enhances the system performance. Solar background, electronics processing bandwidth and signal dynamic range also push for larger pixel size capability to enhance the threshold performance of the sensor system.

In addition to shear bandwidth consideration for a given focal plane array, there are also manufacturing considerations. Although 800×800 arrays have been produced, primarily for the astronomy community, they have $15 \mu\text{m}$ pixels and are normally readout at sub-MHz rates. Discussions with TI indicates that

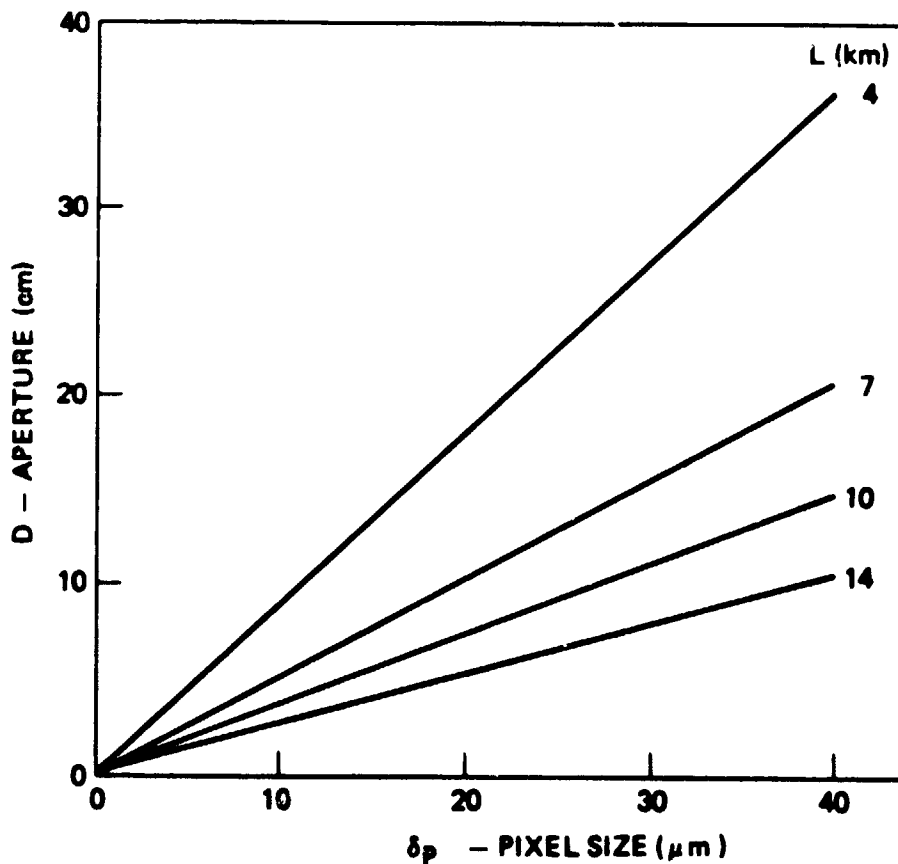


FIGURE A.17 Aperture vs. Pixel Dimensions.

they would probably not be interested in production of such an array with larger pixels, say 20 to 30 μm . The physical size becomes so large that production yields drop dramatically making them prohibitively expensive to produce. Dividing the 800 X 800 in half, i.e., a 400 X 400 sensor with equal chip frame storage makes their production more practical. A number of arrays are now in production for commercial TV and scientific applications which approach the 300 X 400 and 400 X 500 imaging arrays (plus frame storage) with pixel dimensions of 22 to 30 μm .

δ_p selected dimension: $> 25 \mu\text{m}$ also dependent on other system requirements.

A.9.3 Sensor Noise: ϵ

The primary intrinsic sensor noise contributions are dark current and amplifier noise. Analysis indicate that for daytime operation, A leakage of 40 NA/cm^2 would only contribute less than 10% more relative to the solar background noise. Existing data indicates less than 26 NA/cm^2 at 25 C maximum with 8 NA/cm^2 being typical. Hence, for the short integration times associated with LITMAP, there probably will be no cooling requirements due to dark current.

Amplifier noise is a different problem. For sub MHz readout rates, as applied in astronomy for example, the preamplifier noise is on the order of a few tens of electrons rms. As the readout frequency increases, in an attempt to minimize the off focal plane electronics required, the preamp noise increases. Special on chip preamp designs can be tailored to the desired operating frequency regime and special techniques such as correlative double sampling can be applied to minimize the associated readout noise. Systems optimization often results in about equal noise contributions for the most prominent sources, in this application two key contributions are background and readout (preamp) noise.

Desired limits on readout noise will be a contributing factor on defining the upper readout frequency for a given array configuration.

The noise factor ϵ was defined as all other noise contributions divided by the background contribution (all in absolute values, not rms).

ϵ - Desired value: < 1 must be determined for each configuration

A.9.4 Integration Time: T_i

The integration time is a delicate trade between (among other) excessive noise and power dissipation at higher frequencies versus increasing electronics and required full well capacity to handle the solar background at lower bandwidths. Figure A.18 illustrates the relationship between integration time, readout rate and pixels per readout port. The partitioning given on the right side is based on a total array of 800 X 800

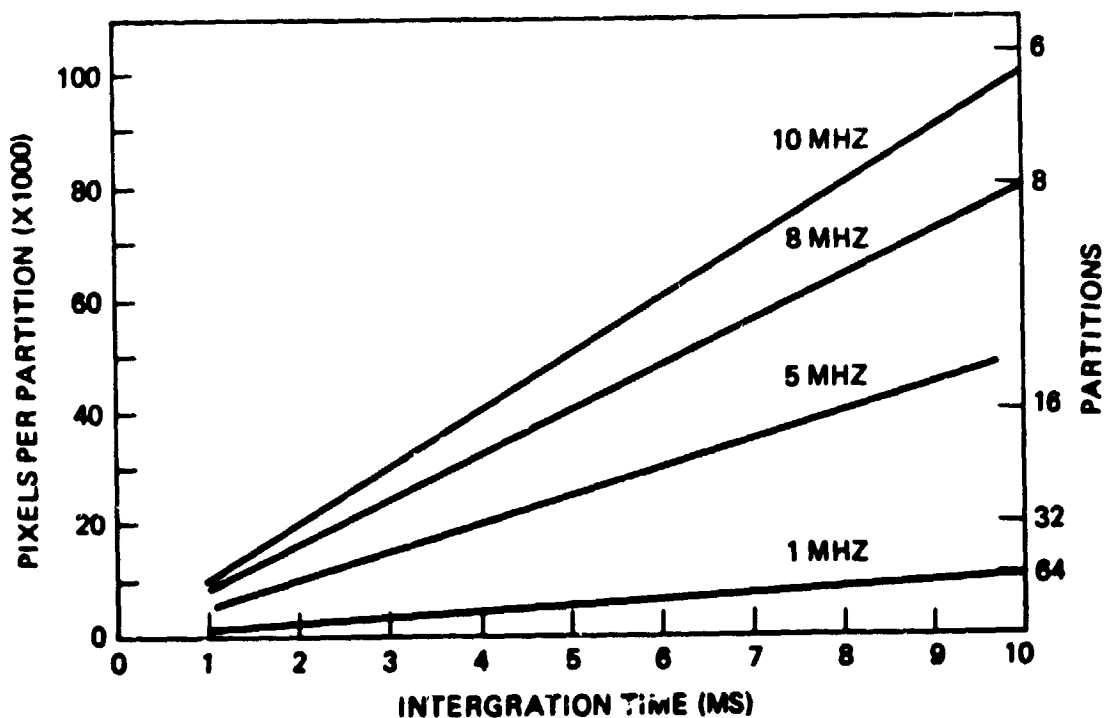


FIGURE A.18 Focal Plane Partitioning vs. Sample Time.

(640,000 pixels). A preliminary analysis indicated the desire to hold the integration time to a nominal 4 milliseconds. With an 8 to 10 MHz readout rate, the full array would have to be partitioned and provided with 16 output ports. For the four array configuration, each array would have four ports. Further system optimization may result in 5 MHz readout rate per port, hence longer integration time (probably not acceptable) or increase partitioning. Electronics weight, power, volume and cost must be traded against array manufacturing constraints. Four to eight ports per array chip appears to be achievable.

Analysis discussed later shows that for SNR, there is an optimum integration time some where around a half to one millisecond. From physical considerations, a longer time must be utilized.

A consideration for the upper integration time limit is the rate of change of the background. Assuming geosynchronous orbit:

- o Day/Night terminator: approximately 10^3 mi/hr
or 444 m/sec. Time to move:

<u>Percent of pixel FOV</u>	<u>Seconds</u>	<u>Frames</u>
10	2.5	625
1	0.25	63
0.1	0.025	6

- o Wind (Clouds): less than 10^2 mi/hr
or 44 M/sec. Time to move:

<u>Percent of pixel FOV</u>	<u>Seconds</u>	<u>Frames</u>
10	25	6250
1	2.5	625
0.1	0.25	63

Note: vertical cloud growth can occasionally exceed the 44 M/sec given above.

For time averaging of the background, a further restriction

may be necessary. For example, for a motion of 0.1% of a pixel in ten frames (i.e., 0.1% in 40 milliseconds) the terminator motion maybe a problem. Satellite jitter must also be assessed carefully.

For LITMAP objectives, the upper integration time will probably be more limited by sensor full well capacity rather than background changes.

T_i	- Selected baseline	:	40×10^{-3} seconds
M	- Partitions	:	16
f	- Frequency	:	10 MHz

A.9.5 Full Well Capacity: FW

This factor does not explicitly appear in the SNR relationship but is one of the limiting factors on the upper end of the integration time. As background and other noise contributions fill the sensor storage area, the allowable signal dynamic range decreases. For excessive integration times, the ability to handle the signal will go to zero and the pixel storage will saturate.

Some representative full well capacity data is illustrated in Figure A.19 for several commercial ICCD's. The virtual phase and some three phase devices fall along the lower solid curve while the four phase devices fall along the upper curve. Although these charge capacities are concept dependent, there is some latitude in well depth to adjust the full well capacity. Figures A.20 to A.22 relates allowable "noise" accumulation to signal dynamic range. The signal dynamic range is defined as maximum signal divided by minimum signal where the minimum detectable signal is defined as:

$$N_s (\text{peak}) = \text{SNR} * N_n (\text{RMS}).$$

Figure A.20 illustrates that larger full well capacities permit larger allocations to background and noise. The large capacity becomes more important as larger dynamic ranges are required coupled with larger backgrounds (e.g., with longer integration times). As seen in Figure A.21, this larger capacity allocation

ORIGINAL PAGE IS
OF POOR QUALITY

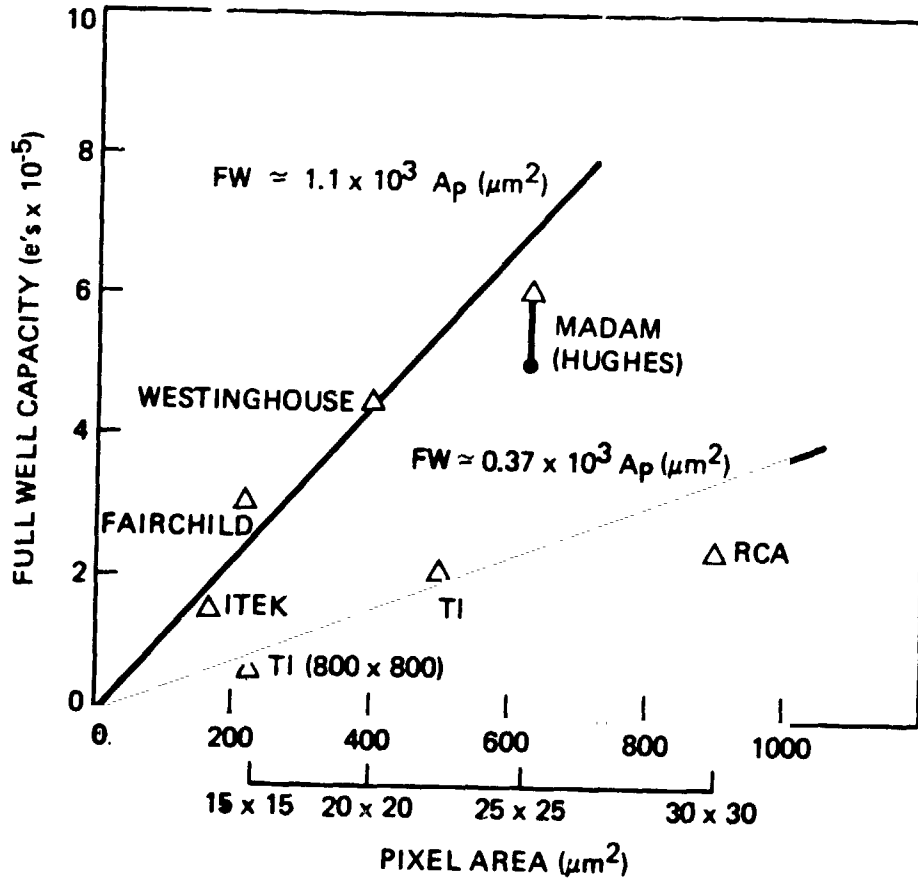


FIGURE A.19 Full Well Capacity.

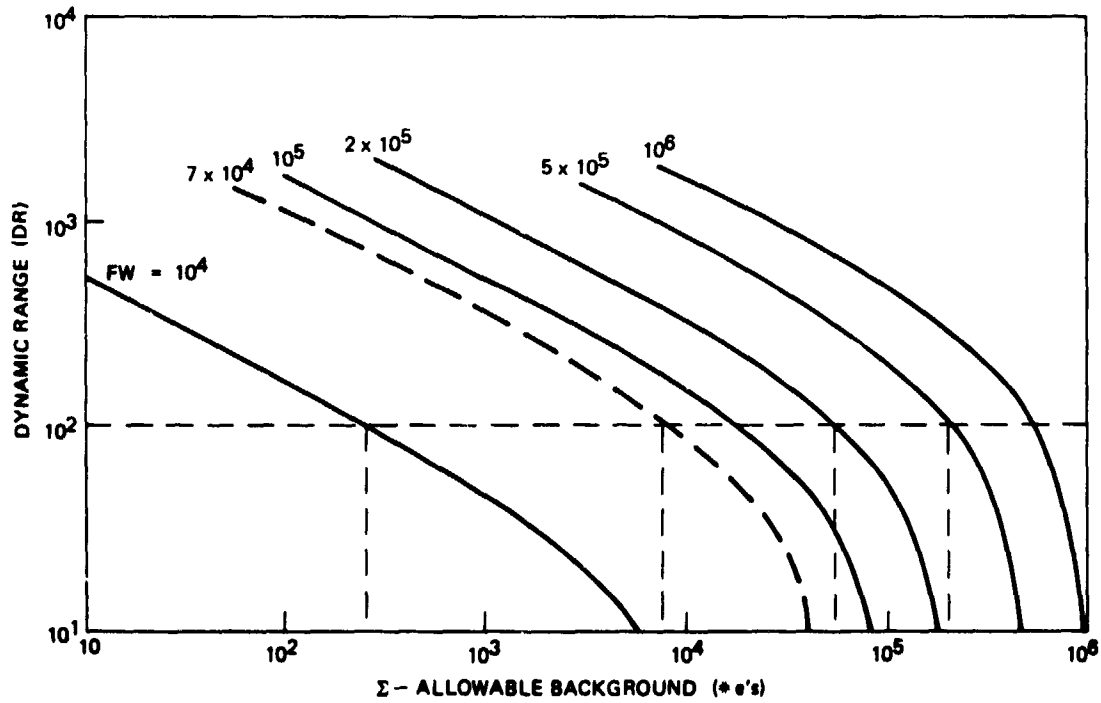


FIGURE A.20 Dynamic Range vs. Allowable Noise.

ORIGINAL PAGE IS
OF POOR QUALITY

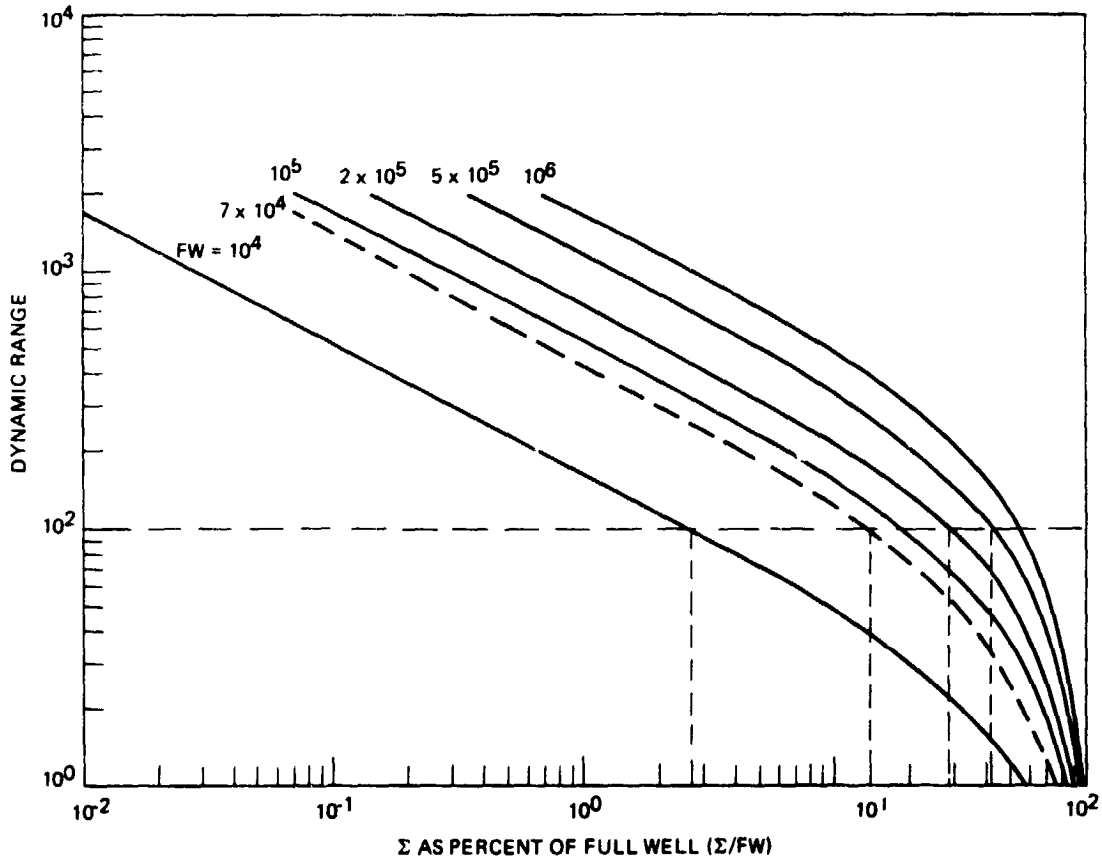


FIGURE A.21 Dynamic Range as Percent of Full Well.

to noise is not only a result of an increase in the absolute full well capacity, but a larger percent of the full well can be allocated to background and noise as the full well capacity

ORIGINAL PAGE IS
OF POOR QUALITY

increases.

Finally Figure A.22 provides curves for fixed dynamic ranges and provides the relationship between absolute electron count for background (and other noise) as a function of the full well capacity. This latter figure illustrates that as the full well capacity goes up two decades, the allowable background goes up 2.5 to 4 decades for dynamic ranges of 10 to 10³. The conclusion: full well capacity is a very important factor when dealing with large backgrounds. For a dynamic range of 100, full capacities of at least 2 X 10⁵ are almost required with values above 5 X 10⁵ being highly desirable. As shown in Figure A.19, these larger capacities primarily comes from larger pixels with some dependency on the CCD technology utilized. The upper curve in Figure A.19 can be represented approximately by

$$FW = 1.1 \times 10^3 A_p (\text{um}^2)$$

where A_p is the pixel area. The allowable background can be estimated by (c.f. broken curve):

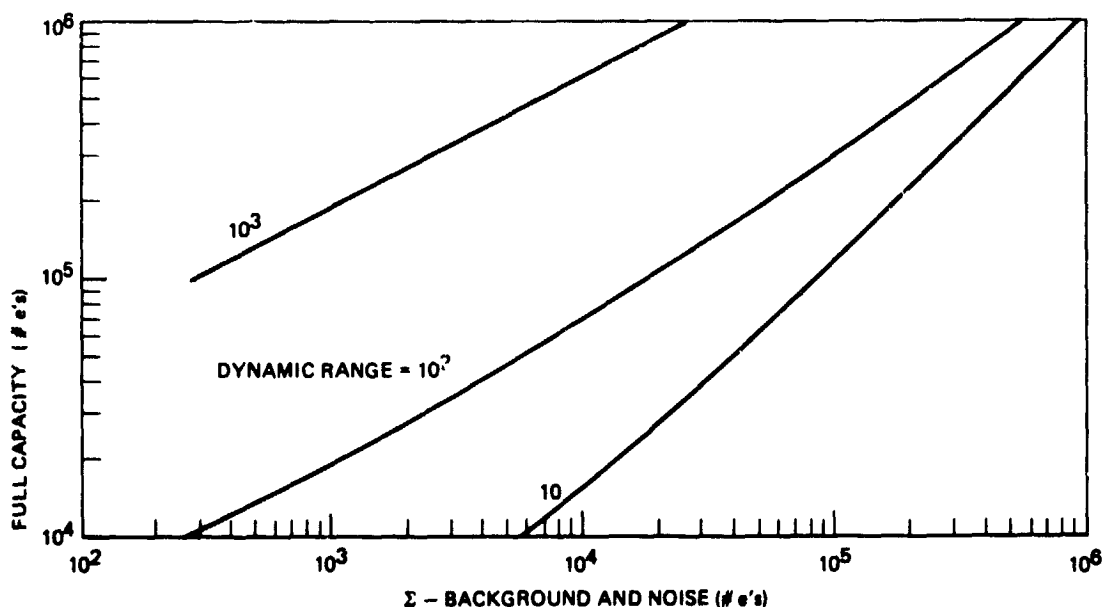


FIGURE A.22 Absolute Noise Limits Relative to Full Well Capacity.

$$N_n^2 = \Sigma FW = -7.86 \times 10^4 + 629 A_p \text{ (um}^2\text{)}.$$

The lower solid curve in Figure A.19 is roughly one third of the upper curve full well capacity, i.e. for the lower curve

$$FW \cong 0.37 \times 10 A_p \text{ (um}^2\text{)}$$

$$\Sigma FW \cong -2.62 \times 10^4 + 210 A_p \text{ (um}^2\text{)}.$$

These sets of curves bound most presently existing commercial ICCD devices.

FW - Selected baseline value: > 200,000 electrons

A.10 THRESHOLD VERSUS DYNAMIC RANGE

Whenever the technology is being pushed, the inevitable question arises as to if performance can be traded versus scientific objectives to relieve some technology stressing issues. LITMAP is no exception and one of the obvious trades is that of threshold setting versus data set completeness.

A previous section discussed observed source strengths. This section addresses the relative impact of raising the threshold on the loss of data. Figure A.23 illustrates several log-normal distribution curves with the dynamic range being defined between the 10% and 90% probability points. The value of 1 on the ordinate is the nominal setting for threshold to provide detection of 90% of the events.

As the threshold is raised, events are lost at the lower end of the curve. A factor of three increase in the threshold for a 10:1 dynamic range would result in a loss of about 40% more of the data. As the dynamic range increases, less sacrifice occurs for a factor of two or three increase in the threshold (hence SNR). For the LITMAP dynamic range design goal of 100:1, an increase of two or three could be tolerated with less than 15% of the data being lost. A word of caution is necessary. Present U-2 data indicates that the dynamic range may be less than 100 between the 10% and 90% points, as low as 12:1. That data set is very small at present, so care should be exercised when making

ORIGINAL PAGE IS
OF POOR QUALITY

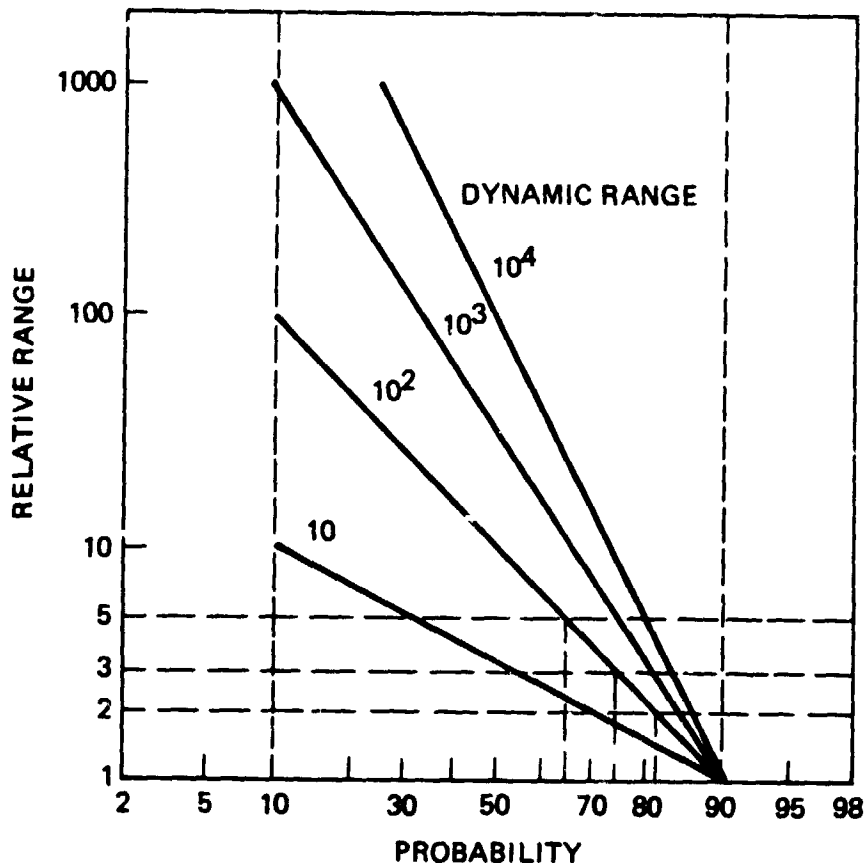


FIGURE A.23 Relative Dynamic Range vs. Probability.

decisions on thresholds. Enough data is available to indicate that the above cloud observations are definitely lower than the 1000:1 dynamic range for below cloud observations. Based on the NASA design goals of 100:1 dynamic range the following system trade guideline has been assumed where E_s is the lowest signal that is desired to be detected.

$$E_T - \text{Threshold: } E_T \leq 3\eta E_s$$

A.11 PARAMETER SELECTION SUMMARY

A summary of the selected parameter values is given in Table A.4. These data provided the input for the baseline

ORIGINAL PAGE IS
OF POOR QUALITY

configuration as given in Table 2.2 of Section 2 and formed the foundation of the parametric analysis of Section 3.

TABLE A.4 Parametric Analysis Selection Summary

<u>Parameter</u>	<u>Value</u>	<u>Units</u>	<u>Comments</u>
FOV	7.37	Degrees	Half Angle (50° latitude)
Pixel Resolution	11 15 20	km km km	Sub-satellite (nadir) Central CONUS 50°N US/CANADA line
Geometric Split, ν	0.6/0.44 1/0.62 1.35/0.70 1.82/0.78		Optimum Subsatellite 37.5°N 50°N
T_L	0.54	Milliseconds	FWHM
Pulse Splitting, ϵ	$[T_i/T_L - (T_i/T_L)^2/3]$ $[1 - (T_L/T_i)/3]$		$0 \leq T_i \leq T_L$ $T_i \geq T_L$
ηE_s	4	$\mu\text{J}/\text{m}^2\text{-sr}$	Single line, NASA/U2
λ	8683	Angstroms	Alternate 7774
SNR	6		From FAR considerations
I_B	300 396	$\text{W}/\text{m}^2 - \mu\text{m-sr}$ $\text{W}/\text{m}^2 - \mu\text{m-sr}$	8683A° 7774A°
Albedo	0.7		Both wavelengths
F/No.	1.0		
K	0.4		Including filter
$\Delta\lambda$	5	Angstroms	
η	0.15		Fraction of optical energy in single line
Q	0.35		Range 0.35 to 0.6

ORIGINAL PAGE IS
OF POOR QUALITY

TABLE A.4 (CONT)

<u>Parameter</u>	<u>Value</u>	<u>Units</u>	<u>Comments</u>
δp	> 25	microns	Needs to be large
ϵ	< 1		Device dependent (desire < 0.5)
T_i	4	Milliseconds	Integration time
M	16		Total number of outputs
F	10	MHz	Rate per output
FW	$> 2 \times 10^5$	Electrons	Full well capacity
E_T	$\leq 3^{\eta} E_s$	$\mu\text{J}/\text{m}^2\text{-sr}$	Threshold relative to NASA/U2 data

B. PARAMETRIC TRADES

B.1 INTRODUCTION

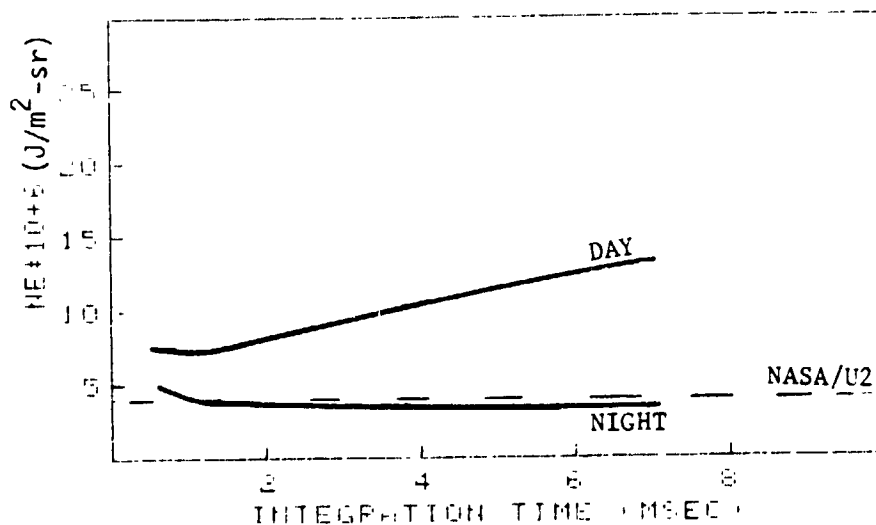
As mentioned in Section 3, a good feeling for the parameter dependencies can be obtained by simple inspection of the basic SNR relationship, which in Section 3 was inverted to provide the attainable spectral threshold energy for a given set of parameters. This inspection approach can be used whenever all terms of interest interact in a product/division manner. Hence, once a given quantitative value is obtained for the threshold energy for a given set of parameters, the adjustment of this threshold can be made by inspection.

This straight forward approach is not as effective when additive/subtractive factors are involved such as when more than one noise term must be considered and for the time and spatial terms which have interactive factors. The following sections will provide some representative parametric trades which were used to determine what parameter set would permit optimization of the LITMAP sensor system. The final selection of an "optimized" parameter set is constrained by the practical limits placed on each parameter as defined in Appendix A.

B.2 BASELINE PARAMETER SET

Appendix A defined a practical parameter set which was deemed to be within the limits of the existing technologies and have a reasonably low risk for implementation but did not necessarily meet all of the requirements of Table 2.1. This parameter set is summarized in Table 2.2 as the Baseline. All parametric analysis started from this baseline with the intent to determine how the overall system (optics/sensor/electronics) could be optimized relative to cost, complexity, schedule and risk.

A graphical presentation of the spectral threshold energy NE ($\text{J}/\text{m}^2\text{-sr}$) as a function of integration time is shown in Figure B.1. Computer printout formats for the baseline data set is illustrated in Figures B.2 (day) and B.3 (night). Note in Figure B.1 that the recent NASA/U2 90% threshold value of $4 \text{ uJ}/\text{m}^2\text{-sr}$ is



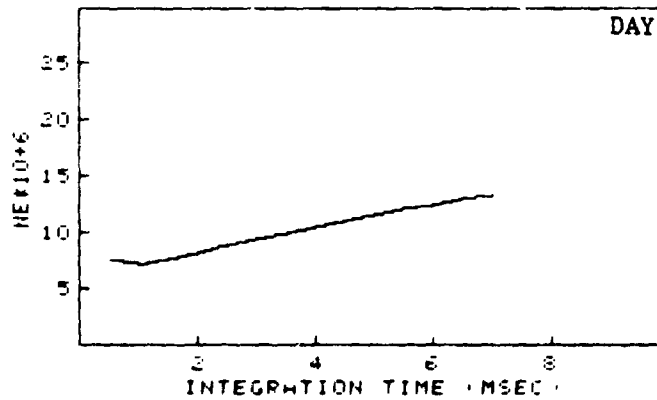
B.1 Threshold Energy for 8683A as a Function of Integration Time for the Baseline Set of Parameters Given in Table 2.2.

approached under night time conditions but a value more near $11 \text{ uJ/m}^2\text{-sr}$ (at 4 milsec) is attainable for worse case daytime conditions. From the dynamic range discussion in Appendix A, even a factor of 2 or 3 increase in threshold for an event dynamic range of 100 would result in losing less than 10% of the data that normally would be attained within the 10 - 90% dynamic range band. Previous analysis by others have shown more optimistic threshold values due primarily to two factors. First, much more optimistic assumptions were taken for parameters such as sensor quantum efficiencies than this study had deemed acceptable based on commercial devices (c.f. Appendix A for discussions). Second, a major contribution to the lower values attained in this study was the inclusion of the spatial and time splitting factors which split lightning pulses, hence lowering their apparent energy. The dashed curves in Figure B.4 result when the splitting factors are excluded. These curves are about a factor of two below the more realistic curves (solid). A third factor which was not included but will have some influence is the

ORIGINAL PAGE IS
OF POOR QUALITY

LIGHTNING MAPPER NOISE CALCULATIONS

Pixel size on Earth (edge of square)	11	IM
Source size	11	IM
Pixel size of CCD	30	Microns
Telescope f/number	1	
Telescope focal length	9.70	CM
Telescope diameter	9.70	CM
	0	
Solar irradiance	300	W/M ² SR μM
Cloud albedo	.7	
Optics transmission, including filter	.4	
Wavelength	868.0	NM
Filter bandwidth	.5	NM
Geometric image splitting factor	.62	
Lightning Pulsewidth	.54	msec
Required S/N	6	
Quantum efficiency	.35	
Satellite altitude	35600	IM
Background	487500	electrons
Amplifier Noise (rms)	150	Electrons



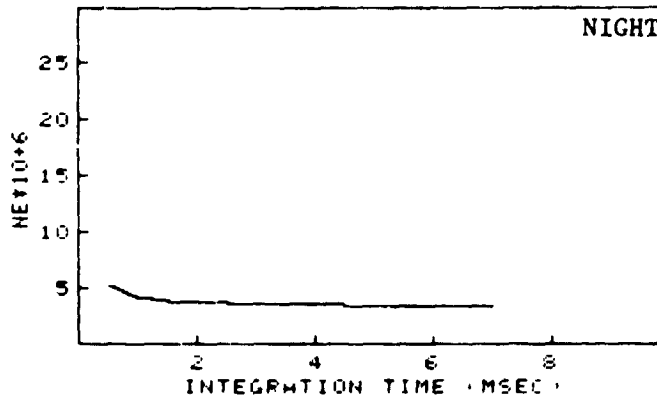
T	T-FACTOR	BACKGROUND (ELECTRONS)	SIGNAL (ELECTRONS)	BACKGROUND NOISE (RMS EL)	SIGNAL μJ/M ² SR	TOTAL NOISE (RMS EL)
.5	.64	22687	1293	150.62	7.54	215.54
1	.82	45374	1581	213.01	7.19	263.54
1.5	.88	68062	1823	260.88	7.73	303.95
2	.91	90749	2037	301.24	8.35	339.53
2.5	.92	113436	2230	336.8	8.96	371.7
3	.93	136124	2407	368.95	9.56	401.28
3.5	.94	158811	2572	398.51	10.12	428.81
4	.95	181498	2728	426.02	10.66	454.67
4.5	.95	204186	2874	451.86	11.17	479.12
5	.96	226873	3014	476.31	11.67	502.38
5.5	.96	249561	3147	499.56	12.14	524.6
6	.96	272248	3275	521.77	12.6	545.91
6.5	.97	294935	3398	543.07	13.04	566.42
7	.97	317623	3517	563.58	13.47	586.2

FIGURE B.2 Computer Printout Format for Baseline/Day

ORIGINAL PAGE IS
OF POOR QUALITY

LIGHTNING MAPPER NOISE CALCULATIONS

Pixel size on Earth (edge of square)	11	FM
Source size	11	FM
Pixel size of CCD	30	Microns
Telescope f/number	1	
Telescope focal length	9.70	CM
Telescope diameter	9.70	CM
	0	
Solar irradiance	0	W/M ² SR uM
Cloud albedo	.7	
Optics transmission, including filter	.4	
Wavelength	868.7	NM
Filter bandwidth	.5	NM
Geometric image splitting factor	.62	
Lightning Pulsewidth	.54	msec
Required S/N	6	
Quantum efficiency	.35	
Satellite altitude	35600	FM
Background	487500	electrons
Amplifier Noise (rms)	150	Electrons



T	T-FACTOR	BACKGROUND (ELECTRONS)	SIGNAL (ELECTRONS)	BACKGROUND NOISE (RMS EL)	SIGNAL uJ/M ² 2SR	TOTAL NOISE (RMS EL)
.5	.64	0	918	0	5.35	153.02
1	.82	0	918	0	4.17	153.02
1.5	.88	0	918	0	3.89	153.02
2	.91	0	918	0	3.76	153.02
2.5	.92	0	918	0	3.69	153.02
3	.93	0	918	0	3.64	153.02
3.5	.94	0	918	0	3.61	153.02
4	.95	0	918	0	3.58	153.02
4.5	.95	0	918	0	3.56	153.02
5	.96	0	918	0	3.55	153.02
5.5	.96	0	918	0	3.54	153.02
6	.96	0	918	0	3.53	153.02
6.5	.97	0	918	0	3.52	153.02
7	.97	0	918	0	3.51	153.02

FIGURE B.3 Computer Printout for Baseline/Night

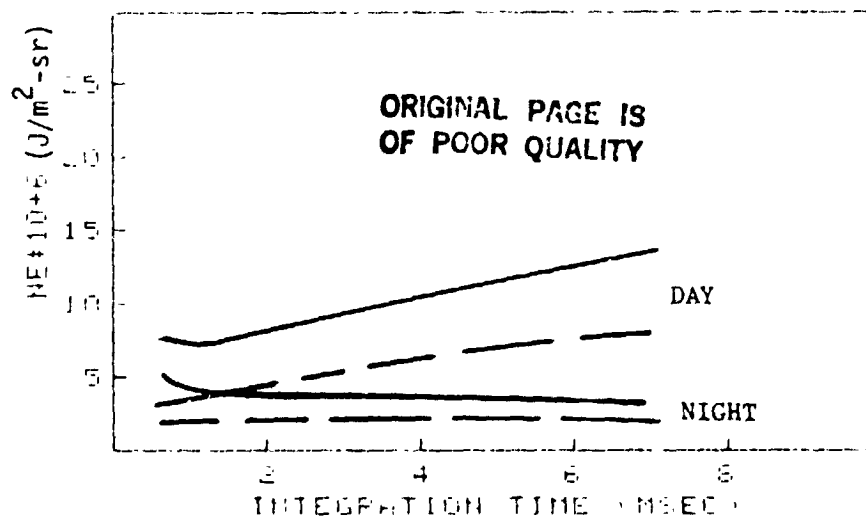


FIGURE 8.4 Baseline with (—) and without (---) Spatial and Time Splitting Factors

frame transfer dead time which will probably be between 10% and 30% depending on the selected integration time. Due to electronic/sensor system constraints, the 10% level is being sought. These factors just emphasize that parameter evaluation and selection must be done carefully. The values selected permit a certain amount of latitude for improvement in some areas to compensate for some inevitable degradation of other parameters.

- o Lightning event splitting (time/spatial) is important.

B.3 OPTIMISTIC SET

Although many parameters can be adjusted slightly, three parameters have been identified which, although will result in some increase in risk and possibly cost, would provide some enhancement of the LITMAP performance. These parameter (K, Q, and pixel size) adjustments are provided in Table 2.2. Figure B.5 shows that these changes will reduce the attainable threshold value to near $5 \mu J/m^2-sr$. Hence desired performance based on the given assumptions, including source image size equal to pixel

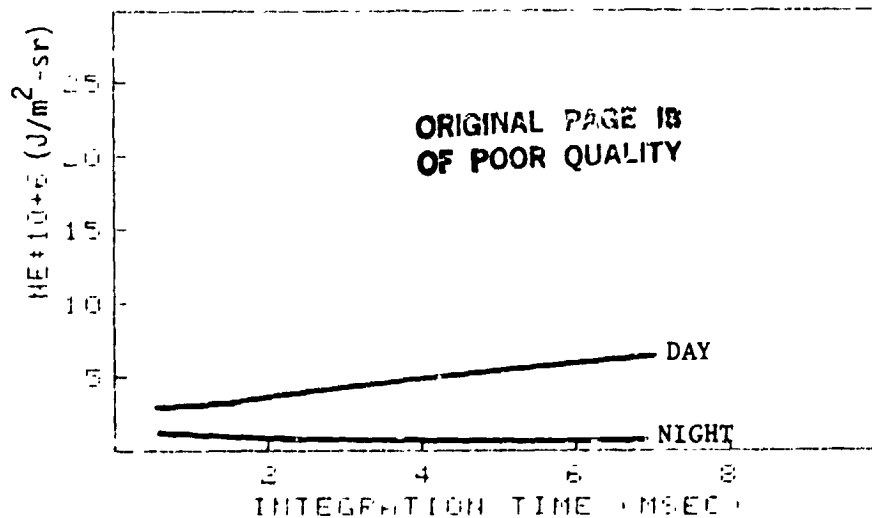


FIGURE B.5 Optimistic Performance

size, approaches the desired detection threshold capability.

- o Increased performance can be attained with some increase in risk and possibly cost.

B.4 LIGHTNING PULSE DURATION

The effect of dividing lightning events between two frames is illustrated in Figure B.6 along with effects of pulse duration. All of the curves in this appendix have this general shape. A finer step and larger range for the integration time was used in Figure B.6 to emphasis the shape of this curve. From hardware constraints, times shorter than one millisecond would not be practical so most of the parameter trades were done with fewer data points and longer times.

The minimum threshold point is at the minimum of the curves in Figure B.6. The left hand (small integration time) rise is due to the time splitting factor and the gradual right hand rise is due to the longer integration of the solar background. The minimum occurs where the integration time equals the pulse duration time. To avoid large changes in threshold as a

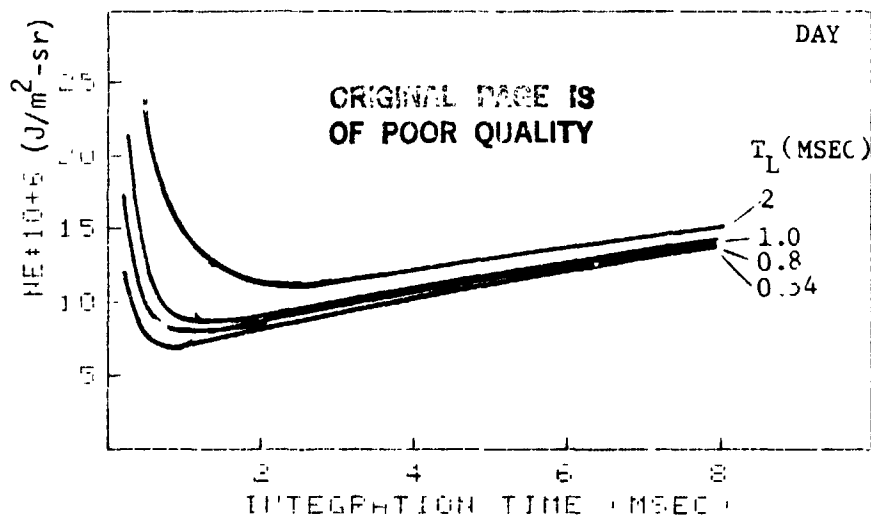


FIGURE B.6 Pulse Duration Effects

function of pulse duration, integration times longer (rather than smaller) than the pulse duration is desired. This integration time requirement is also driven by hardware, hence the analysis in Appendix A resulted in a baseline selection of 4 milliseconds as the integration time. This selection somewhat minimizes the variations due to pulse durations from sub milliseconds to one or two milliseconds. Not that the longer pulses will have some increase in their threshold, but these pulses tend to be the more intense pulses, hence will be detected inspite of this increase.

- o Pulse duration and time splitting considerations drive the integration time toward several milliseconds. This result is also compatible with some of the hardware constraints (e.g. data rate).

B.5 FILL FACTOR

The source size relative to individual pixel FOV dimension influences the threshold performance capability of the LITMAP instrument. Figure B.7 illustrates the effects where all parameters were set at their baseline values (including fixed

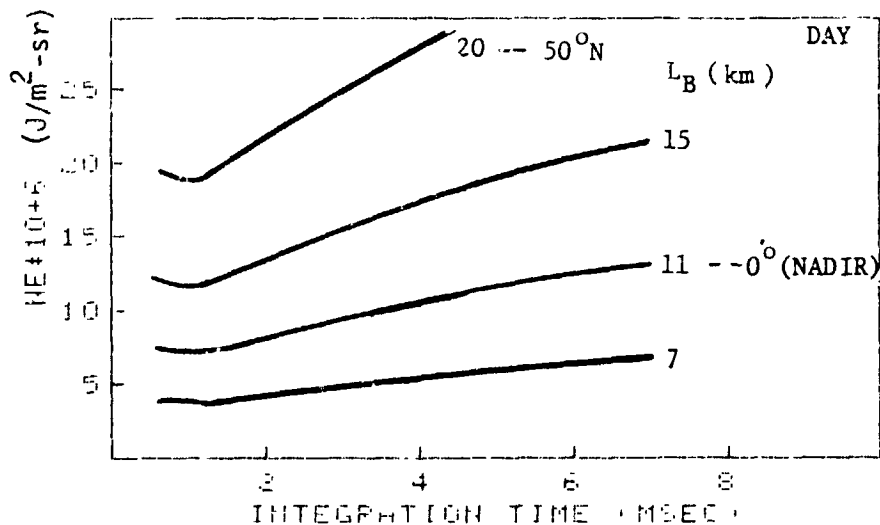


FIGURE B.7 FOV Effects - Day

source size) and the FOV varied. The 0°N (subsattellite point) and 50°N (maximum viewing angle) limits are included. The analysis was done such the maximum permissible aperture was always used as constrained by the FOV and detector pixel size. This gave the minimum threshold for a given set of conditions. As expected, the FOV to source size has strong effect on the threshold capability. It is thus emparative that the effective source size be quantified. This will be discussed a little more in a subsequent section.

For the present situation, with a fixed effective source size, the background area viewed is larger as the viewing angle moves away from the sub-satellite point. A threshold degradation of about 2.7 results at the maximum viewing angle.

Spatial splitting has been included and does have an effect which is very apparent in the nighttime plots of Figure B.8 corresponding to the same conditions of Figure B.7. Without the splitting factor the nighttime capability would be only amplifier noise dependent, hence constant (without noon light etc.). But

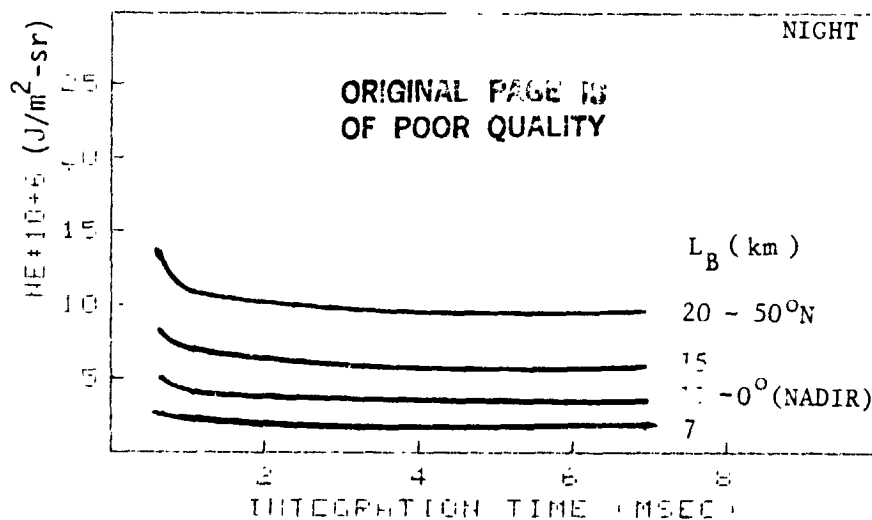


FIGURE B.8 FOV Effects - Night

as seen in Figure B.8, the nighttime capability degrades (threshold increases) as the FOV increases, primarily because of the effect through the spatial splitting factor which requires larger effective source strengths as the FOV increases relative to source size.

The composite result for the FOV effect coupled with the spatial splitting falls between a linear and square dependency as illustrated in Figure B.9 where the solid line is for computed values. All curves were made equal at the nominal value of 11 km baseline sub-satellite resolution point.

- o Off nadir viewing angles will have a threshold degradation of up to a factor of about 3.

B.6 PIXEL SIZE

One of the key parameters that can be varied to enhance the LITMAP instrument performance is that of sensor pixel size. Larger pixels permits larger apertures and full well capacities. This latitude must then be traded with achievable array size

ORIGINAL PAGE IS
OF POOR QUALITY

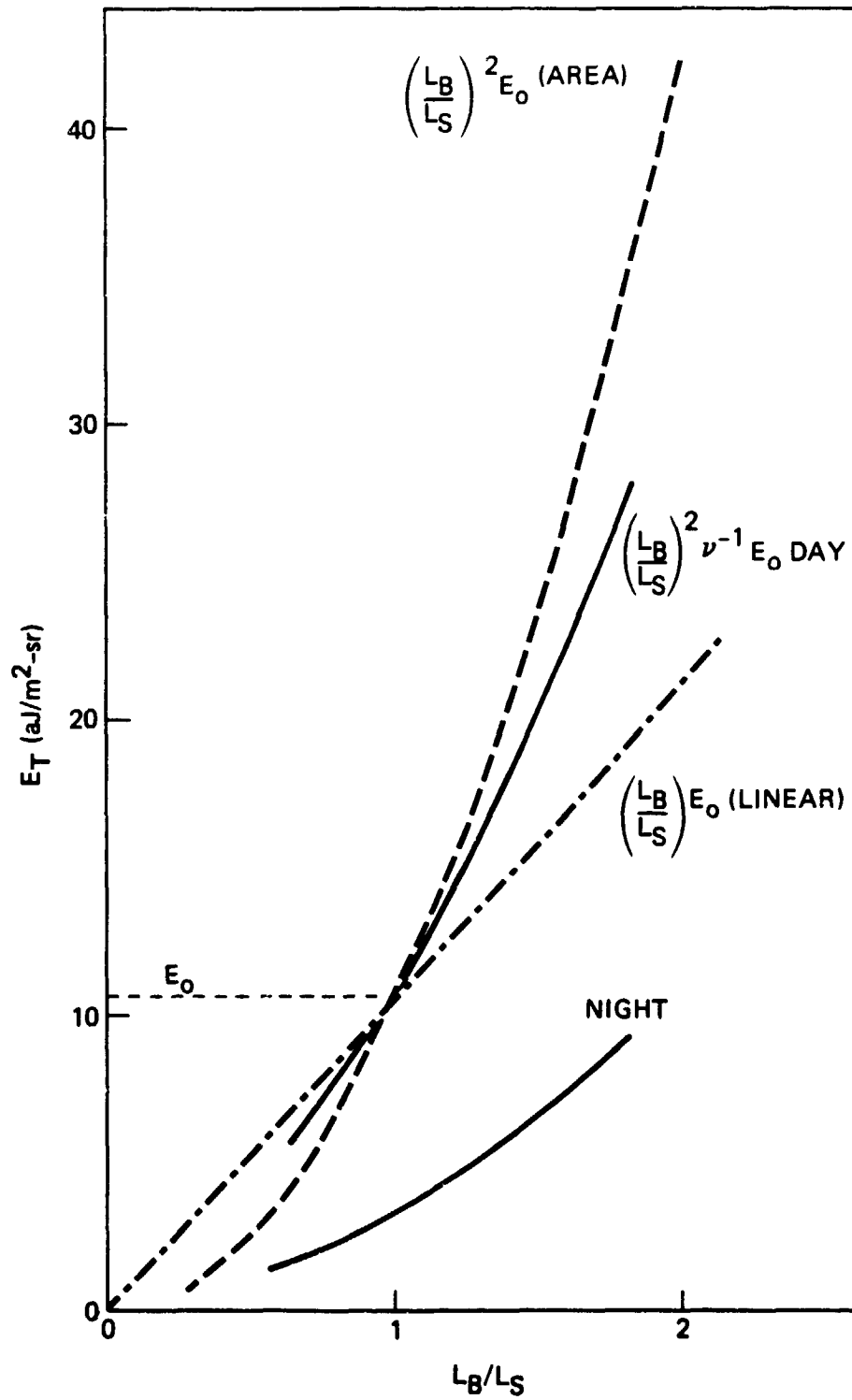


FIGURE B.9 Threshold Dependency on FOV.
Baseline conditions and $L_S = 11$ km.

which usually results in building a mosaic of smaller arrays. This mosaic approach introduces its own complications including optical/focal plane complexities.

Performance for pixel sizes from 15 to 40 microns are illustrated in Figure B.10 for daytime operation. The 15 micron pixel size as used for the large 800 X 800 NASA/JPL Galileo project is not suitable for LITMAP, both from sensitivity (limited aperture size) and full well (background handling) requirements. Figure B.11 again illustrates that the larger aperture permitted by a larger pixel results in a lower detectable energy level.

- o Large pixel size is necessary (> 20 microns)

B.7 READOUT NOISE

The process of extracting the photon produced electrons from the sensor array will induced noise contributions in addition to those associated with solar background and signal. The primary contributor, as indicated in Appendix A, is the readout amplifier associated noise. This noise contribution is often specified as the number of rms noise equivalent electrons.

For the baseline conditions, the effect of varying the amplifier noise is summarized in Figures B.12 (day) and B.13 (night). For normal solar background and cloud albedo, a significant contribution from the amplifier noise does not occur until somewhere above 200 e rms. From Figure B.12, the present baseline concept could accommodate up two or three hundred electron rms noise contribution without serious degradation of performance. But as noted in Figure B.13, as the amplifier noise increases, the night performance degrades. As this contribution approaches 400 e rms, the day/night performances will be about equal for a 4 millisecond integration time. For larger noise contributions, the performance will become amplifier limited, not solar background limited.

- o Amplifier noise must be kept significantly below the solar contribution if enhanced night performance is desired (i.e., $N_{amp} (rms) < N_{sol} (rms)/2$).

ORIGINAL PAGE IS
OF POOR QUALITY

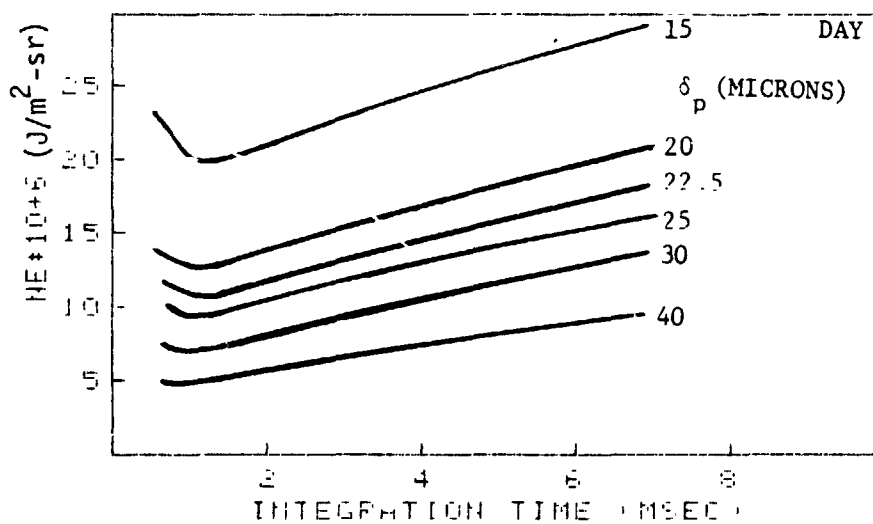


FIGURE B.10 Pixel Size Effects - Day

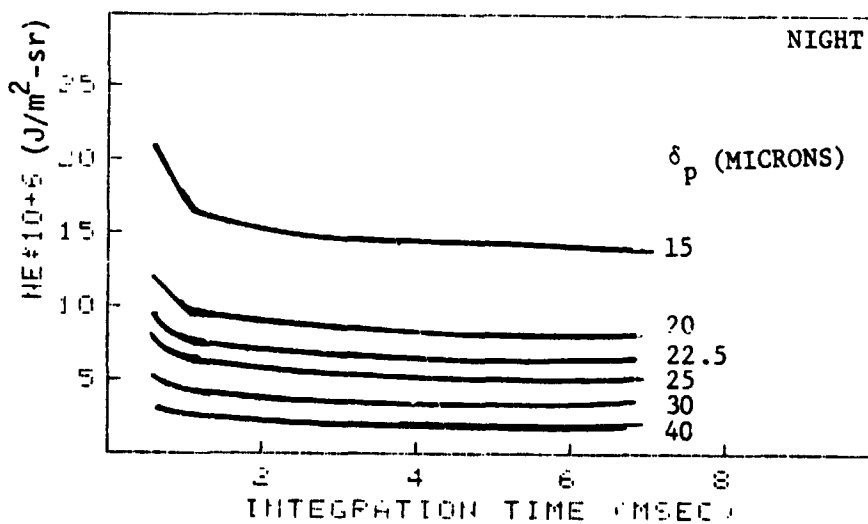


FIGURE B.11 Pixel Size Effects - Night

ORIGINAL PAGE IS
OF POOR QUALITY

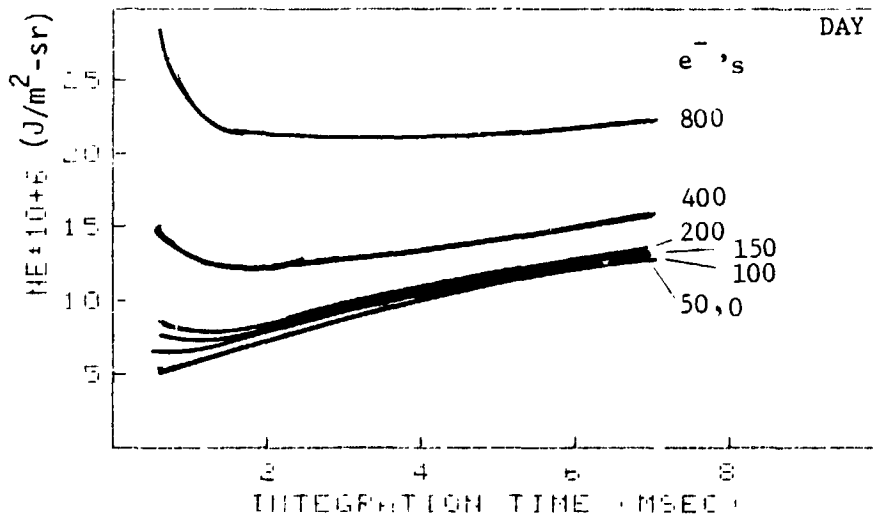


FIGURE B.12 Amplifier Noise Effects - Day

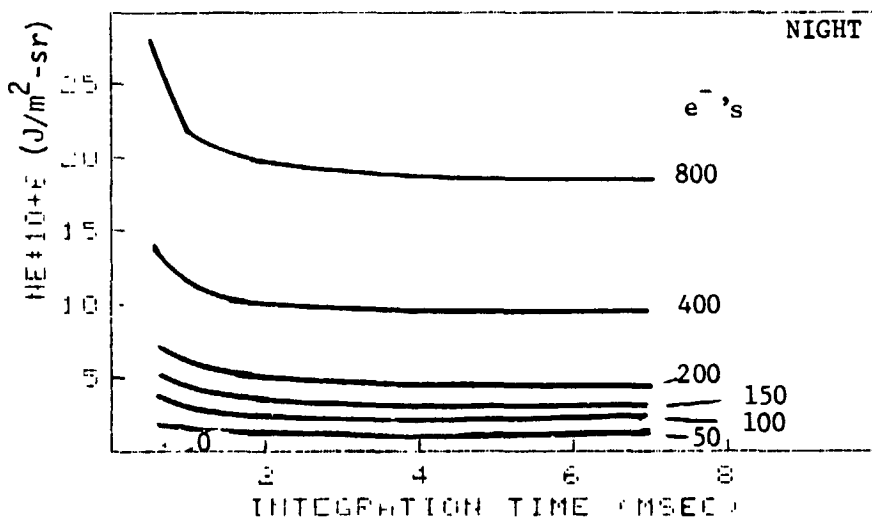


FIGURE B.13 Amplifier Noise Effects - Night

ORIGINAL PAGE IS
OF POOR QUALITY

B.8 WAVELENGTH

Primary focus has been on the 8683A wavelength. Other candidates exist and should possibly be evaluated. The baseline performance at 8683 and alternate 7774 angstroms were compared. The following values were assumed:

<u>Parameter</u>	<u>Baseline</u>	<u>Alternate</u>	<u>Units</u>
Wavelength	8683	7774	A
Q	0.35	0.5	-
I _B	300	396	w/m ² -sr-um

Figure B.14 illustrates that the threshold values are about the same for the conditions considered. Other factors such as sensor materials and/or larger absolute strength for one of the lines may result in a preference. At the present, the 8683 A line has been baselined although it has a somewhat lower detection quantum efficiency when silicon dioxide is used for the structural elements. If tin oxide is used, as for the Westinghouse devices, both spatial line detection efficiencies are about equal and fairly high (> 50%). Hence the tin oxide material would be a good candidate for the "optimistic" system.

- o Relative optical magnitudes of the spectral lines are needed.

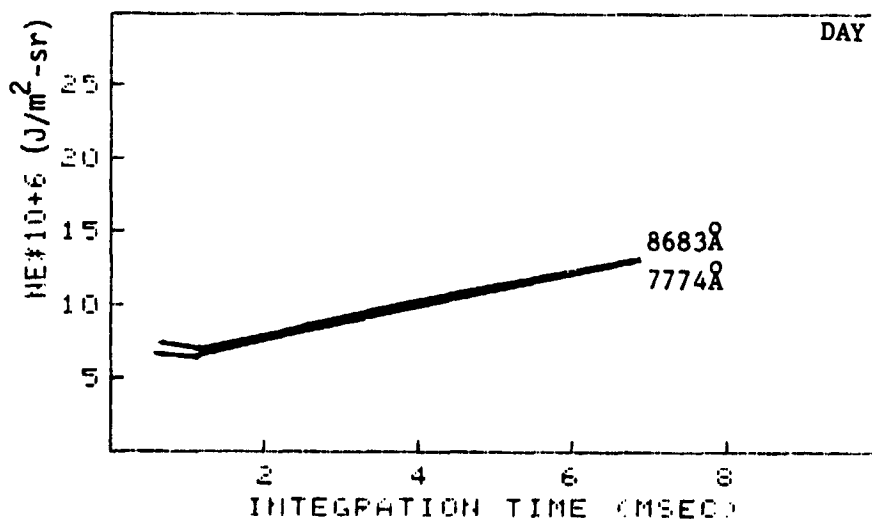


FIGURE B.14 Wavelength Selection

B.9 FILTER BANDPASS

The filter bandpass must be as narrow as possible to reject the solar background. Birefringent filters have been developed that can provide large FOV coverage while maintaining narrow passbands but suffer from lower transmission, high cost and high risk. Interference filters, although more technologically available, exhibit a FOV angular dependency which does not accommodate a large FOV (18°) and narrow bandwidth ($<5 \text{ \AA}$) simultaneously.

The effect of optical bandpass on the daytime threshold performance is illustrated in Figure B.15. A 25A bandpass would degrade the system performance by a factor of 2 relative to a 5A filter. This degradation is in addition to the factor of 2 which occurs if optical splitting factors are not included.

As a result of these considerations, the FOV was divided into smaller portions which permitted the use of interference filters possessing around 5A passband to be used. If the need is sufficient, some improvement could be realized through the use of a birefringent type of filter.

- o Narrow bandpass is necessary ($<5\text{A}$).

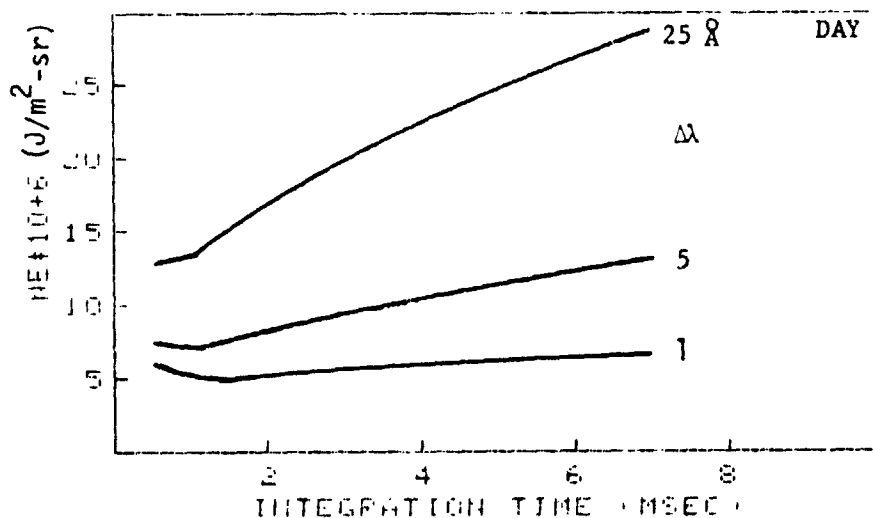


FIGURE B.15 Optical Bandpass Effects

B.10 EVENT SOURCE SIZE

Physical, complexity and cost constraints place restrictions on the allowable number of array elements that can be utilized. This limited array size coupled with full disc coverage places a severe restriction on the source energy that can be resolved during day operations. As discussed earlier, this detection is also complicated by the geometric splitting.

The baseline concept assumes that the source and pixel FOV are of equal size, 11km. Figure B.16 illustrates the increase in the required threshold energy as the source moves from 11 km dimensions (lower curve) to 5 km. The night performance is not as bad as illustrated in Figure B.17. If the $4 \text{ uJ/m}^2\text{-sr}$ is a true indication of the source strength, and if the effective source size is considerably less than 11 km square, then the threshold will be much larger. This condition would result in pushing the LITMAP instrument design hard toward the technology limits to provide the performance desired from a geosynchronous orbit. An alternative would be to decrease the pixel FOV to match source size. If the full disc coverage then requires too many array elements, a move to a very LITMAP compatible step/stare concept could be made.

- o Event source size must be quantified.

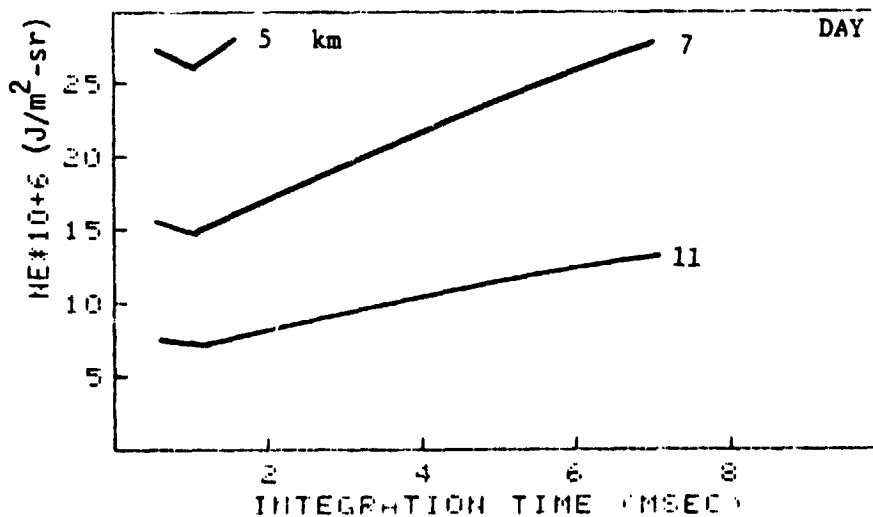


FIGURE B.16 Source Size Effects - Day

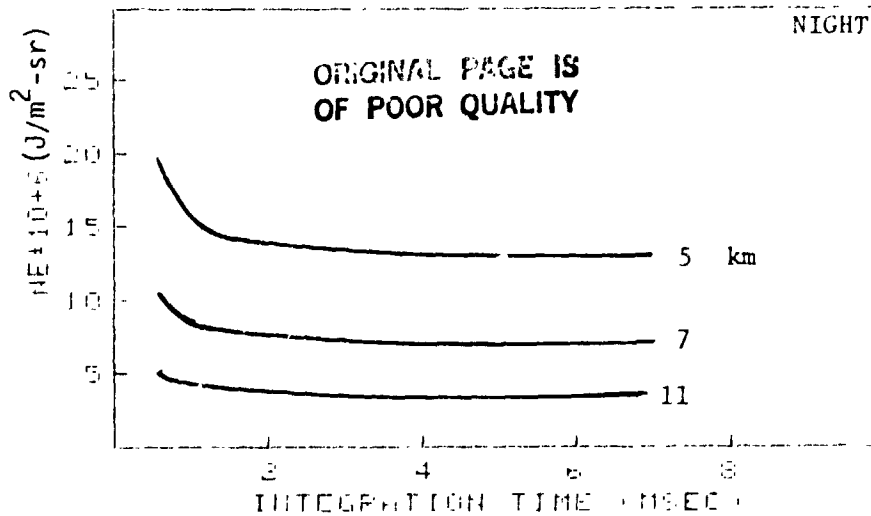


FIGURE B.17 Source Size Effects - Night

B.11 EXISTING DEVICES

The capability of existing imaging array devices were assessed to put the overall system trade evaluations into perspective with the real world. A 22.4 micron TI (TV: IC-202) device is compared with a RCA (SID 501D) 30 micron device. As can be seen in Figure B.18, the RCA device comes close to the LITMAP baseline limit. The smaller pixel device has a higher threshold capability. Performance of other devices are illustrated in Figure B.19 (8683A) and Figure B.20 (7774A). For ease of wavelength dependency comparison, Figure 21, 22 and 23 illustrates the 8683A and 7774A results for RCA, Westinghouse and Hughes. Where the detection quantum efficiencies are nearly equal for the two wavelengths (as in the Westinghouse device) the 8683A line comes out ahead, otherwise the 7774A line has a small edge. The device pixel sizes and quantum efficiencies are given in a device characteristics table located in Section 5.

- o Existing commercial devices approach the LITMAP baseline performance specifications (array partitioning required to handle data rate).

ORIGINAL PAGE IS
OF POOR QUALITY

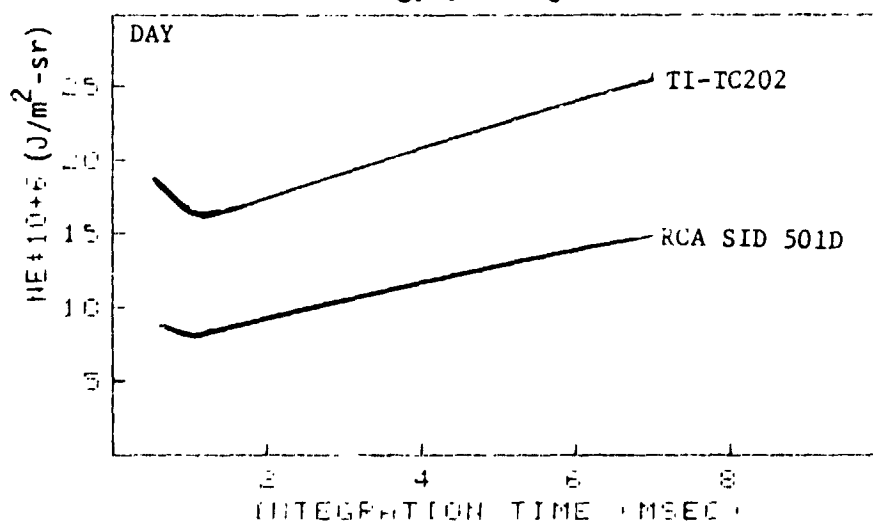


FIGURE B.18 Actual Devices - RCA, TI

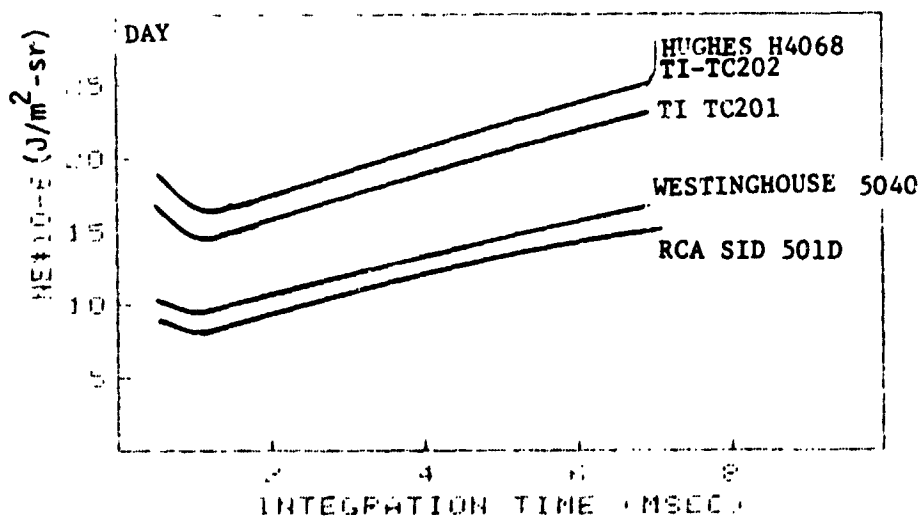


FIGURE B.19 Actual Devices - 8683A

ORIGINAL PAGE IS
OF POOR QUALITY

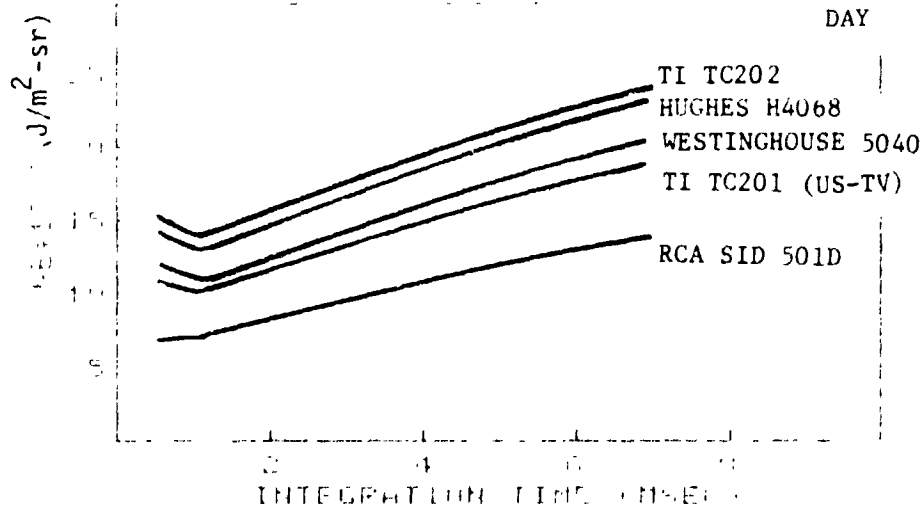


FIGURE B.20 Actual Devices - 7774A

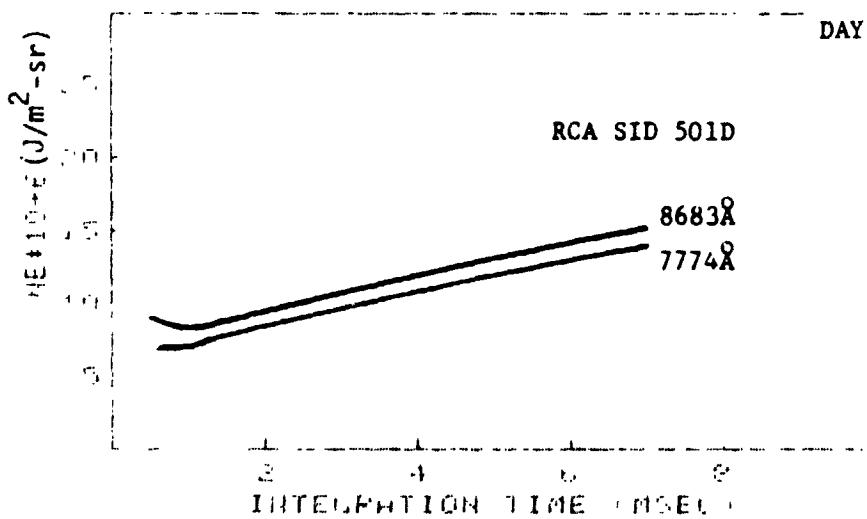


TABLE B.21 RCA: 8683A and 7774A (SID 501D)

ORIGINAL PAGE IS
OF POOR QUALITY

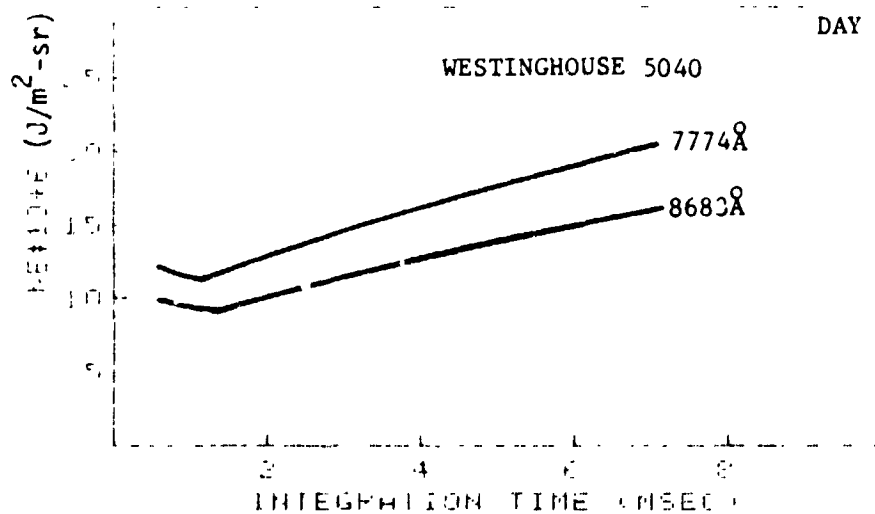


FIGURE B.22 Westinghouse: 8683A and 7774A (5040)

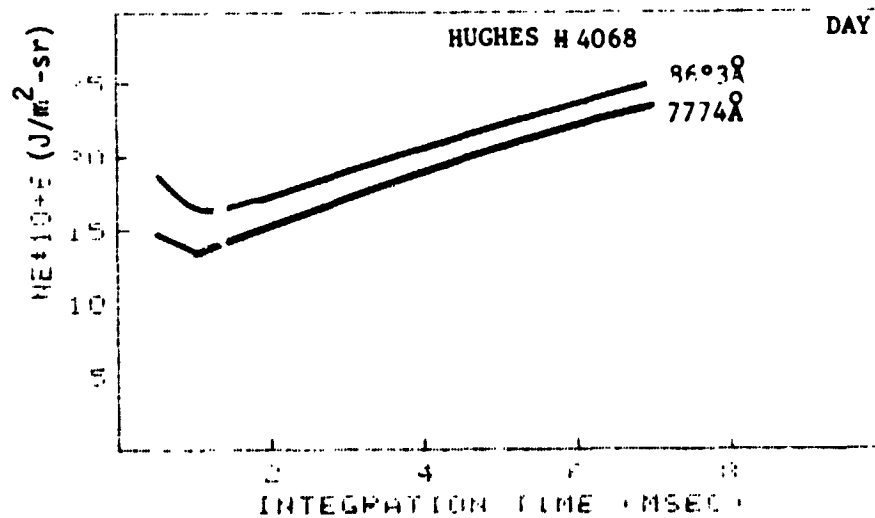


FIGURE B.23 Hughes: 8683A and 7774A (H4068)

ORIGINAL PAGE IS
OF POOR QUALITY

B.12 SUMMARY

This section has illustrated the threshold dependency on the various sensor design parameters. These analyses were also weighed against electronic and physical constraints as well as cost and schedule. Table B.1 summarized the results of this appendix.

TABLE B.1 Parametric Trade Results

<u>FACTOR</u>	<u>COMMENT</u>
o Baseline	Lightning event splitting (time/spatial) is important.
o Optimistic	Increased performance can be attained with some increase in risk and possible cost.
o Pulse Duration	Pulse duration and time splitting considerations drive the integration time toward several milliseconds. This result is also compatible with some of the hardware constraints (e.g, data rate).
o Fill Factor	Off nadir viewing angles will have a threshold degradation of up to a factor of about 3.
o Pixel Size	Large Pixel size is necessary(> 20 microns)
o Readout Noise	Amplifier noise must be kept significantly below the solar contribution if enhanced night performance is desired (i.e., $N_{\text{amps}} \text{ (rms)} < N_{\text{sol}} \text{ (rms)}/2$).
o Wavelength	Relative optical magnitudes of the spectral lines are needed.
o Filter Bandpass	Narrow bandpass is necessary (< 5Å).
o Event Source Size	Event source size must be quantified.
o Existing Device	Existing commercial devices approach the LITMAP baseline performance specifications (array partitioning required to handle data rate).